Bioactive properties of glasses/glass-ceramics synthesized from agricultural and food wastes

A
Thesis
Submitted in the partial fulfilment
of the requirements for the award of the degree of

DOCTOR OF PHILOSOPHY

By
Shivani Punj
(Registration No. 901612021)

Under the supervision of

Dr. Kulvir Singh
(Professor and Head)

School of Physics and Materials Science
Thapar Institute of Engineering and Technology
(Deemed-to-be-University)
Patiala-147004, Punjab, India
June -2022

Certificate

I hereby certify that the work which is presented in the thesis entitled **"Bioactive properties of glasses/glass-ceramics synthesized from agricultural and food wastes"** in the partial fulfillment of requirements for the award of the degree of DOCTOR OF PHILOSOPHY in the School of Physics and Materials Science, Thapar Institute of Engineering and Technology, Patiala (Punjab), India is an authentic record of my own research work carried out under the supervision of Dr. Kulvir Singh. The matter embodied in this thesis has not been submitted in part or full to any other university or institute for the award of any degree.

Shivani Punj

(Shivani Punj) **Dated:** 01-07-2022

Registration No. 901612021

It is certified that the above statement made by the student is correct to the best of my knowledge and belief.

(Dr. Kulvir Singh)

Professor and Head
School of Physics and Materials Science
Thapar Institute of Engineering and Technology,
Patiala-147004 (Punjab), India.
Supervisor

Acknowledgment

At this moment of accomplishment, foremost, I would like to express my sincere gratitude to my supervisor, Dr. Kulvir Singh (Professor and Head, Thapar Institute of Engineering and Technology, Patiala) who provided me an opportunity to join as his student and gave access to the laboratory and research facilities. I thank him for his continuous support of my Ph.D. study, and research for his patience, motivation, enthusiasm, and immense knowledge. He always encouraged and supported me just like a father in difficult times during my Ph.D. pursuit. He never let me down whenever I approached him. Throughout my thesis-writing period, he encouraged me by giving valuable points. I could not have imagined having a better advisor and supervisor for my Ph.D. study. My deepest personal regards are due for him forever.

I gratefully acknowledge Dr. Parkash Gopalan (Director, TIET Patiala) and Dr. Rafat Siddique (Dean, research and sponsored projects, TIET Patiala) for allowing me to work under their kind support.

I would like to thank all doctoral committee members: Dr. Bhupendra Chudasama, Dr. B.C. Mohanty, Dr. Amjad Ali, for sparing their valuable time for the progress monitoring of my research work and giving such insightful comments which helped me to improve my research from various perspectives. I am highly thankful to Dr. Manoj Baranwal (Associate Professor, Department of Biotechnology, TIET, Patiala) for his support to complete my ongoing research work. I would like also thank to Dr. Devender Kumar (Assistant Professor, Department of Mechanical Engineering, TIET, Patiala) for his unconditional help to the laboratory work.

I would like to thank Mr. Puroshottam, Mr. S.P. Verma, Mr. Parminder, Ms. Amandeep Kaur, Ms. Neelam Sadana, Mr. Lalji Verma, and Mr. Vijay, for their official and technical support. All the staff members of SAI labs (TIET, Patiala) and SAIF lab (Panjab University Chandigarh) are also acknowledged who offered their services for characterization work.

It gives me great pleasure to thank my colleagues Dr. Paramveer Kaur, Tarisha Walia, Manmeet Kaur, Taranveer Kaur, Vimi Dua, Navneet Kaur, Santosh, and Neha Srivastava for their cooperation and help received during this period that allowed me to overcome the more persistent obstacles to thesis completion. I would like to thank my seniors Dr. S.S. Danewalia, Dr. Gaurav Sharma, Dr. Neetu Bansal, and Dr. Savidh khan for their valuable help during the initial stage of my work.

I am thankful to the Department of Science and Technology, New Delhi, for giving me financial assistance for Project under Women Scientist Scheme, award letter no. (SR/WOS-A/PM-23/2018).

I am greatly indebted to my grandfather Sh. Diwan Chand Sharma and my mother Smt. Anuradha Punj, who have stood by me in every thick and thin of my life. I have no words to acknowledge their unconditional love and endless efforts in taking care of my son, which only encouraged me to take up my research work. My grandfather always stood as a pillar of strength for me with unending faith and empathy. He has always shared his valuable thoughts and inspired me to work harder. I thank my husband, Sh. Jashandeep Singh for his love, patience, and support throughout my work. I am not able to find words to express my feelings for my son Devanshbir who endured many uneventful days while I worked instead of giving him my undivided attention.

Besides this, I also thank those who could not find the separate name but helped me directly and indirectly in the beautiful journey to the completion of this project.

Above all, I bow my head to God, the almighty for providing me with this opportunity and granting me the capability to proceed successfully.

Shivani Punj

(Shivani Punj)

List of Publications (From thesis)

1. **Shivani Punj**, K. Singh, Blue-green light emitting inherent luminescent glasses synthesized from agro-food wastes, ***J. Mater. Sci. Mater. Electron*** 30 (4) (2019) 3871-3881. **IF (2.779)**
2. G. Sharma, M. Kaur, **Shivani Punj**, K. Singh, Biomass as a sustainable resource for value-added modern materials: a review, ***Biofuel. Bioprod. Biorefin***. 14(3) (2020) 673-695. **IF (5.239)**
3. **Shivani Punj**, K. Singh, Bioactive calcium silicate glass synthesized from sustainable biomass waste, ***Biofuel. Bioprod. Biorefin.*** 14(6) (2020) 1141-1151. **IF (5.239)**
4. **Shivani Punj**, Jashandeep Singh, K. Singh, Ceramic biomaterials: Properties, state of the art and future prospectives, ***Ceram. Int.*** 47(20) (2021) 28059-28074. **IF (5.532)**
5. **Shivani Punj**, Neha Srivastava, Manoj Baranwal, Kulvir Singh, In-vitro biological evaluation of diopside bio-ceramic synthesized from sustainable agro-food waste ashes, ***Silicon*** (2021) 1-11. **IF (2.941)**
6. **Shivani Punj**, Jashandeep Singh, K. Singh, Structural and optical properties of agro-food wastes derived glasses synthesized in two different crucibles, ***Mater. Today. Proc.*** (2022) DOI: 10.1016/j.matpr.2022.01.123

Other than thesis

1. Taranveer Kaur, **Shivani Punj**, Ravindra Kumar, Kulvir Singh, Effect of minor phase (CuO) on sinterability, grain size, and dielectric properties of $CaCu_3Ti_4O$ ceramics, ***App. Phys. A*** 126(10) (2020) 1-6. **IF (2.584)**

Conferences and workshops

Poster presentations

1. National Conference on Recent advances in condensed matter physics held at KU, 12-13 October 2018.

   Shivani Punj, K. Singh, *Effective utilization of the agro-food wastes materials in engineering and medical applications*.

2. Materials Research Society of India Symposium (MRSI-2020) on " 2nd Indian Materials conclave and 31" AGM meeting of MRSI, held at CSIR-Central Glass & Ceramic Research Institute, Kolkata, 11-14th February 2020.

   Shivani Punj, K. Singh, *Structural properties of agro-food wastes derived bioactive glass.*

3. International Symposium on Materials of the Millennium: Emerging Trends and Future Prospects (MMETFP-2021) held at Gujrat, 19-21th November 2021.

   Shivani Punj, Jashandeep Singh, Kulvir Singh, *Structural and optical properties of agro-food wastes derived glasses synthesized in two different crucibles*

Workshops attended

1. Recent Advances in Nanoscience and Nanotechnology (RANN-2020) held at NIT Srinagar, 24-28th August 2020. (online)
2. Advanced Energy Materials (TEQIP III) held at Dr. B.R Ambedkar, held at NIT, Jalandhar, 12-16th September 2020. (online)
3. Recent Trends in Advanced Materials and Devices held at NIT, Jalandhar, 21-25th September 2020. (online)
4. Current Trends in Condensed Matter Physics held at NIT Jalandhar, 25-29th September 2020. (online)

List of abbreviations

AES- Avian eggshells

β-TCP – β-Tricalcium phosphate

BCP-Biphasic calcium phosphate

bSNPs-Biogenic silica nano particles

BA-Brown ash

BOs -Bridging oxygens

CBG-Conventional bioglass

CC- Corn Cob

CH-Corn husk

CHA-Corn husk ash

CCD-Charge coupled device

c-HAp- Carbonated hydroxyapatite

Ca-P -Calcium Phosphate

CHNSO-Carbon hydrogen nitrogen sulfur oxygen

DTA/TGA- Differential thermal analysis/thermogravimetric analysis

DMEM-Dulbecco's modified Eagle's medium

DMSO-Dimethyl sulfoxide

DSC- Differential scanning calorimetry

DCPD-Dicalcium phosphate dihydrate

ESP-Eggshell powder

ESM- Egg shell membrane

EDS-Energy dispersive spectroscopy

FTIR-Fourier transform infrared spectroscopy

FESEM-Field emission scanning electron microscopy

FWHM-Full width at half maximum

h- Hours

HAp- hydroxyapatite

HOB- Human osteoblasts cells

hLFCs-Human lung fibroblast cells

MTT-3-(4,5-Dimethylthiazol-2-yl)-2,5 diphenyl tetrazolium bromide assay

MP-AES - Microwave Plasma Atomic Emission Spectroscopy

NBOs- Non bridging oxygens

NCCS-National Center for Cell Science

OD-Optical density

pH- Potential of hydrogen

PCL-Polycaprolactone

Pt-Rh -Platinum-Rhodium

PPB-Parts per billion

PS- Peanut shells

RH-Rice husk

RHA-Rice husk ash

R-SBgC- Rice husk silica based bioactive glass-ceramics

SAOS-Sarcoma Osteogenic

SBF-Simulated body fluid

SG-Silica gel

SCB-Sugarcane bagasse

SCL-Sugarcane leaves

SCLA-Sugarcane leaves ash

SEM-Scanning electron microscope

WA-White ash

WS-Wheat straw

WSA-Wheat straw ash

wt % -Weight percentage

XRD- X-ray diffraction

Index

Chapter 4 Results and discussion-I

Chapter 5 Results and discussion-II

Chapter 6 Results and discussion -III

Chapter 7 Conclusion and future scope

List of figures

List of tables

Abstract

Agro-food wastes/ashes such as corn husks, sugarcane leaves, wheat straws, and eggshell powder are used as resource materials to prepare the glasses via the melt-quench technique. These agro-food wastes/ashes/powders contain silica, calcium, magnesium, potassium, and some other trace elements that are usually required to make bioglass/glass-ceramics. Moreover, agro-food wastes are also sustainable, and cost-effective sources to synthesize bioglasses/glass-ceramics. The effect of different agro-food waste ashes like sugarcane leaves ashes, wheat straw ashes, and eggshell powder with fixed corn husk ashes are investigated. The formed glasses/glass-ceramics are investigated for their physical, structural, thermal, and mechanical properties to check their suitability and applicability as biomaterials. Bioactive properties of the glasses/glass-ceramics are investigated *in-vitro* using simulated body fluid. Further, the biocompatibility of these glasses/glass-ceramics is observed on osteoblastic-like human cell lines (MG-63) using 3-(4,5-Dimethylthiazol-2-yl)-2,5diphenyl tetrazolium bromide assay to investigate their applicability. The thesis work is represented in seven chapters.

Chapter 1 deals with the basics of glass/glass-ceramics, bioglasses/glass-ceramics, and their basic requirements to qualify as bioactive materials. Different testing methods used to test the bioactivity of glasses/glass-ceramics followed by the mechanism of formation of HAp layer on the glass/glass-ceramics surface after soaking in simulated body fluid (SBF) are also given in this chapter. The biocompatibility testing methods are also given in brief. The 3-(4,5-Dimethylthiazol-2-yl)-2,5 diphenyl tetrazolium bromide assay is a reliable method. It is directly related to the number of viable (living) cells introduced to test the biocompatibility of glass/glass-ceramics. Further, the potential agro-food wastes and their constituents are also discussed in this chapter.

Chapter 2 This chapter contains the literature survey on various agro-food wastes/ powder/ashes and their use as resources to synthesize different bioactive materials. The

different agro-waste materials along with their ashes have been studied to extract silica as alternative resource material to commercial silica production to synthesize bioglasses/glass-ceramics. Apart from this, other structural, thermal, mechanical, bioactive, and biocompatible properties of agro-food wastes derived bioglasses/glass-ceramics and calcium phosphate ceramics, silicate-calcium based bioceramics have been summarised. Based on the literature survey, the motivation of the present study followed by objectives are also given in the last of this chapter.

Chapter 3 The compositions of raw materials such as corn husk ash (CHA), sugarcane leave ash (SCLA), wheat straw ash (WSA), and eggshell powder (ESP) are analyzed by energy dispersive spectroscopy (EDS). Based on chemical analysis, different compositions with variable agro-food wastes contents are proposed such as [(60) CHA-(40-x) SCLA-(x) ESP] where, x=10, 20, and 30 (wt %) and [(60) CHA-(40-x) WSA-(x) ESP] where, x=10, 20, and 30 (wt %). These compositions are synthesized by recrystallized alumina crucibles via melt quench techniques. The two samples from each series with similar compositions [60 CHA-30SCLA-10 ESP], [60 CHA-10 SCLA-30 ESP] and [60 CHA-30WSA-10 ESP], [60 CHA-10WSA-30 ESP] in wt % are selected to prepare in platinum-rhodium (Pt-Rh) crucible. Agro-food wastes derived glasses are also replicated using conventional chemical oxides based on the best bioactive results for comparison. The chemical compositions of the as-prepared samples have been examined via energy dispersive spectroscopy (EDS). The Archimedes principle has been used to study the density of the as-prepared samples. The structural and thermal properties of the samples are analyzed by X-ray diffraction (XRD), Fourier transform infrared spectroscopy (FTIR), and differential scanning calorimetry (DSC). The mechanical property such as microhardness of these samples are studied using a Vickers hardness tester. The bioactivity of these glasses/glass-ceramics are checked through an *in-vitro* test after soaking the samples in simulated body fluid (SBF) for 7 to 28 days, parameters like weight

change of the samples and pH change of the SBF are checked after every 7 days. The soaked glasses in SBF are characterized by XRD, FTIR, scanning, and field emission scanning electron microscope (SEM and FESEM) with EDS and microwave plasma atomic emission spectroscopy (MP-AES) to know the physicochemical reactions take place on the surface of glasses. The biocompatibility of as-prepared glasses/glass-ceramics with concentrations of 1, 2, 5, and 10 mg/ml, are studied on osteoblast-like human cell lines (MG-63) using 3-(4,5-Dimethylthiazol-2-yl)-2,5 diphenyl tetrazolium bromide, assay. The cell viability is determined using the Elisa microplate reader.

Chapter 4 is related to the obtained results and their interpretations. This chapter is divided into two sections. In the first section, the effect of SCLA on replacing ESP with the fixed composition of CHA is studied, whereas, in the second section the effect of WSA on replacing SCLA in the base glass is discussed in detail. The effect of SCLA and WSA on the physical, structural, thermal, mechanical, bioactive, and biocompatible properties are investigated thoroughly. The XRD patterns show the confirmation of the amorphous nature of the glasses. The microhardness of the SCLA glasses is in the range of 5.64 to 6.26 GPa, which is within the range (4-10 GPa) of reported conventional chemical-derived silicate glasses. The addition of (30 wt %) ESP ($CaCO_3$) at the cost of (10 wt %) SCLA, depolymerize the silica-phosphate glass network and increases the hydrophilic nature of the glasses increasing the surface reactivity and bioactivity of the glasses that are accessed in SBF. Moreover, weak bands 562, 602 cm^{-1} due to P-O bonding (amorphous) as well as 1423-1465 cm^{-1} stretching of carbonate bands on the glass surface after soaking in SBF have appeared in the FTIR spectra. The spherical sponge type of amorphous carbonated HAp (c-HAp) adhered on the surface of soaked glasses is confirmed via SEM and EDS. Initially, all glasses show a Ca/P ratio is high 4.91 as hydroxyapatite layer (HAp) is taken place and became less ~ 2 in all the glasses which is higher than standard HAp (1.67). All glasses have shown good (> 90 %) cell viability on human

osteoblastic-like cell lines (MG-63) by varying concentrations (1mg/ml to 10 mg/ml) of glass. When SCLA is replaced by WSA, WSA becomes more reactive than SCLA towards recrystallized alumina crucible as determined via EDS analysis. WSA glasses have shown an increase the compactness, rigidity (5.34 to 6.47 GPa), and less depolymerize the silicate-phosphate glass network than SCLA glasses, due to the presence of higher K_2O and alumina contents is confirmed by DSC and FTIR. In-vitro studies, the dissolution rate becomes lower due to the incorporation of alumina contents in the glass network that reduce the bioactivity as well as change the morphology of HAp from sponge to flakes type is confirmed by FESEM. The higher alumina (10.8 wt %) containing glass (10 wt % WSA) inhibits the bioactivity as well as become toxic (cell viability ≤ 68 %) at a higher concentration (10 mg/ml). This is due to the increase of a higher amount of alumina which strengthens the glass network and enrichment of the Al-OH group that decreases the release of silicon as well as a lack of silanol groups that inhibit the apatite formation on its surface is confirmed by FTIR and MP-AES.

Chapter 5 In this chapter, the effect of Al_2O_3 on bioactivity has been discussed to synthesize similar compositions in the Pt-Rh crucible. So, this chapter deals with composition [60 CHA-30SCLA-10 ESP], [60 CHA-10 SCLA-30 ESP] in wt % and [60 CHA-30WSA-10 ESP], [60 CHA-10WSA-30 ESP] in wt % are prepared using Pt-Rh crucible. The glasses synthesized in the Pt-Rh crucible have shown a lower amount of alumina (0.78 wt % to 1.02 wt %) in comparison to those synthesized in an alumina crucible (4 wt % to 10.8 wt %) is confirmed by EDS. With the decrease of alumina contents, the glass-forming ability of agro-food wastes derived glasses has reduced on replacing of SCLA with WSA. This is due to the presence of different alkali and alkaline earth metal ions in agro-wastes/ashes that have higher combinational entropy which plays a different role in the formation of glasses is confirmed by DSC. The microhardness of these Pt-Rh synthesized glasses lies in the range of 5.59 to 6.57 GPa. The diffusion of alumina from the crucible is decreased the water adsorption tendency. Since water

adsorption tendency enhances the bioactivity of the glasses. In the in-vitro study, more depolymerized the glass network and Si-OH (silanol) groups increased on its surfaces is confirmed by MP-AES and FTIR. The WSA-based glasses are formed globular type amorphous c-HAp with a Ca/P ratio of 1.7 to 4.0 is also confirmed by FTIR and FESEM with EDS. The cell viability of 10 wt % WSA-based glass on MG-63 cell lines has shown > 88 % at a higher concentration of 10 mg /ml, which could be beneficial for bone bonding applications. However, due to the release of more Mg^{2+} ions in SCLA glasses, bioactivity is decreased and also inhibits to form amorphous c-HAp on the glass surface. SCLA glasses have formed flakes and cauliflower-type amorphous HAp with Ca/P ratio of 1.6 to 3.9 is confirmed by MP-AES, FTIR, and SEM with EDS in these samples.

Chapter 6 based on bioactivity, biocompatibility, and other properties, two of the best compositions have been synthesized using conventional chemicals for comparison with agro-food wastes derived glasses. These glasses have been synthesized using the melt-quench technique following similar conditions for comparison and differentiate among conventional and agro-food wastes derived glasses. The glasses are derived from conventional chemicals show more density and rigidity (6.47-6.83 GPa) in the glass structure due to the formation of more covalent bonds Si-O-M or P-O-M (M=Al or Mg) than glasses derived from agro-food wastes, which is an agreement with a characteristic temperature of the glass determined by DSC and FTIR. In the in-vitro study, the SCLA-based conventional chemical glass has shown to release more Mg^{2+} ions in the SBF, reduce the overall rate of calcium phosphate precipitates, and slow (28 days) the transformation of amorphous HAp to amorphous c-HAp. It also changed the morphology of HAp from sponge to irregular flakes with a reduced Ca/P ratio of 3.98 to 2.18 than the glass derived from agro-food wastes. The conventional chemical oxide-based glass has also become toxic at a higher concentration (10 mg/ml) of glass, due to leaching out of more Ca^{2+} ions in SBF than the glass derived from agro-food wastes. However, WSA- based

conventional chemical glass has shown similar bioactive and biocompatible properties as observed for agro-food wastes derived glass.

Chapter 7 contains the conclusion and future scope of the present work. The results obtained within the present study reveal that the glass synthesized in an alumina crucible using a higher amount of (30 wt %) ESP contents in place of (10 wt %) SCLA has shown good bioactivity. This glass also shows good biocompatibility on human osteoblastic-like (MG-63) cell lines (> 90 % at higher concentration (10 mg/ml)), as compared to the similar composition of glass synthesized in Pt-Rh crucible and using conventional chemical oxides. This is due to the presence of different alkali and alkaline earth metal ions in agro-wastes/ashes controlling the dissolution rate of the glass in comparison to a reported conventional chemical-derived glasses. SCLA-based glass showed a high tendency to form spherical sponge-type amorphous c-HAp within 14 days of soaking in SBF, due to lower release of Mg^{2+} and higher release of K^{+} ions also help to incorporate the Ca-P precipitates on the glass surface. However, it inhibits the formation of crystalline HAp on the glass surface. Conventional chemical-based glasses with a Ca/P ratio >1 (for human bone the Ca/P ratio is 1.67) used as implants have been reported in the previous studies. The present glass has shown a Ca/P ratio >1.67, which is expected to be useful for bone bonding applications. On the other hand, WSA (10 wt %) based glasses have also shown good bioactivity and biocompatibility same as SCLA (10 wt %) only when it is synthesized in Pt-Rh crucible. Therefore, it is less cost-effective than the glass synthesized in an alumina crucible. In future, agro-food wastes materials could be used as resource materials in biomedical applications.

.

Chapter 1 Introduction

1. Glasses and glass-ceramics

Glasses do not have any structural periodicity due to the random arrangement of atoms. However, they exhibit some characteristic temperatures like glass transition (T_g), crystallization temperature (T_c) etc in comparison to crystalline and non-crystalline. These characteristic temperatures depend on the glass constituents and processing parameters [1]. Experimentally to test the glassy nature of the materials, the two techniques such as X-ray diffraction (XRD) and thermal analysis like differential scanning calorimetry (DSC) are used. XRD pattern showed a broad hump that confirmed the amorphous nature of the material. DSC used to measure characteristic temperature T_g onset crystalline temperature T_x , T_c and melting temperature (T_m) in the glasses. The amorphous nature of glass is also exhibited in the glass transition temperature like T_g. For instance, Figure 1.1 shows the XRD and DSC graph of 5CaO-20P_2O_5-60SiO_2-5B_2O_3-10ZnO (in mol %) based glass composition [2].

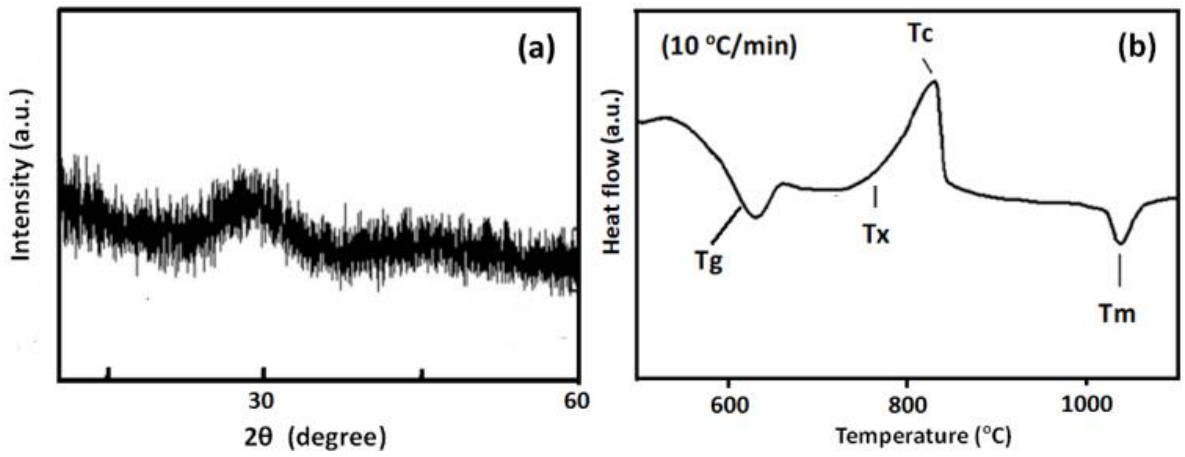

Figure 1.1 (a) XRD of glass sample (b) DSC curve for glass sample indicated the T_g, T_x, T_c, and T_m

The glasses contain, usually, three basic components i.e., glass network former, glass modifiers, and intermediates. These components are required some specific properties to act as

glass former or glass modifiers as proposed by many researchers [1, 3]. Glasses have unique compositional flexibility. Moreover, the properties of glasses can be altered by doping or adding replacements to the glass compositions [4]. This feature plays a vital role in glasses that are used in biomedical fields [5]. Based on thermal history, the glasses convert into glass-ceramics by controlled heat treatment. Usually, glass-ceramics exhibit better mechanical properties than glasses of similar compositions [1].

1.1 Bioglass and bioglass-ceramics

Hench and his colleagues (1971) discovered the bioglass (45S5) i.e., $45SiO_2$, 24.5CaO, $24.5Na_2O$, and $6P_2O_5$ in weight percent [6]. The bioglass is being used as implants in the human body to mend and replace damaged or diseased bones due to their bioactive and biocompatible properties [7]. The bioactive properties of developed materials can be checked *in-vitro, in-silico, and in-vivo* techniques. In *in-vitro* testing, the bioglasses are formed a bone-like apatite layer on its surface. It is formed when they are soaked in simulated body fluid (SBF), or an aqueous solution that has approximately the same ion concentration and pH as human blood plasma. The ions produced by the bioglass particles combine with local ions of SBF to form a hydroxyapatite layer (HAp) or carbonated hydroxyapatite (c-HAp). The composition of the HAp layer is similar to that of bone minerals, it creates a strong chemical linkage between bioactive glass and the surrounding bone [8]. It is an important feature of bioactive glass that makes it particularly attractive for use as an implant material in the regeneration of new bones or repair of the fractured bone. Bioglasses are not only capable of forming a HAp layer, but also osteoinductive, i.e., they can stimulate bone cells to regenerate and self-repair, significantly speeding up tissue healing kinetics [9]. It can also be utilized as bone grafts, implants, coatings, and dentistry. Kokubo et al. (1982) also reported some work on the bioglasses [10]. Glass-ceramics were developed in order to improve the mechanical properties of glasses. But, it was reported that the glass-ceramics exhibit lower bioactivity than parent

glass [5]. One feature that distinguishes bioactive glasses from other bioactive ceramics is the ability to control the rate of tissue bonding by controlling a variety of chemical properties [11]. Some glass-ceramics can also form this, but their heterogeneous macrostructure limits their applications [12]. Varying the initial composition of bioglass and processing conditions can be used to develop different bioglasses/glass-ceramics. For instance, Na_2O replaced by K_2O, CaO replaced by MgO, and B_2O_3 are used instead of SiO_2 in the glasses that have different bioactive properties [13-16]. In the same line, the presence of MgO in the bioactive glasses improved mechanical properties, biocompatibility, and biodegradability [15, 17, 18]. It also considerably helps in bone growth. It also affects the rate of HAp formation but depends upon the amount present in the glass composition to tailor the bioactive properties. There are some other elements which also include ZnO, AgO, TiO_2, Fe_2O_3, and Al_2O_3 in the glass composition [19, 20]. These oxides also provide therapeutic functions to bioglasses for regenerative medicines, tissue engineering applications, and bone cancer research [21]. Moreover, adding some dopants to the major compositions of glass/glass-ceramics influences various properties but at the same time, a high dose of doped ions can cause toxicity in the human body [22]. On the other hand, biocompatibility is also a basic property of any bioactive glasses/glass-ceramics. It concerns the capability of the material to perform its intended function without causing any undesirable or inappropriate adverse response to the body [23]. Therefore, a balance between various properties is required for the proper selection of materials, their constitutes, concentration, process parameters, and design.

1.2 Basic requirements for bioactive glasses/ glass-ceramics

In addition to the above bioactive glasses/glass-ceramics properties, other properties are also required such as chemically compatible, non-toxic, non-irritable, non-allergenic, and non-carcinogenic for the living body. When bioactive glass/glass-ceramics come into contact with living tissues, their surface chemistry must be optimized to meet the need of the host tissues.

A bio-adhesive contact must be established between the materials and living tissues. The structure of bioactive glasses/glass-ceramics should be known when designing alternative compositions to understand their behavior as biomaterials. There is also a need to design such types of materials that are not only osteoconductive but also possess a controllable degradation rate [24]. Because dissolution rate plays an important role in bioactivity, reactivity, and solubility of the bioactive materials [25]. It also gives information of apatite formation during biomineralization of glass dissolving in the body fluid and the release of calcium-phosphate (Ca-P) ions [26]. The dissolution rate should be compatible with the rate of bone formation. If the dissolution rate is too low, the ionic concentrations are inappropriate to promote cellular proliferation and differentiation. On the other side, if the dissolution rate is too fast, the ionic concentration may be higher than the effective level. The rate of dissolution and ion release in glass is affected by the glass network structure and type of constituent's ions present in the glass. Highly polymerized glass networks dissolve slowly, vice-versa [27]. Some studies showed no correlation between network connectivity and dissolution behavior in SBF [28]. The results exhibited that the dissolution behavior was affected by the presence of ionic species in the glass. It includes valance and ionic radii that examine their leaching behavior [29]. The dissolution rate and connectivity of the glass network could be tailored by adjusting the composition and fabrication techniques of glass. The bioactive glasses/glass-ceramics should be mechanically compatible with surrounding tissues, in order to prevent structural failure during the handling of the materials. Lastly, the bioglass/glass-ceramics should be cost-effective while still maintaining the desired properties in order to be commercialized.

1.3 Testing of bioglasses/bioglass-ceramics

Primarily, the developed biomaterials could be tested for their bioactivity by *in-silico, in-vitro,* and, *in-vivo* methods.

1.3.1 *In-silico*

In-silico testing is done through a computer simulation that provides a significant contribution to the biomedical field and clinical trials. For instance, *in-silico* testing is gaining popularity for predicting how pathogens, genes, and drugs will act and interact in the human body [30].

1.3.2 *In-vivo*

In-vivo testing is performed within the living organism under controlled physicochemical conditions. It is most commonly used in animal testing and clinical trials involving human participants [31].

1.3.3 *In-vitro*

In-vitro testing is performed outside of the living organism. It is performed under laboratory conditions. For instance, cell culture experiments were conducted using test tubes, petri dishes. *In-vitro* testing is used as a safety tool before real testing of materials *in-vivo*. *In-vitro* testing is beneficial both ethically and economically because it reduces the number of animals required for *in-vivo* testing. Previously, *in-vitro* tests were carried out by immersing the glass in either distilled water or a Tris-buffered solution, but since the innovation of SBF by Kokubo et al. [32] has become the most extensively used solution for *in-vitro* testing. SBF contains all the necessary inorganic components found in human blood and properties that are nearly identical to human blood plasma as given in Table 1.1. However, the concentration of HCO_3^- is lower than blood plasma. If the concentration of HCO_3^- in SBF is higher than 5 mM, then it is only valid for dynamic test, where the solution circulates permanently and thus lack of pH stability is less significant for *in-vitro* test.

Table 1.1 Ionic concentrations of SBF and human blood plasma (mM)

	Na^+	K^+	Mg^{2+}	Ca^{2+}	Cl^-	HCO_3^-	HPO_4^{2-}	SO_4^{2-}
Plasma	142.0	5.0	1.5	2.5	103.0	27.0	1.0	0.5
SBF	142.0	5.0	1.5	2.5	147.8	4.2	1.0	0.5

The pH of the solution is buffered between 7.25 and 7.4 at 37 ^{o}C during *in-vitro* studies [32]. Later on, different types of SBF were also proposed to check the *in-vitro* bioactivity of the materials. But Kokubo protocol is still widely used to check the *in-vitro* bioactivity of the materials. Several properties of bioactive glasses have been studied in SBF by observing the changes in weight of the glass, surface morphology, as well as changes in pH, and ionic concentrations of the solution. The SBF method is an efficient method to test the *in-vitro* bioactivity of bioglasses/glass-ceramics for the assessment of the apatite formation potential. However, the reliability of this method depends on the type of bioglasses/ glass-ceramics tested. For instance, silicate-based bioglasses and bioglass-ceramics, including silicate bioglass 45S5, diopside-based ($Ca_2MgSi_2O_6$) ceramics, etc., have been shown excellent apatite forming abilities in SBF [33, 34]. Other studies also showed that these silicate bioglasses/glass-ceramics possess good *in-vivo* bioactivity [18, 31]. As a result, it can be said that the *in-vivo* bioactivity of glasses can be deduced precisely from their nature in SBF. In spite of this, different important immersion conditions, such as surface to volume ratio, static or dynamic arrangements, and geometry of test samples, are also major factors to validate the *in-vitro* testing of bioactivity. On the other hand, the *in-vitro* method is also conducted using tissues or cell culture to determine the biocompatibility of the bioglasses/glass-ceramics.

1.4 Mechanism of bioactivity

When glass comes into contact with body fluid (SBF) in an *in-vitro* test, a series of physicochemical reactions occur at the glass-tissue interface [35]. During chemical reactions, a layer of carbonated hydroxy apatite (c-HAp) forms to which bone can bond. Bonding is based on three general processes: leaching, dissolution, and precipitations. Leaching is described as the release of ions, which occurs primarily through the exchange of alkali or alkaline earth metal ions with H^+ or H_3O^+ in the testing solution. Because they are not part of the glass network, glass modifier ions leach very easily from the surface of the glass when immersed in

the aqueous solution. The ion exchange process causes an increase in the concentration of hydroxide ions, resulting in an increase in the basicity of the solution to pH >7. The network dissolution occurs at the same time, as a result, breaking of the network forming silica bonds (-Si-O-Si-O-Si-O-Si-) by the attack of hydroxyl ions (OH^-). It displaces the silica into the solution as silicic acid ($Si(OH)_4$). Glass composition is important in this step because the rate of silica dissolution is highly dependent on glass composition. If the weight percentage of SiO_2 exceeds 60 %, the rate of silica dissolution rapidly decreases due to an increase in bridging oxygens (BOs), that formed a strong glass network [36]. Hydrated silica formed on the glass surface by polycondensation process with nearby silanols, resulting in the silica gel layer. Calcium and phosphate ions released from the glass combine with those from the solution to form a calcium-phosphate (Ca-P) layer on the glass surface during the precipitation process. The Ca-P layer formed may be structurally amorphous or crystalline in nature influenced by many factors. Actually, when carbonate ions incorporate from solution to layer, it slowly crystallizes to form c-HAp. The time taken to form the HAp layer varies from hours to many days and also depends upon many factors such as the composition of the immersed materials, rate of ion exchange, hydroxylation, and pH of the solution.

Hench and others described the 1-5 reaction steps for the formation of the c-HAp layer on the surface of glasses as shown in Figure 1.2 [6, 37].

Step 1. Rapid exchange of alkali or alkaline earth metal ions Na^+ or K^+ with H^+ or H_3O^+ from solution $Si\text{-}O\text{-}Na^+ + OH \rightarrow Si\text{-}OH^+ + Na^+$ (solution) + OH^-.

Step 2. -Si-O-Si-O-Si- bonds break through the action of hydroxyl ions and form Si-OH (silanols) $Si\text{-}O\text{-}Si + H_2O \rightarrow Si\text{-}OH + OH\text{-}Si$.

Step 3. Condensation of Si-OH groups near the glass surface: re-polymerization of the silica-rich layer.

Step 4. Migration of Ca^{2+} and PO_4^{3-} groups to the surface through the SiO_2-rich layer forming an amorphous Ca-P rich film on top of the SiO_2-rich layer.

Step 5. Incorporation of hydrolysis (OH^-), carbonate (CO_3^{2-}) or fluorine (F^-) from solution and crystallization of the Ca-P to c-HAP or fluorapatite layer.

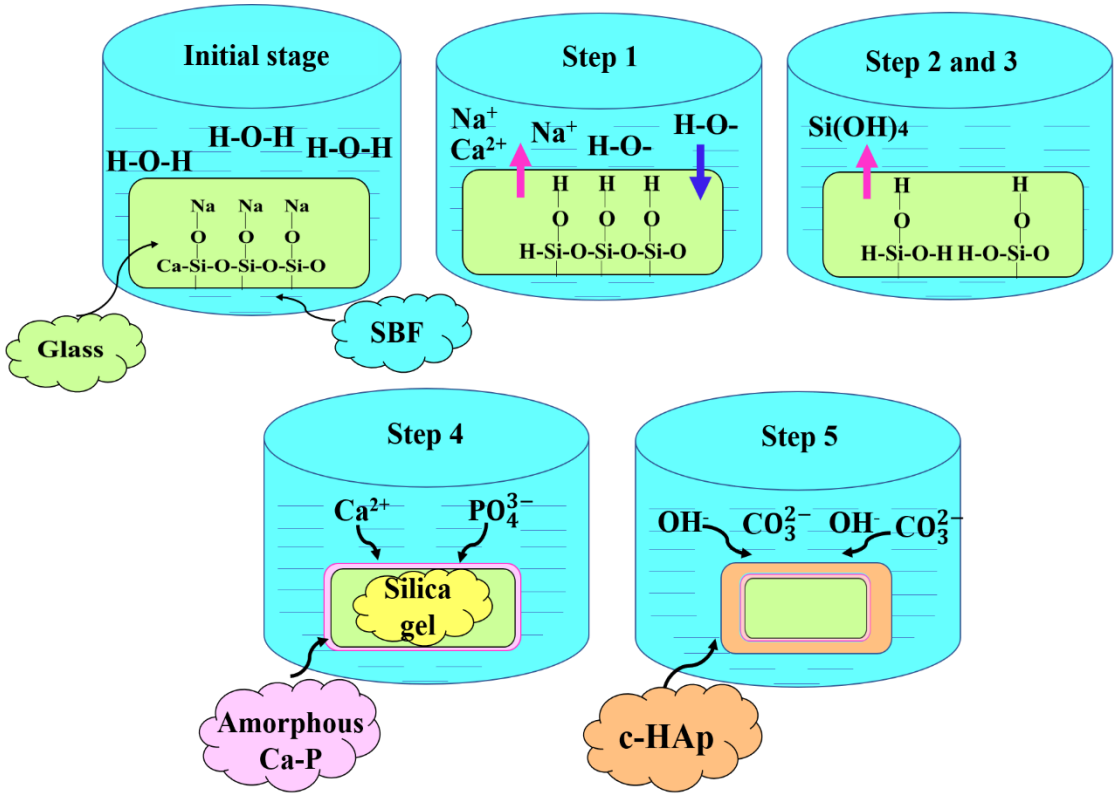

Figure 1.2 Mechanism of bioactive glass surface modification in response to SBF

The first 1-5 steps that take place on the glass side of the interface are independent of the presence of tissues. The tissue interaction occurs after the glass reactions. The c-HAp layer provides an optimal environment for the next 6-11 biological reaction stages, which include cell colonization, proliferation, and differentiation to form osteoblasts (new bone growth) with a good mechanical bond to the implant surface. The action of bioglass in the creation of new soft (peripheral nerves, heart, lungs, and ophthalmology) or hard tissues (bones) greatly depends on the structural properties and composition of the glass.

1.5 Testing of biocompatibility

The primary assessment of the experimental evolution of biocompatibility is the cytotoxicity test [23]. In the biomedical field, cytotoxicity tests determine whether the material is toxic or not in contact with particular cell lines. The most common type of biocompatibility test is the use of a cell culture system to detect cytotoxicity, cell proliferation, cell adhesion, or cell death. In cell culture studies, cultivated human and animal cells have been used to assess the biocompatibility of developing materials. Various cell lines or tissues also affect the performance of the cytotoxicity or cell viability assay [38]. Different types of cell culture tests are used to determine the biocompatibility: diffusion of agar, dilution extract, direct contact method, etc [39]. However, among these methods, the direct contact method is widely studied by various researchers to assess the biocompatibility of biomaterials [40, 41]. Because the selection of a particular assay is essential to obtain reliable and accurate results. The choice of cell types depends on the desired application of biomaterials. For instance, when a material is to be used as bone analogue material, then human osteoblast cell (HOB) lines are to be used. Osteoblasts are bone-forming cells with a single nucleus. An ordered group of osteoblasts formed HAp, which is accumulated into the organic matrix to form strong and dense bone matrix. Hence, it provides better compressive strength to the bone. Another parameter of cell culture testing is the time of culture. Generally, the tests are reported to be carried out for 24 hours, however, slowly growing cells, like HOB, need to be cultured for three to seven days. Here, fixed density of cells is incorporated onto the material surface and the numbers of cells are measured after some time. Cell spreading and proliferation assays are performed in these cases after seeding (using 96 well plate), to assess the effect of biomaterials. For instance, 3-(4,5-Dimethylthiazol-2-yl)-2,5 diphenyl tetrazolium bromide, (MTT) assay is a sensitive and

reliable colorimetric assay (an assay which measures changes in color) used to quantify cellular proliferation (cell growth), viability and cytoxicity of cells [38].

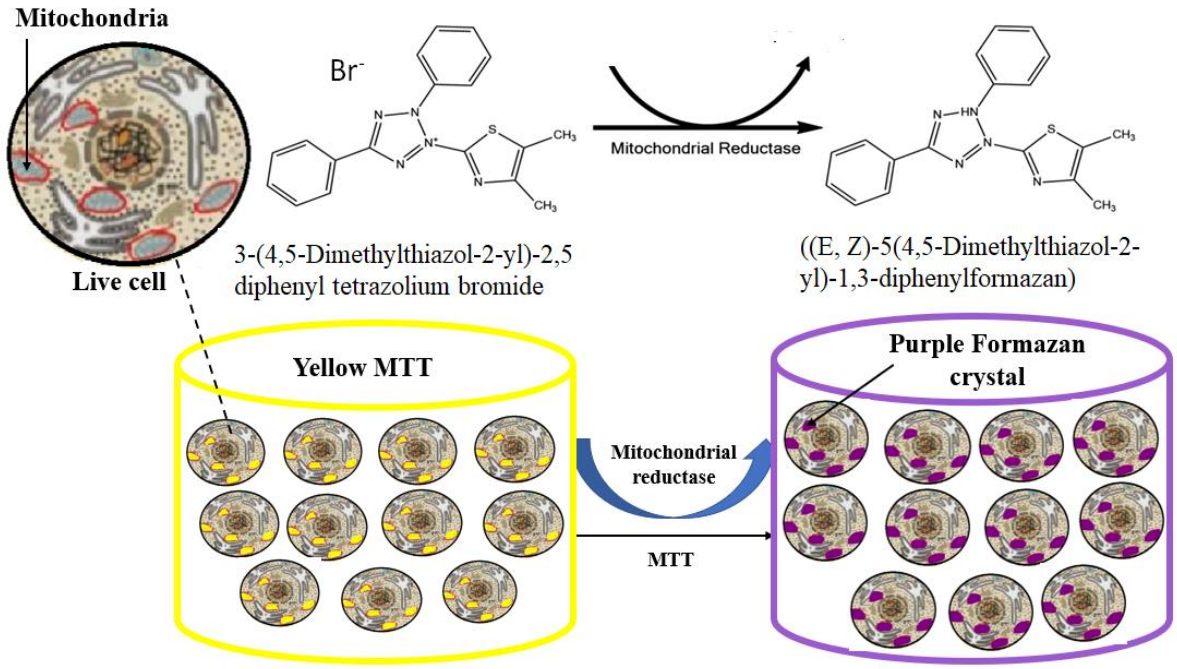

Figure 1.3 Principle of MTT assay used to assess viability via yellow MTT reduced to purple color

Yellow MTT has a large expanded chemical formula that is reduced to purple formazan in the mitochondria of living cells as given in Figure 1.3. This reduction takes place only when mitochondrial reductase enzymes are active, and therefore, conversion is directly related to the number of viable (living) cells. The cytotoxicity of the biomaterial is determined by the ratio of the number of viable cells to the total number of cells seeded. Hence, cytotoxicity of a material is a major concern for materials that are to be used as biomaterials. Eventually, the structural dependence of biomaterials on cell attachment, proliferation, and growth is evident via the release of ions and consequently with pH change [42].

1.6 Agro-food wastes as a resource

Agro-food wastes refer to the residues produced during the production and processing activities of agro sectors [43]. Some of the common agricultural wastes include rice husk (RH), rice straw, sugarcane leave (SCL), sugarcane bagasse (SCB), corn cob (CC), corn husk (CH), wheat straw (WS), peanut shells, etc. The agricultural wastes contain organic matters such as cellulose, proteins, lignin, etc., and other components such as carbon, phosphorous, potassium, calcium and magnesium, and silicon that are required for the growth of crops [44]. During the cultivation and manufacturing processes of these crops, the most considerable agriculture waste is discharged to nature [45]. Agro-food wastes are utilized in various fields such as textile, compost, organic fertilizers, animal feed, biofuel, and biogas in place of heat and energy production [43, 46-49]. Even above uses, enormous wastes are left untreated and unutilized. Untreated waste management is an expensive process. Therefore, it is disposed off either unplanned dumping or mostly burnt in the open fields, converted into ashes. Sugar mills and rice mills usually use agro wastes to generate heat and electricity. Disposal of agricultural waste ashes causes wastage of valuable nutrients of lands, and the surrounding area, contributing to air pollution, and water contamination due to their small particle size and lightweight. In general, agro waste ashes contain a good amount of silica (30-78 %) along with potassium oxide (K_2O), magnesium oxide (MgO), calcium oxide (CaO), and sodium oxide (Na_2O), and some other trace elements [50]. Similar to agro wastes, food wastes also consist of large amounts of organic materials such as carbohydrates, fats, proteins, etc. [51]. For instance, eggs are a very common and cost-effective diet for humans. The egg shells are often discarded in landfills without any pre-treatments. Decomposition of egg shells leads to the release of ammonia (NH_3) and hydrogen sulphide (H_2S) with an offensive odor, that causes environment-related problems. Eggshells exhibit an ample amount of calcium carbonate as approximately

94 %, along with trace elements are 1 % of calcium phosphate, 1 % of magnesium carbonate, and 4 % of other organic matters. Undoubtedly, an effective way to properly manage agricultural waste ashes and food waste not only eliminates the disposable problem but also solves the pollution-associated problem. It helps to protect the environment and the health quality. However, technological advances have transformed waste ashes into cost-effective valuable materials in a variety of fields [52, 53]. Some of the agricultural waste ashes exhibit an ample amount of SiO_2. Similarly, eggshell powder has $CaCO_3$. These two components are the major constituents of lime silicate glasses. Therefore, these sustainable and cost-effective could be used to synthesize glasses, glass-ceramics, and ceramic materials for various applications. Additionally, the use of the biogenic forms of silica, calcium oxides along with other trace elements as an alternative to conventional chemicals to produce glasses/glass-ceramics [50, 54, 55]. These glasses/glass-ceramics can be further used as biomaterials for biomedical applications [56].

As discussed above, bioglasses/glass-ceramics have different properties that can be tailored by varying the compositions and process parameters according to the requirement of the medical applications. Bioglasses, bioglass-ceramics, and ceramic could be synthesized using agro-food wastes since agro-food wastes exhibit SiO_2, CaO, MgO, K_2O, etc [57-60]. These oxides are essential parts of bioglass as reported by many researchers [15, 34, 50, 56]. Bioactive glass/glass-ceramics are being synthesized by using agro-food wastes with optimized properties and compositional constituents for better performances. In the following chapter, the literature survey related to agro-food waste ashes as resource materials to synthesize bioglasses and ceramics will be discussed.

References

[1] J.E. Shelby, Introduction to Glass science and Technology, 2nd ed. The Royal Society of Chemistry, 2005.

[2] G. Kaur, G. Pickrell, G. Kimsawatde, D. Homa, H. Allbee, N. Sriranganathan, Sci. Rep. 4 (2014) 1.

[3] W.D. Kingery, H.K. Bowen, D.R. Uhlmann, Introduction to ceramics, 2nd ed. John wiley & sons, 1976.

[4] V. Singh, S. Devi,V.S. Pandey, R.S. Bharj, S. Tyagi, Trans. Indian. Inst. Met. 71 (2018) 177.

[5] G. Kaur, O.P. Pandey, K. Singh, D. Homa, B. Scott, B. Pickrell, J. Biomed. Mater. Res. 102 (2014) 254.

[6] L.L. Hench, An introduction to bioceramics, 2nd ed. World Scientific, 2003.

[7] L.L. Hench, T. Kokubo, Handbook of biomaterial properties, 2nd ed. Springer Boston, 1998.

[8] A. Camaioni, I. Cacciotti, L. Campagnolo, A. Bianco, Hydroxyapatite (HAp) for Biomedical Applications, 1st ed. Elsevier 2015.

[9] S.K. Nandi, A. Mahato, B. Kundu, P. Mukherjee, Adv. Tech. Bone Regen. 13 (2016) 276.

[10] T. Kokubo, M. Shigematsu, Y. Nagashima, M. Tashiro, T. Nakamura, T. Yamamuro, S. Higashi, Bull. Inst. Chem. Res. Kyoto Univ. 60 (1982) 260.

[11] L.-C. Gerhardt, A.R. Boccaccini, Mater. 3 (2010) 3867.

[12] M. Montazerian, E. Dutra Zanotto, J. Biomed. Mater. Res. Part A. 104 (2016) 1231.

[13] P. Dey, S.K. Pal, I. Banerjee, S. Sarkar, J. Aust. Ceram. Soc. 56 (2020) 1309 .

[14] M. Tylkowski, D. Brauer, J. Non-Cryst. Solids. 376 (2013) 175.

[15] M. Priya, K.S. Thind, K. Singh, V. Kumar, D.P. Singh, J. Phys. Chem. Solids. 8 (2009) 1137.

[16] K.K. Dey, M. Ghosh, R. Prakash, K. Sharma, D. Singh, Appl. Phys. A. 127 (2021) 545.

[17] M. Vallet-Regi, A. Salinas, J. Roman, M. Gil, J. Mater. Chem. B. 9 (1999) 515.

[18] O.H. Andersson, K.H. Karlsson, K. Kangasniemi, J. Non-Cryst. Solids. 119 (1990) 290.

[19] K. Jurczyk, M. Kubicka, M. Ratajczak, M. Jurczyk, K. Niespodziana, D. Nowak, M. Gajecka, C. Jurczyk, Trans. Nonferrous Met. Soc. 26 (2016) 118.

[20] B. Karakuzu-Ikizler, P. Terzioglu, Y. Basaran-Elalmis, B.S. Tekerek, Bioact. Mater. 5 (2020) 66.

[21] S.S. Danewalia, K. Singh, Ceram. Int. 42 (2016) 11858.

[22] I. Atkinson, E. Anghel, L. Predoana, O. Mocioiu, L. Jecu, I. Raut, C. Munteanu, D. Culita, M.J. Zaharescu, Cerm. Int. 42(2016) 3033.

[23] P. Kaur, K. Singh, A.K. Yadav, H.Sood, Biomed. Phys. Eng. Express. 4 (2018) 035038.

[24] N.A. Gestel, J. Geurts, D.J. Hulsen, B. van Rietbergen, S. Hofmann, Biomed. Res. Int. 2015 (2015) 21.

[25] Z. Imran, I. Zonera, F. Umer, A. Leghari, A. Humera, World J. Dent. 3 (2012) 199.

[26] K.Singh, I. Bala, V. kumar, Ceram. Int. 35 (2009) 3401.

[27] J.R. Jones, D.S. Brauer, L. Hupa, D.C. Greenspan, Int. J. Appl. Glass Sci. 7 (2016) 423.

[28] I. Elgayar, R. Hill, X. Chen, N. Bubb, D. Wood, Int. J. Appl. Glass Sci. 8 (2017) 418.

[29] S. Kapoor, A. Goel, A. Tilocca, V. Dhuna, G. Bhatia, K. Dhuna, J.M. Ferreira, Acta Biomater. 10 (2014) 3264.

[30] E. Ferrero, I. Dunham, P. Sanseau, J. Transl. Med. 15 (2017) 1.

[31] T. Kokubo, H. Kushitani, S. Sakka, T. Kitsugi, T. Yamamuro, J. Biomed. Mater. Res. Part B 24 (1990) 721.

[32] T. Kokubo, H.J.B. Takadama, Biomater. 27 (2006) 2907.

[33] C. Ohtsuki, T. Kokubo, T. Yamamuro, J. Non-Cryst. Solids. 143 (1992) 84.

[34] F. Baino, J. Barberi, E. Fiume, G. Orlygsson, J. Massera, E. Verne, J. Healthcare. Eng. 2019 (2019) 5153136.

[35] J.R. Jones, D.S. Brauer, L. Hupa, D.C.S. Geenspan, Int. J. Appl. Glass. Sci. 7 (2016) 423.

[36] R.Agarwal, A.J.Garcia, Adv. Drug. Deliv. Rev. 94 (2015) 53.

[37] N. Ojha, Mater.Sci. (2016) 5894.

[38] O.S. Aslanturk, Intech open 2 (2018) 64.

[39] S. Kamiloglu, G. Sari, T. Ozdal, Front. Food Nutr. Res. 1 (2020) 332.

[40] P. Singh, M. Baranwal, S.M. Reddy, Pharm. Biol. 54 (2016) 2269.

[41] V.Gupta, S.Tyagi, A.K. Paul, J. Nanosci. Nanotechnol. 19 (2019) 646.

[42] E. Mancuso, O. Bretcanu, M. Marshall, K.W. Dalgarno, Ceram. Int. 43 (2017) 12651.

[43] K. Senthilkumar, M.N. Kumar, V.C. Devi, K. Saravanan, S. Easwaramoorthi, Waste. Biomass. Valorization. 1 (2020) 9.

[44] R. Millati, R.B. Cahyono, T. Ariyanto, I.N. Azzahrani, R.U. Putri, M. Taherzadeh, Sustainable Resource Recovery Zero Waste Approaches, 1st ed. Elsevier 2019.

[45] S. Karekezi, K. Lata, S.T. Coelho, Int. Conf. Renew. Energy Power Engg. 4 (2004) 4.

[46] S. Devi, C. Gupta, S.L. Jat, M. Parmar, Open Agric. 2 (2017) 486.

[47] A. Swami Nathen, S. Robert Ravi, Int. J. Eng. Res. Appl. 7 (2017) 76.

[48] M. Pointner, P. Kuttner, T. Obrlik, A. Jager, H. Kahr, Agron. Res. 12 (2014) 391.

[49] R.A. Patil, U.B. Deshannavar, Int. J. Eng. Res. 10 (2017) 232.

[50] G. Sharma, M. Kaur, S. Punj, K. Singh, Biofuel. Bioprod. Biorefin. 14 (2020) 673.

[51] T.A. Ahmed, L. Wu, M. Younes, M. Hincke, Front. Bioeng. Biotechnol. 9 (2021) 548.

[52] R.Mehra, S. Kaur, R. Parkash, Indoor. Built. Environ. 29 (2020) 286.

[53] F. Akhter, S.A. Soomro, A.R. Jamali, Z.A. Chandio, M. Siddique, M. Ahmed, Biomass Convers. Biorefin. 4 (2021) 1.

[54] S.S. Danewalia, G. Sharma, S. Thakur, K. Singh, Sci. Rep. 6 (2016) 1.

[55] B. Aktas, M. Albaskar, S. Yalcin, K. Dogru, Arch. Mater. Sci. Eng. 82 (2016) 57.

[56] H. Ismail, H. Mohamad, Mater. 14 (2021) 5193.

[57] S. Yucel, D. Ozçimen, P. Terzioglu, S. Acar, C. Yaman, Adv. Sci. Lett. 19 (2013) 3477.

[58] W. Leenakul, T. Tunkasiri, N. Tongsiri, K. Pengpat, J. Ruangsuriya, Mater. Sci. Eng. C 61 (2016) 695.

[59] W.-F. Ho, H.-C. Hsu, S.-K. Hsu, C.-W. Hung, S.-C. Wu, Ceram. Int. 39 (2013) 6467.

[60] A. Ratep, Silicon 12 (2020) 1425.

Chapter 2 Literature Review

2.1 Agro-food wastes derived modern materials

Abundant amounts of agro-food waste residue are generated that cause major health and environmental problems due to improper management. On the other side, agro-food wastes contain valuable minerals that could serve as resource materials for the formation of modern materials such as glass-ceramics and ceramics, electronic materials, etc [1, 2]. The minerals content in agro-food wastes depends on crops, regions, fertilizers used during crops growth, soil quality, etc. [3, 4]. As given in chapter 1 (section 1.6) the common agro-food wastes exhibit majorly carbon, silicon, magnesium, potassium, etc. Therefore, these agro-food wastes and their ashes could be used as valuable resource materials. Presently, various costly minerals are being used to synthesize various glasses using costly conventional chemicals. Recently, many researchers have used agro-food wastes as initial resources to synthesize different value-added materials [2, 5-7]. Since agro-food wastes and their ashes contain carbon, silicon, potassium, magnesium, etc [4]. The various mineral contents present in common agro-food waste ashes are given in Table 2.1 [4, 5, 8]. Basically, the agro-food waste ashes are the second generation of agro wastes. These wastes are dumped in the open air after using them to generate heat and electricity in various industries and open air burning in the field. As given in Table 2.1, the common agro-wastes ashes are composed of SiO_2, CaO, MgO, Na_2O, K_2O, and with minor trace content of TiO_2, Al_2O_3, and Fe_2O_3. Silica is majorly present in most of the common agro-food waste ashes. In some agro wastes ashes also contain a higher amount of K_2O, CaO in peanut shells, wheat straw, and P_2O_5 in corn husk ash as also given in Table 2.1. On the other hand, in food wastes such as egg shells having main component is calcium carbonate ($CaCO_3$) that is also more desirable for lime silicate glass formation [9].

Table 2.1 Various mineral contents present in common agro-food wastes/ashes

Oxide contents in wt%	**SiO_2**	**CaO**	**MgO**	**Na_2O**	**K_2O**	**P_2O_5**	**Al_2O_3**	**Fe_2O_3**	**TiO_2**	**SO_3**	**References**
Rice husk ash	87-97	0.2-0.6	0.2-1.6	-	0.1	-	1.7-2.9	-	-	0.1-1.5	[3, 4]
Sugarcane baggase Ash	55-75	2.2-8.0	1.7-4.0	0.6-	0.4-1.6	0.5-1.1	0.8-1.9	1.8-2.0	0.3-1.3	0.1-0.9	[4, 8, 10]
Cornhusk /Cob ash	35.7-79.3	5.8-11	1.5-9.9	0.9-5.1	3.8-20.2	11-22.5	0.4-1.5	0.2-4.4	-	0.6-1.07	[4, 5]
Peanut shells	17.6-29.3	9.8-21.9	6.7-9.7	0.1-4.9	18.3-25.7	7.4	3.7-5.9	1.3-3.4	0.2-0.6	3.2	[4, 11]
Wheat straw ash	30-73.9	5.21-11	1.8-5.0	-	11.5-30.5	-	0.91	1.51	1.92	-	[5, 7, 12]
Egg shells	0.1-0.2	94-99	0.3-0.8	0.1	0.1	-	-	-	-	-	[4, 5, 13]

Although, the variety of minerals present in agro-food wastes/ashes provide flexibility in the choice of glass compositions. On the other hand, the control of the amount of various minerals is very difficult. This problem could be addressed to use mineral extraction techniques by calcination at different temperatures or pre-acid treatments performed similarly to those used by industries [14]. Various researchers also used agro-food wastes to synthesize glasses and glass-ceramics that also depend on the burning conditions such as time, temperature as well as acid pre-treatments [15-18]. For instance, burning rice husk (RH) at controlled conditions < 700 ^{o}C yields amorphous ash. Whereas, > 800 ^{o}C resulted in crystalline ash. It has also been reported that > 700 ^{o}C also gives amorphous ash, but the time of sintering should be short [18]. For instance, some studies reported that up to 900 ^{o}C the silica can be obtained in amorphous form when the time of sintering is < 1 hour [19]. On the other hand, 15 h exposers of RH the crystallization takes place even at 300 ^{o}C [19]. Therefore, the duration of time and temperature must be carefully selected during the processing of agro wastes to ensure the ash of maximum reactivity. The amount of extracted silica from agro-waste ashes can also be increased by acid pre-treatments. Silica > 90 % can be extracted from rice husk ash (RHA) with few metallic impurities, by mineral acid leaching sintered at 600 ^{o}C under an inert atmosphere [20, 21]. Sugarcane bagasse ash (SCBA) is a major by-product of the sugarcane industry and contains 55-75 % of silica. The amount of silica can be increased by acid pre-treatments that allow increasing the silica up to 80 % with some trace elements [8, 10]. 95 % purity of silica can also be obtained from sugarcane waste by thermally treated 900 ^{o}C for 7 h. Similarly, corn cobs (CC), obtained from maize corn, contain 35 % of amorphous silica, by using the precipitation method obtained 50-60% of silica with trace elements [22]. Wheat husk ash (WSA) is obtained after burning wheat husk at 400 to 1000 ^{o}C for 5 h. Amorphous silica can be obtained at 700 ^{o}C for 5 h contains up to 93.9 % silica with minor trace elements [22]. WSA also contain major amount of SiO_2 (35 wt

%) and K_2O (30 wt %) with minor trace elements [12]. Pre-treatment of wheat straws by ethanol extraction or calcined ash was boiled in nitric acid solution helped to reduce the potassium contents [23-25]. After acid and calcination treatments, high purity silica (> 90 wt%) can be obtained which is a good resource to prepare mesoporous silica materials [25]. On the other hand, food waste such as eggshell powder (ESP) has the main component is calcium carbonate ($CaCO_3$). High-temperature treatment of crushed eggshells produces 99 % of calcium oxide along with trace elements [13]. It has been observed that the addition of ESP in glass compositions reduces the melting temperature of the glasses as well as modifies the different properties [3].

2.2 Agro-food wastes derived bioceramics/bioglasses

Apatite formation on the material in simulated body fluid (SBF) is a well-known method for predicting *in-vitro* bioactive properties. Bioceramics/bioglasses are found to be bioactive based on these mechanisms: Bioceramics/bioglasses form a bone-like apatite layer on its surface during soaking in SBF. It has been considered that when they interact with SBF there is an exchange of ions and formed abundant silica hydrogel in the form of silanol (Si-OH) groups. It provides favorable sites for apatite formation. When Si-OH groups bind with calcium-phosphate ions to form an amorphous apatite. Further, it combines with carbonates and crystallizes to form hydroxycarbonate apatite that aid in bonding with bones. The same composition containing glasses with different process parameters responds differently to bio-mimic body fluid. Various researchers used extracted silica from RHA as alternative resource material for commercial silica production and also used it to synthesize bioglasses/glass-ceramics [20, 26, 27]. The amorphous silica obtained from rice husk has been extracted as sodium silicate and used as a silica precursor for the sol-gel synthesis of bioceramics [28]. According to the literature, few reports are based on bioglass made from the melt quench technique using rice husk as a silica source [26, 29, 30]. For instance, bioactive glass with

composition $46SiO_2$-$24Na_2O$-$24CaO$-$6P_2O_5$ in wt % (46S6) was synthesized via melt quench method at 1400 ^oC in a platinum pot using biogenic silica extracted from RHA. The 46S6 glasses were soaked in SBF for 7 days at a concentration (surface area/volume ratio) of 20 mg/ml. The glass sample weight to volume ratio also effects the apatite layer formation. The increased surface area for the reaction leads to a faster apatite layer formation rate. The SEM results showed partial HAp formed after 7 days of soaking in SBF [31]. Yucel et al. [29] have synthesized strontium (Sr) substituted melt-derived bioglasses by extracting silica from RHA. When Sr is substituted for Ca in ($45SiO_2$-$24.5Na_2O$-$14CaO$-$6P_2O_5$-$10.5SrO$ in wt %) bioglass has not shown significant change in the glass structure. However, the thickness of the apatite layer on the glass surface increases with the increase of soaking time in SBF from 7 to 21 days. It has been reported that Ca act as a modifier in silicate glass system. As Sr and Ca have the same charge and comparable ionic radii. As a result, Sr may play here similar role as Ca, in the glasses. The Sr^{2+} has lower field strength than Ca^{2+}, resulting in a more loosely cross-linked glass network that increases the bioactivity [29]. These bioglasses have also shown continuous weight loss but with a slow rate of up to 7 days of soaking, due to the release of Ca^{2+}, Na^{2+}, Si^{4+}, and P^{5+} ions to tris-(hydroxymethyl)-aminomethane (Tris) buffer solution [32]. The degradation behavior of the glasses also gives information about bioactivity, pH lies in the range of 7.4-8.2 which was favorable to osteoblasts [33]. The substitution of Mg and Al up to 1wt % in 45S5 bioglasses using biogenic silica derived from RHA has shown no negative effect on bioactivity and biodegradability of glasses after soaking in tris buffer for 21 days. The hardness of these glasses is also enhanced with the combination of Mg and Al [34]. Mesoporous bioglass (MBG) has also been prepared from RHA via the sol-gel method for anticancer drug delivery and bone regeneration [35]. The results showed no cytotoxicity in normal cells and MBG-folic acid with calprotectin (a water-insoluble anticancer drug) that kills the cancer cells efficiently [36, 37].

The use of eggshells and its membrane as an alternative for synthetic CaO in the production of biomaterials has grown tremendously over the past few years. In an *in-vivo* investigation, nanocoating of copper-doped bioglasses (uniform thickness 40-50 nm) was prepared using an eggshell membrane (ESM) indicated a better angiogenesis rate and better antibacterial activity than conventional bioglasses [38]. However, very few reports use a combination of RHA and ESP as resource materials to make glasses via the melt-quench method and studied their bioactivity. The *in-vitro* bioactivity of ternary glasses (compositions $45SiO_2$-25CaO-$25Na_2O$, 25CaO-25MgO-$50SiO_2$, $50SiO_2$-25CaO-$25Na_2O$ in wt%) have also observed using natural (RHA;SiO_2), ESP (CaO)), and synthetic minerals (Na_2O, MgO) [39, 40]. The XRD results have shown the diffraction peaks (angle 2θ = 25.87, 31.78.49.46, and 53.14) after soaking in SBF, confirmed crystalline HAp formation on the surface of the glass. FTIR analysis also exhibited the occurrence of different functional groups which were related to the formation of HAp. The SEM and EDS results have obtained a globular shape of HAp particles with molar ratio of Ca/P=1.68 [30]. Literature has also demonstrated that the RHA extracted silicate-based glasses has feasibility of converting into highly useful glass-ceramics [26, 28].

In general, the vitrification of silicate or a mixture of various other materials is followed by a crystallization process to form glass-ceramics. Two steps are involved in the crystallization process to obtain glass-ceramics. The first stage is nucleation, followed by the second stage i.e., growth. The rate of nucleation is temperature-dependent, once stable nuclei are formed, the crystal growth begins. The different sintering temperatures were used to study the bioactive and mechanical properties of glass-ceramics. Generally, proper crystallinity can turn the glass into inert materials or decreases apatite forming kinetics on the glass surfaces [28]. However, semi-crystalline properties exhibited by the glass are expected to increase dissolution rate and bioactivity. On the other hand, density, mechanical properties, and

chemical durability are enhanced with the increase in the sintering temperature of glasses. The change in these properties increases the compressive strength due to the sintering phenomenon: particles rearranged, mass diffusion to pores, and grain growth takes place in the glasses. For instance, Nayak et al. [28] investigated the glasses (50 SiO_2-25Na_2O-25CaO mol%) sintered at 900-1050 ^oC for 2 h via the sol-gel method. Glasses sintered at 1000 ^oC formed crystalline phases (combeite ($Na_6Ca_3Si_6O_{18}$), and devrite ($Na_2Ca_3Si_6O_{16}$) have shown good mechanical strength. Whereas at 1050 ^oC strength was low due to the production of cracks in it, during sintering there is a mismatch of thermal expansion between ceramics and glassy matrix leading to cracks in the glass-ceramics. On the other hand, 45S5 bioglass was prepared via the melt-quench method and further sintered at different temperatures ranging from 650-1050 °C for 2 h. The XRD results showed that (sintering temperature was > 650 °C) amorphous phase changed into crystalline phases ($Na_2Ca_2Si_3O_9$, $Na_2Ca_4(PO_4)_2$ SiO_4, and $Ca_3Si_2O_7$) their intensity also increased. When sintering temperature was around 1050 °C resulting in maximum mechanical values, with a high density of 2.27 g/cm^3, 16.96 % porosity, and the Vickers micro hardness value of 364 HV. The samples also showed a bioactive nature [26]. Thus, the thermal behavior and temperature dependence properties of glasses also influence bioactivity. It has also been observed that the higher the sintering temperature resulting in more structural changes takes place and more crystalline phases formed rather than an amorphous phase that reduces the bioactivity. The permeability of the glass-ceramics is less in SBF solution and the less effective contact area between sample and solution for dissolution. Therefore, both bioactivity and degradability decreased with an increase in sintering temperature. The same research group [41] also reported that the biodegradability test in which the rate of silica network dissolution and apatite phase formation was also dependent on the impurity cation (CaO, K_2O, Fe_2O_3) contents which were inherited from the rice husk composition [42]. Silicate-based bioactive glass-ceramic (R-

SBgC) with the composition of $50SiO_2$-$25Na_2O$-25CaO (mol %) prepared from RHA were combined with polycaprolactone (PCL) to fabricate a composite scaffold using thermally induced phase separation (TIPS) method. The results revealed that an increase in R-SBgC in the PCL matrix produced a bioactive material. It has a higher density, and compressive modulus resulting in reduced scaffold porosity. These properties were useful in the development of the ideal scaffold intended for use as a bone substitute in non-load bearing sites [43]. The same research group has also synthesized a similar composition of bioactive glass-ceramics using a sol-gel method, that might be used for tissue engineering applications [44]. Despite bioglasses/glass-ceramics, attempts are also being made to synthesize calcium-phosphate-based ceramics such as tricalcium phosphate and HAp using natural resources and food wastes [45-47]. Silicate-calcium-based ceramics such as diopside, wollastonite, and larnite phases are synthesized using agro-food waste/ashes. These materials are being used in the health sector, particularly in orthopedics, dentistry, prosthesis, and composite applications. The literature survey related to natural sources directly or indirectly use for forming biomaterials are given in section 2.2.

2.2.1 Calcium-phosphate bioceramics

Commercially available calcium phosphate bioceramics such as tricalcium phosphate (TCP), biphasic calcium phosphate (BCP), and hydroxyapatite (HAp) are costly because high purity reagents are required for their production [48]. The HAp could also be obtained from natural materials like fish bone [49], bovine bone [50, 51], coral [52, 53], and oyster shells [54] using different processing methods. Moreover, these raw materials exhibit some inherent properties such as the pore structure, c-HAp, etc. On the other hand, some different issues arise due to the HAp materials which were prepared from bovine and human resources by treating them with dilute HCI acid. Sometimes, it is not enough to remove some of the troublesome particles from the body. For instance, prions, a small proteinaceous infectious particle, even

can survive after acid treatments. High-temperature calcination above 850 ^{o}C could solve this problem and minimize the transmission of associated diseases in various natural sources. Similarly, corals are not found worldwide, some coral species are in danger of extinction [55]. As a result, it is crucial to investigate raw materials that are sustainable, low cost, and easily accessible. Alternative to this, Avian egg shells (AES) were also utilized to replace the synthetic CaO that has a similar composition (composed of 94 % $CaCO_3$, 1 % CaP, 1 % $MgCO_3$, and 4 %, organic matter) as accompanied by coral. AES has been utilized as a potential bone substitute in facial reconstructive surgery after being treated with dilute sodium hypochlorite [56]. Similarly, chicken egg shells are also being used to form calcium salts such as β-tricalcium phosphate (β-TCP), biphasic calcium phosphate (BCP), CaO nanoparticles and HAp [30, 40, 57, 58]. These different types of calcium salts commonly used to incorporate in the inorganic components of native bone which enhanced the osteoconductivity of the produced materials. In recent years, several methods, adopted to synthesize HAp from chicken egg shells contain 95-98 % of $CaCO_3$ with minor amount of trace elements such as Mg, Sr, Si, Na, F. It was found from that the presence of foreign ions cause perturbed the lattice structure of HAp, shift in functional group of vibration frequencies and thermal stability of commercially synthesized HAp [48]. Microwave processing method was used to obtain nanocrystalline apatite with varying Ca/P ratios (1.5,1.60 and 1.67) using chicken egg shells. Differential thermal analysis (DTA) results revealed that nanocrystalline apatites were thermally stable up to 650 ^{o}C. The presence of minor amount of trace elements did not show any worse effect on bioactivity [46]. Ca-hydroxyapatite (HAp) nano powders were synthesized using egg shells that has been calcined at 900 ^{o}C for half an hour and other uncalcined egg shells. The XRD results exhibited that after calcination, single crystalline HAp phase formed, whereas uncalcined egg shell has both amorphous and crystalline phases. The SEM micrographs of HAp samples revealed that the calcined sample having combination

of spherical, hexagonal and cylindrical shapes with crystallite size 30-60 nm and Ca/P molar ratio 1.66 [48]. Uncalcined egg shell-based sample, did not show clear crystalline phase, and has Ca/P molar ratio of 1.50, resulting in Ca-deficient HAp [48]. Nanocrystalline hydroxyapatite (NHAp) is obtained from eggshell waste using microwave irradiation. It has platelet-like agglomerated morphology, stability at high temperatures, and osteoblast cell adhesion. It can be utilized for hard tissue replacement [59]. NHAp is also fabricated by using an ultrasonication-mediated method. The mechanical properties of NHAp have been influenced by calcination at 600 ^{o}C and exhibited almost close results as compared to prepare commercial HAp. *In-vitro* studies also revealed that the nanocrystalline HAp enhanced bioactivity as well as biocompatibility on human fetal osteoblastic-like cells [60]. Microwave-processed HAp has the advantages of shorter processing time, high reaction rates, narrow size distribution, and high purity. Therefore, it could be used for applications such as coatings for implant materials. With the increase of sintering temperature 1000 to 1150 °C for 20 minutes decrease in particle size of HAp leads to enhanced mechanical properties, such as compressive strength, hardness and, fracture toughness [61]. HAp powder was synthesized from egg shell by wet chemical method, using phosphoric acid (H_3PO_4). The results revealed that sintered (at 900 °C) HAp powder resembles the feature of pure and single apatite phase having favourable Ca/P molar ratio ranging from 1.7 to 2.4 [62]. Mechanochemical method had also increased the phase purity of HAp samples derived from egg shells. The higher heating temperature of HAp samples resulted in higher degree of crystallinity and larger particle size in the range 8-47 nm and 250-550 nm, respectively [57]. The solid-state reaction method has used to fabricate HAp/TCP using egg shells with reactant materials (calcium pyrophosphate ($Ca_2P_2O_7$) and dicalcium phosphate dihydrate (DCPD)). Combined ESP and DCPD sintered at 1150 ^{o}C for 3h showed only a single HAp phase. When ESP and $Ca_2P_2O_7$ sintered at 1100 ^{o}C for 3h showed almost pure β-TCP and minor phase of HAp. Further, with

increase of heat treatment duration from 3h to 5h at 1100 ^{o}C then β-TCP phase stats to decrease and HAp phase disappeared. HAp/TCP based bioceramics used for bone grafts and drug delivery and protein purification applications [55]. Pure and biocompatible HAp and β-TCP powders were fabricated using eggshell and phosphoric acid. The crystallization behavior of the fabricated HAp and β-TCP was affected by the mixing ratio of ESP and phosphoric acid i.e., 1:1.1, 1:1.3, 1:1.5. At 1:1.3 and 1.:1.5 wt %. β-TCP was effectively synthesized at 900 ^{o}C and >1000 ^{o}C, β-TCP starts to decrease and formed α-TCP [63]. Hydrothermally treated ESP generated HAp also show good biocompatibility on MC3T3-E1 cells, i.e., a mouse calvaria-derived osteoblast-like cell line [64].

2.2.2 Silicate-calcium based bioceramics

Silicate bioceramics are preferred over HAp and TCP because they have greater mechanical strength and the ability to form a Si-OH bond over their surface, inducing stable apatite formation [65]. Some reports have shown that the TCP has not much ability to induce HAp formation on its surface. Moreover, HAp implants can hardly resorb *in-vivo* and barely induce osteogenic differentiation [66]. Recent studies on the effect of silica incorporation in HAp matrix have revealed that it has excellent properties than pure HAp. Rapid bioactivity interactions in silica-based biomaterials have been found, while pure HAp took several days due to its low resorbability [67]. Silica substituted HAp also stimulates human osteoblast-like cells for osteoblastic differentiation [68]. Similarly, bio-silica and nano-silica particles also inhibit osteoclast differentiation [69]. In the biomedical field, silica is also an essential contributor to bone health, and improves bone density, due to its deficiency causes poor skelton development [70, 71]. The major importance of silicon is also considered to protect against aluminum toxicity for gastrointestinal and dialysis patients studied by Parry et al. [72]. This is due to alumina having a close chemical affinity with silicates. It formed hydroxy aluminosilicates, through silicic acid that protect against the cellular toxicity of aluminum.

Athinarayanan et al. [73] have also synthesized biogenic silica nanoparticles (bSNPs) through acid pre-treatment of sugarcane baggase. It was done in an autoclave, which removes metal ions and promote hydrolysis of organic substances. The XRD results has shown crystalline nature of bSNPs. TEM is confirmed irregular shape with porous morphology of bSNPs. bSNPs is also synthesized using corn cob. It has unique spherical shape with a narrow size distribution that is used for dental applications [74-76]. The particle size, morphology of bSNPs can be controlled using different chemical, thermal, biological methods [77-79]. These methods are non-toxic, cheap and environment friendly due to the usage of agro wastes as substrate for performing reactions to obtain valuable products [80-83]. Three types of amorphous silica, namely brown ash (BA), white ash (WA), and silica gel (SG) have been prepared from rice husk. Brown ash can be prepared by burning husk at 700 °C and it contains about 96 % silica. White ash contains 99.78 % silica, and can be prepared by combustion and followed by acid treatments. Silica gel can be prepared from BA through the alkaline extraction of silica and acid neutralization process. The bioactivity of these different ashes evaluated at different temperatures - i.e., 900 °C for BA, 1100 °C for SG and 1200 °C for WA after dipping into SBF and tris buffer solution [28]. BA and SG ceramics show more bioactivity than WA ceramics [41]. This is due to the formation of silanol groups on the surface of the silica particles in the presence of the hydrolysis process. In the case of SG, hydrolysis might be more straightforward due to the inherent gel formation of materials. White ash shows a low response for bioactivity due to the presence of fewer impurities when treated at high temperatures (1200 °C) [41]. ESP was also utilized to synthesize akermanite ($Ca_2MgSi_2O_7$), diopside ($CaMgSi_2O_6$), and nanocrystalline larnite (Ca_2SiO_4) phases via sol-gel and mechanical milling method [84]. The results indicated the HAp formed on ($Ca_2MgSi_2O_7$) after 7 days of soaking in SBF, which helps in promoting cell proliferation, osteogenesis, angiogenesis and suppress osteoporotic bone regeneration when studied for an

in-vitro test. The bonding strength of $CaMgSi_2O_6$ bioceramics was about 350±7 MPa with excellent fracture toughness of 4±0.3MPa [85-88]. Wollastonite ($CaSiO_3$), diopside ($CaMgSi_2O_6$), forsterite, and pseudo-wollastonite ceramics were made by sintering the RHA and ESP at 870-1300 ^oC for 4 h. Researchers have shown that wollastonite glass-ceramics has more ability to form HAp than pseudo wollastonite due to more degradability of wollastonite glass-ceramics in SBF [27, 89, 90]. XRD results revealed that when wollastonite doped with silver (upto 6 mol%) the intensity of diffraction peaks increased with increased exposure time in SBF solution from 7 to 21 days [91]. There are very few reports on ceramics using SCBA. Ceramic SiO_2-CaO-Na_2O formed by using silica source from SCBA > 970 ^oC. The major phase is wollastonite is formed at > 970 ^oC and below this rankinite, phase is formed [17]. SCBA is also used as a raw material to prepare ceramics (wollastonite) as a replacement for silica which is used as coating materials. The SEM results showed a microporous network of elongated crystals with some areas with dendritic, feather-like ordering, which crystallized at 1050 ^oC. Vickers microhardness value was 564.4 HV [92, 93].

2.3 Agro-food waste/ashes derived materials and biocompatibility

Biocompatibility is very important other than bioactivity for an implant. Researchers have been using different cell lines in cell culture to study the biocompatibility of the bioceramics derived from agro-food waste/ashes. The cytotoxicity of rice husk derived 46S6 bioactive glasses was determined with a concentration of 20 mg/ml on sarcoma osteogenic (SAOS-2) osteoblast-like cells cultured in DMEM-F12 media by MTT assay. 46S6 glass has shown no toxic effect during the test [31]. The substitution of strontium in 45S5 bioactive glasses (using RHA) to study their cytotoxicity by MTT assay. As strontium has been considered a promising incorporation agent to enhance the replications of preosteoblast cells and reduce the osteoclast activity. The results have shown good metabolic activity and cell viability, due to the controlled degradation rate of strontium and silica ions in DMEM cell culture media

determined by ICP-OES [32]. It has also been found that pH change also directly affects the growth of cells, metabolic activity, and membrane potential due to their acidic and basic properties. The fast increment in pH because of H^+ cation occurs due to more ion dissolution of the glass [32]. Human osteosarcoma MG-63 cell lines were also used to test the cytocompatibility of RHA and ESP based bioglasses (SiO_2-CaO-Na_2O) with different concentrations (1000-50 µg/mL) and compared to blank control via MTT assay. The cell viability has been observed at >70 % even at a higher concentration i.e., 1000 µg/mL. These bioglasses have demonstrated no toxicity effect that can be used in biomedical applications [30]. The osteoblast-like MG-63 cells have also shown no cytotoxicity on diopside ceramics [88]. The biocompatibility of bSNPs derived from RHA and SCBA was also assessed using MTT assay on human lung fibroblast cells (hLFCs) at different concentrations of bSNPs (0, 25, 50, 100, 200, and 400 µg/mL). The cell viability >85% has been found for bSNPs even at a higher concentration of 400 µg/mL, indicating bSNPs are biocompatible. These can be used in 3D scaffolds of lung cells and tissue engineering applications [73, 94]. The copper doped wollastonite particle's toxicity was also determined via MTT assay using murine mesenchymal stem cells (mMSC) at different concentrations (0.01, 0.03, 0.05, 0.1, and 0.5 mg/ml) for 24 and 48 h time intervals. This materials were found non-toxic only up to concentration of 0.05 mg/mL [95]. The hemocompatibility of silicate ceramics was also evaluated at different concentrations (62.5, 125, and 250 µg/mL) using red blood cells. The hemolysis assay reveals that wollastonite, diopside, and forsterite phases were hemcompatible even after 72 h of incubation [89].

3. Motivation of the study

From the above literature survey, it is clear that limited work on waste derived glasses/glass-ceramics especially bioactive properties has been carried out so far. Only RHA has been used as a silica source individually to synthesize bioceramics, glasses, and glass-ceramics. Most

researchers used either RHA or egg shells to synthesize HAp and bioceramics with conventional chemicals like P_2O_5, Na_2O, etc. Very few reports used a combination of RHA and ESP along with some conventional mineral oxides to develop bioceramic materials. Moreover, sugarcane leaves ashes, corn husk, and wheat straw waste ashes are not used to synthesize bioactive and biocompatible glass and glass-ceramics. Based on the above observations and literature survey, the following objectives are proposed for the present research.

4. Objectives

1. Glasses/glass-ceramics will be synthesized using agro-food waste materials such as corn husk ash (CHA), sugarcane leave ash (SCLA), and eggshell powder (ESP).
2. Physical, structural, and mechanical properties of as-prepared glasses will be studied using XRD, SEM with EDS, TGA/DTA, FTIR, and micro hardness tester.
3. Bioactive properties of these glasses/glass-ceramics will be checked *in-vitro* with simulated body fluid (SBF) along with MP-AES or ICP analysis of SBF after dipping samples.

To achieve the above-mentioned objectives, various experimental and testing techniques have been employed. The details of sample preparations and various characterization and testing techniques have been given in the next chapter.

References

[1] R. Rawlings, J. Wu, A. Boccaccini, J. Mater. Sci. Mater. Electron. 41 (2006) 733.

[2] S.S. Danewalia, G. Sharma, S. Thakur, K. Singh, Sci. Rep. 6 (2016) 1.

[3] S. Chandrasekhar, K. Satyanarayana, P. Pramada, P. Raghavan, T. Gupta, J. Mater. Sci. Mater. Electron. 38 (2003) 3159.

[4] I. Cornejo, S. Ramalingam, J. Fish, I. Am. Ceram. Soc. Bull. 93 (2014) 24.

[5] G. Sharma, M. Kaur, S. Punj, K. Singh, Biofuel. Bioprod. Bioref. 14 (2020) 673.

[6] A. Muthadhi, R. Anitha, S. Kothandaraman, Civ. Eng. Environ. Syst. 88 (2007) 50.

[7] H. Biricik, F. Akoz, I. Lhan Berktay, A.N. Tulgar, Cem. Concr. Res. 29 (1999) 637.

[8] K.L. Singh, S.A. Jawaid, Abstr. Appl. Anal. 1 (2013) 42.

[9] B. Aktas, M. Albaskara, S. Yalcin, K. Dogru, Acta Phys. Pol. A 132 (2017) 442.

[10] K. Ganesan, K. Rajagopal, K. Thangavel, Cem. Concr. Compos. 29 (2007) 515.

[11] B. Aktas, M. Albaskar, S. Yalcin, K. Dogru, Arch. Mater. Sci. Eng. 82 (2016) 57.

[12] J. Dodson, Diss. University of York, 2011.

[13] K. Prabakaran, A. Balamurugan, S. Rajeswari, Bull. Mater. Sci. 28 (2005) 115.

[14] K. Matori, M. Haslinawati, Z. Wahab, H. Sidek, T. Ban, W. Ghani, Int. J. Basic Appl. Sci.1(2009) 512.

[15] A. Ratep, Silicon 12 (2020) 1425.

[16] A.J.A. Al-Nidawi, K.A. Matori, A. Zakaria, M.H.M. Zaid, Results Phys. 7 (2017) 955.

[17] S.R. Teixeira, M. Romero, J. M. Rincon, J. Am. Ceram. Soc. 93 (2010) 450.

[18] P.K. Mehta, U.S. Patent No. 4,105, 459 1978.

[19] M. Nehdi, J. Duquette, A. El Damatty, Cem. Conc. Res. 33 (2003) 1203.

[20] N. Yalcin, V. Sevinc, Ceram. Int. 27 (2001) 219.

[21] C. Real, M.D. Alcala, J.M. Criado, J. Am. Ceram. Soc. 79 (1996) 2012.

[22] M. Pointner, P. Kuttner, T. Obrlik, A. Jager, H. Kahr, Agron. Res. 12 (2014) 391.

[23] H.J. Naqvi, A. Saeed, A. Umair, F.H. Shah, J. Pak. Inst. of Chem. Eng. 39 (2011) 51.

[24] P. Terzioglu, S. Yucel, T.M. Rabagah, D. Ozcimen, Biol. Res. 8 (2013) 4406.

[25] Y. Ma, H. Chen, Y. Shi, S. Yuan, Mater. Res. Bull. 77 (2016) 258.

[26] W. Leenakul, T. Tunkasiri, N. Tongsiri, K. Pengpat, J. Ruangsuriya, Mater. Sci. Eng. C. 61 (2016) 695.

[27] H. Ismail, H. Mohamad, Mater. 14 (2021) 5193.

[28] J.P. Nayak, Diss. 2010.

[29] S. Yucel, D. Ozcimen, P. Terzioglu, S. Acar, C. Yaman, Adv. Sci. Lett. 19 (2013) 3477.

[30] S. Palakurthy, K.V. Reddy, S. Patel, P.A. Azeem, Prog. Biomater. 9 (2020) 239.

[31] S. Yucel, Z. Aydın Sinirlioglu, B. Karakuzu, T.M. Temel, Y. Elalmış, A.C. Ozarslan, In Advance Materials Research, Trans-Tech Publications Ltd. (2015).

[32] S.Yucel, P. Terzioglu, Z.A. Sinirlioglu, B.S. Tekerek, Y.B. Elalmis, Sigma J. Eng. Natural Sci. 33 (2015) 23.

[33] A.C. Ozarslan, S. Yucel, Mater. Sci. Eng. C. 68 (2016) 350.

[34] B. Karakuzu-Ikizler, P. Terzioglu, Y. Basaran-Elalmis, B.S. Tekerek, S. Yucel, Bioactive Mater. 5 (2020) 66.

[35] S.-Y. Chen, P.-F. Chou, W.-K. Chan, H. Lin, Ceram. Int. 43 (2017) 2239.

[36] K.G. Patel, N. M.Mishra, R. Rakshit Shettigar, Int. J. Chem. Eng.Appl. 7(2016) 344.

[37] R. Shamsudin, F.A. Abdul Azam, A. Hamid, M. Azmi, H. Ismail, Mater. Sci. 10 (2017) 1188.

[38] J. Li, D. Zhai, F. Lv, Q. Yu, H. Ma, J. Yin, Z. Yi, M. Liu, J. Chang, C. Wu, Acta Biomater. 36 (2016) 254.

[39] P. Srinath, P.A. Azeem, K.V. Reddy, S.R. Kumar, S AIP Conf. Proceed. AIP Publishing LLC, 2115 (2019) 030233.

[40] E.R. Essien, V.N. Atasie, E.U. Udobang, Bull. Mater. Sci. 39 (2016) 989.

[41] J. Nayak, J. Bera, Silicon 4 (2012) 57.

[42] F. Andreola, M. Martín, A.M. Ferrari, I. Lancellotti, F. Bondioli, J.M. Rincon, M. Romero, L. Barbieri, Ceram. Int. 39 (2013) 5427.

[43] F. Naghizadeh, N. Sultana, M.R.A. Kadir, T.M. Tengku Md Shihabudin, R. Hussain, T. Kamarul, J. Nanomater. 2014 (2014) 1.

[44] F. Naghizadeh, M.R.A. Kadir, A. Doostmohammadi, F. Roozbahani, N. Iqbal, M.M. Taheri, S.V. Naveen, T. Kamarul, J. Non-Cryst. Solids. 427 (2015) 54.

[45] S. Vichaphund, M. Kitiwan, D. Atong, P. Thavorniti, J. Europ. Ceram. Soc. 31 (2011) 2435.

[46] A. Siddharthan, T.S. Kumar, S. Seshadri, Biomed. Mater. 4 (2009) 045010.

[47] A. Arboleda, M. Franco, J. Caicedo, L. Tirado, C. Goyes, Ing. Compet. 18 (2016) 71.

[48] S. Ahmed, M. Ahsan, Bangladesh J. Sci. Indust. Res. 43 (2008) 501.

[49] M. Ozawa, S. Suzuki, J. Am. Ceram. Soc. 85 (2002) 1315.

[50] S. Salman, O. Gunduz, S. Yilmaz, M. Ovecoglu, R.L. Snyder, S. Agathopoulos, F. Oktar, Ceram. Int. 35 (2009) 2965.

[51] F.N. Oktar, S. Agathopoulos, L.S. Ozyegin, O. Gunduz, N. Demirkol, Y. Bozkurt, S. Salman, J. Mater. Sci. Mater. Med. 18 (2007) 2137.

[52] J. Hu, J. Russell, B. Ben-Nissan, R. Vago, Australia. 11 (1999) 59.

[53] M. Sivakumar, T.S. Kumar, K. Shantha, K.P. Rao, Biomater. 17 (1996) 1709.

[54] S.-C. Wu, H.-C. Hsu, Y.-N. Wu, W.-F. Ho, Mater. Charact. 62 (2011) 1180.

[55] W.-F. Ho, H.-C. Hsu, S.-K. Hsu, C.-W. Hung, S.-C. Wu, Ceram. Int. 39 (2013) 6467.

[56] L. Dupoirieux, D. Pourquier, F. Souyris, J. Craniomaxillofac. Surg. 23 (1995) 187.

[57] A. Hamidi, M. Salimi, A. Yusoff, AIP Conf. Proceed, AIP Publishing LLC, 1835 (2017) 020045.

[58] K. Ronan, M.B. Kannan, ACS Sustain. Chem. Eng. 5 (2017) 2237.

[59] D.S.R. Krishna, A. Siddharthan, S. Seshadri, T.S. Kumar, J. Mater. Sci. Mater. Med. 18 (2007) 1735.

[60] V.H. Ingole, K. Hany Hussein, A.A. Kashale, K. Ghule, T. Vuherer, V. Kokol, J.Y. Chang, Y.C. Ling, A. Vinchurkar, H.N. Dhakal, J. Biomed. Mater. Res. Part A. 105 (2017) 2935.

[61] S. Bose, S. Dasgupta, S. Tarafder, A. Bandyopadhyay, Acta Biomater. 6 (2010) 3782.

[62] H. Khandelwal, S. Prakash, J. Miner. Mater. Charac. Eng. 4 (2016) 119.

[63] S.J. Lee, S. Oh, In Key Engineering Materials, Trans-Tech Publication Ltd. 240 (2003) 35.

[64] J.W. Park, S.R. Bae, J.Y. Suh, D.H. Lee, S.H. Kim, H. Kim, C.S. Lee, J. Biomed. Mater. Res. Part A. 87 (2008) 203.

[65] A. Udduttula, S. Koppala, S. Swamiappan, Transac. Indian Ceram. Soc. 72 (2013) 257.

[66] M. Bohner, Biomater. 30 (2009) 6403.

[67] M. Vallet-Regí, D. Arcos, J. Mater. Chem. B. 15 (2005) 1509.

[68] D. Reffitt, N. Ogston, R. Jugdaohsingh, H. Cheung, B.A.J. Evans, R. Thompson, J. Powell, G. Hampson, Bone 32 (2003) 127.

[69] M. Wiens, X. Wang, H.C. Schroder, U. Kolb, U. Schlobmacher, H. Ushijima, W.E. Muller, Biomater. 31 (2010) 7716.

[70] R.J. Singh, J. Nutr. Health. Aging. 11 (2007) 99.

[71] J. Eisinger, D. Clairet, Mag. Res. 6 (1993) 247.

[72] R. Parry, D. Plowman, H.T. Delves, N.B. Roberts, J.D. Birchall, J.P. Bellia, A. Davenport, R. Ahmad, I. Fahal, P. Altmann, Nephrol. Dial. Transplant 13 (1998) 1759.

[73] J. Athinarayanan, V.S. Periasamy, M. Alhazmi, A.A. Alshatwi, J. Biomed. Mater. Res.Part B. 105 (2017) 340.

[74] J. Shim, P. Velmurugan, B.-T. Oh, J. Indus. Eng. Chem. 30 (2015) 249.

[75] A.M. Carvalho, R.A. Cordeiro, H. Faneca, Pharmaceutics. 12 (2020) 649.

[76] Y. Zhou, G. Quan, Q. Wu, X. Zhang, B. Niu, B. Wu, Y. Huang, X. Pan, C. Wu, Acta Pharm. Sin. B. 8 (2018) 165.

[77] E.A. Okoronkwo, P.E. Imoisili, S.A. Olubayode, S.O. Olusunle, Adv. Nanopart. 5 (2016) 135.

[78] N. Permatasari, T.N. Sucahya, Nandiyanto, Indonesian J. Sci. Technol. 1 (2016) 82.

[79] C. Kongmanklang, K. Rangsriwatananon, J. Spectrosc. 2015 (2015) 1.

[80] A. Zielonka, E. Zymanczyk-Duda, M. Brzezinska-Rodak, M. Duda, J. Grzesiak, M. Klimek-Ochab, Fungal Biol. 122 (2018) 333.

[81] U. Vijayalakshmi, V. Vaibhav, M. Chellappa, U. Anjaneyulu, J Indian Chem. Soc. 92 (2015) 675.

[82] A. Pieła, E. Zymanczyk-Duda, M. Brzezinska-Rodak, M. Duda, J. Grzesiak, A. Saeid, M. Bioorg. Chem. 99 (2020) 103773.

[83] N.K. Mohd, N.N.A.N. Wee, A.A. Azmi, AIP Conf. Proceed., AIP Publishing LLC, 1885 (2017) 020123.

[84] R. Choudhary, S. Koppala, S. Swamiappan, J. Asian Ceram. Soc. 3 (2015) 173.

[85] L. Xia, Z. Yin, L. Mao, X. Wang, J. Liu, X. Jiang, Z. Zhang, K. Lin, J. Chang, B. Fang, Sci. Rep. 6 (2016) 22005.

[86] A. Kazemi, M. Abdellahi, A. Khajeh-Sharafabadi, A. Khandan, N. Ozada, E. C, J. Mater. Sci. 71 (2017) 604.

[87] R. Choudhary, S. Koppala, A. Srivastava, S. Sasikumar, J. Sol-Gel Sci. Technol. 74 (2015) 631.

[88] P. Srinath, P.A. Azeem, K.V. Reddy, P. Chiranjeevi, M. Bramanandam, R. P. Rao, Adv. Powder Technol. 32 (2021) 875.

[89] R. Choudhary, S.K. Venkatraman, I. Bulygina, F. Senatov, S. Kaloshkin, N. Anisimova, M. Kiselevskiy, M. Knyazeva, D. Kukui, F. Walther, Mater. Sci. Eng. C 118 (2021) 111456.

[90] S.S. Hossain, S. Yadav, S. Majumdar, S. Krishnamurthy, R. Pyare, P. Roy, Ceram. Int. 46 (2020) 833.

[91] S. Palakurthy, Ceram. Int. 45 (2019) 25044.

[92] S.R. Teixeira, A.E. Souza, C.L. Carvalho, V.C. Reynoso, M. Romero, J. M. Rincon, Mater. Charac. 98 (2014) 209.

[93] I. Kashif, A. Ratep, Silicon 10 (2018) 2677.

[94] A.A. Alshatwi, J. Athinarayanan, V.S. Periasamy, Mater. Sci. Eng. C. 47 (2015) 8.

[95] S. Azeena, N. Subhapradha, N. Selvamurugan, S. Narayan, N. Srinivasan, R. Murugesan, T. Chung, A. Moorthi, Mater. Sci. Eng. C. 71 (2017) 1156.

Chapter 3 Materials and Methods

All the glasses/ glass-ceramics are synthesized by the melt-quench technique using different agro-food waste sources and crucibles. The as-quenched samples were characterized and testing by various techniques. The details are given below.

3.1 Preparation of glasses

Glasses were prepared using different weight percent of corn husk ash (CHA), sugarcane leave ash (SCLA), wheat straw ash (WSA), and eggshell powder (ESP). The SCLA, CHA, and WSA were obtained from a local sugar mill, corn, and wheat agricultural farms, respectively. On the other hand, the eggshells were taken from the hostel of the Thapar Institute of Engineering and Technology, Patiala Punjab, India. The presence of different elements and their amounts in raw materials such as CHA, SCLA, WSA, and ESP were given in Table 3.1. The composition of glasses was selected as [(60) CHA - (40-x) SCLA - (x)ESP] where, x =10, 20, and 30 (wt %). The samples were labeled as CSE-1, CSE-2, and CSE-3.

Table 3.1 The percentage of elements present in various agro-food waste deduced from energy dispersive spectroscopy (EDS)

Elements	CHA (wt %)	SCLA (wt %)	WSA (wt %)	ESP (wt %)
Si	3.72	36.24	15.39	0.07
Na	6.64	0.30	1.17	–
Ca	3.97	2.99	2.34	70.21
P	2.06	–	-	0.02
Mg	6.61	3.87	1.07	0.63
K	37.09	8.19	29.27	–
Al	2.94	–	1.81	0.03
Ti	–	0.41	0.23	–
Fe	4.26	0.62	1.23	–
O	32.71	47.38	47.49	29.04

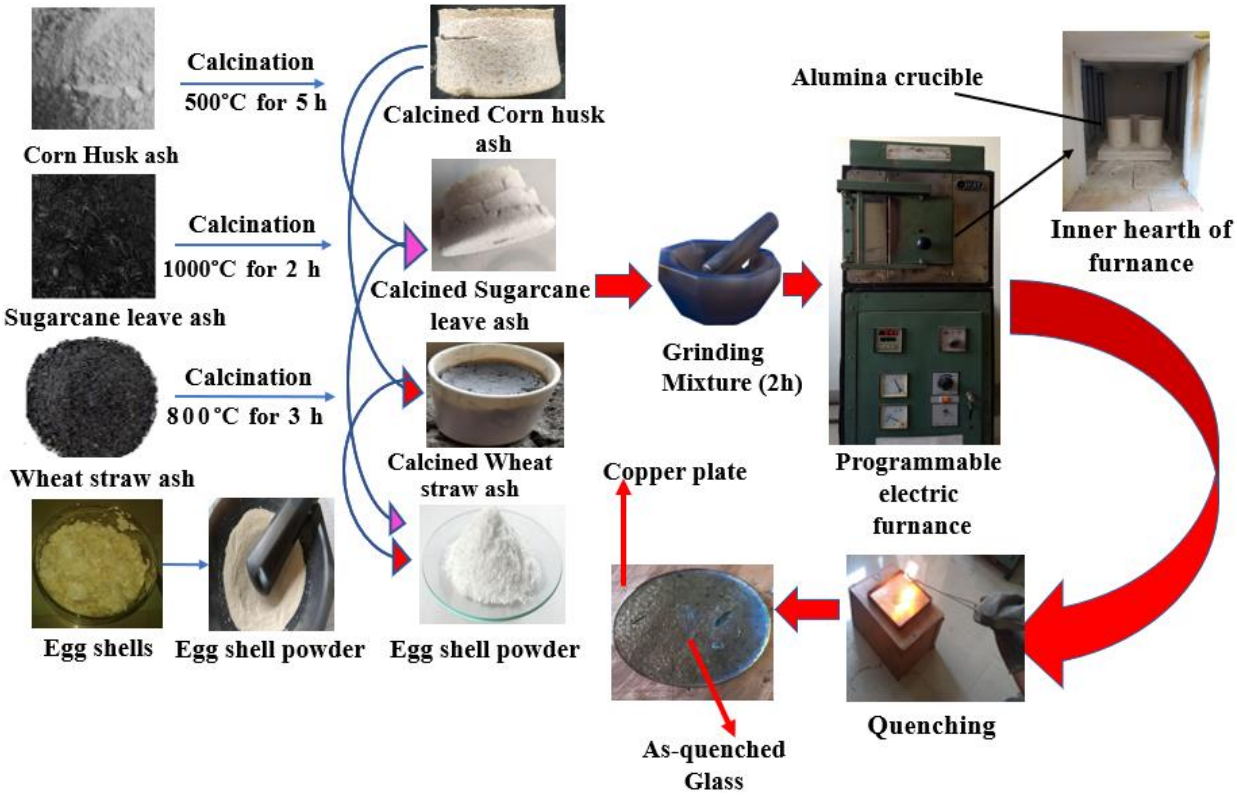

Figure 3.1 Synthesis procedure of glasses using agro-food wastes ashes in an alumina crucible

Second series of glass composition was selected as [(60)CHA - (40-x)WSA - (x)ESP] 10, 20, and 30 (wt %). The second series labelled as CWE-1, CWE-2, CWE-3. Here, SCLA was replaced by WSA. All glass series were prepared by the melt-quench technique. As shown in Figure 3.1, the ashes of different materials such as CHA, SCLA, and WSA were calcined at 500 °C for 5 hours (h), 1000 °C for 2 h, and 800 °C for 3 h, respectively. Eggshells were taken, washed with distilled water to remove impurities from them, and kept in a 1 M HCl solution for 2 h followed by distilled water washing. Then, egg shells were kept in the oven at 70 °C for 6 h to remove water from the eggshell. Finally, egg shells were ground in an agate mortar to convert into powder. The calcined powders of different ashes and eggshell powder were taken according to stoichiometric formulae and mixed in an agate mortar pestle for 2 h. After grinding, the mixture was put into recrystallized alumina crucible (100 ml) and melted at 1550 °C at a heating rate 5 °C min^{-1} in a programmable electric furnace (model:

Okey with $MOSi_2$ heating element). At intermediate temperatures i.e., 300, 600, 900, and 1200 °C, the furnace was held for 30 minutes each for enhancing the fusibility among agro-food waste ashes. At 1550 °C, the samples were kept for 1 h to get homogeneous melt. The melt was quenched in the air using thick (6.84 mm) copper plates. The as-quenched samples were crushed into powder for further investigation. Energy dispersive analysis (EDS) was performed on the quenched samples as discussed in chapter 4. It showed that some alumina content was also present in the sample. It might be picked up when it was melted in an alumina crucible. So, two samples with compositions [60CHA - 30SCLA - 10ESP] and [60 CHA -10SCLA - 30ESP] in wt % were selected to prepare in platinum-rhodium (Pt-Rh) crucible via melt quench method. To remove the volatile substances, the SCLA, CHA and ESP were combined in stoichiometric amounts and calcined at 1100 ^{o}C for 3h before melting in a Pt-Rh crucible. The calcined powder was ground in an agate mortar pestle for 2 h. After grinding, the mixture was put into a Pt-Rh crucible and melted at 1550 °C at a heating rate of 5 °C min^{-1} in a programmable electric furnace. Further steps were performed in the same way as did for the similar compositions melted in an alumina crucible. The prepared samples are labeled as PCSE-1 and PCSE-3. Another series of samples were also prepared in Pt-Rh crucible using WSA in place of SCLA in the same way as done for the above series and designated as PCWE-1 and PCWE-3.

3.1.1 Synthesis of glasses by conventional chemicals

Based on bioactive results, synthesized one glass from each series using the conventional chemicals for comparison. Glasses with composition $47.9SiO_2$-$23.5CaO$-$4.6P_2O_5$-$6.4MgO$-$7K_2O$-$8Al_2O_3$-$0.8Na_2O$-$0.2TiO_2$-$1.4Fe_2O_3$ and $43.6SiO_2$-$21CaO$-$1.5P_2O_5$-$5.5MgO$-$15K_2O$-$12Al_2O_3$-$0.7Na_2O$ $0.3TiO_2$-$0.4Fe_2O_3$ in wt % were prepared in Pt-Rh crucibles using melt-quench technique. These glasses were designated as MCSE-3 and MCWE-2. The starting chemical purity was ≥ 99 % (LobaChemie). These chemicals were used without further

purification. All the initial chemicals were taken as oxides except Na_2CO_3 and K_2CO_3.

Table 3.2 Sample labels with compositions and samples synthesized using different crucibles along with calcined and melting temperature in hours (h)

Composition (wt %)	**Sample label**	**Calcination Temperature (°C) / Time period (3h)**	**Crucibles**	**Synthesis conditions Temperature (°C) / Time period (1h)**
60CHA-30SCLA-10 ESP	CSE-1		Alumina	1550
60CHA-20SCLA-20 ESP	CSE-2		Alumina	1550
60CHA-10SCLA-30 ESP	CSE-3		Alumina	1550
60CHA-30WSA-10 ESP	CWE-1		Alumina	1550
60CHA-20WSA-20 ESP	CWE-2		Alumina	1550
60CHA-10WSA-30 ESP	CWE-3		Alumina	1550
60CHA-30SCLA-10 ESP	PCSE-1	1100	Platinum-rhodium	1550
60CHA-10SCLA-30 ESP	PCSE-3	1100	Platinum-rhodium	1550
60CHA-30WSA-10 ESP	PCWE-1	1100	Platinum-rhodium	1550
60CHA-10WSA-30 ESP	PCWE-3	1100	Platinum-rhodium	1550
47.9SiO_2-23.5CaO 4.6P_2O_5-6.4MgO-7K_2O-8Al_2O_3-0.8Na_2O-0.2TiO_2-1.4Fe_2O_3	MCSE-3	1100	Platinum-rhodium	1550
43.6SiO_2-21CaO-1.5P_2O_5-5.5MgO-15K_2O-12Al_2O_3-0.7Na_2O-0.3TiO_2-0.4Fe_2O_3	MCWE-2	1100	Platinum-rhodium	1550

The starting powders were mixed in acetone media and ground for 1h in an agate mortar pestle. The powder of the above-mentioned chemicals was calcined at 1100 °C for 3h prior to

melting in the Pt-Rh crucible. The calcined powder was ground in an agate mortar pestle for 2 h. After grinding, the mixture was put into a Pt-Rh crucible and melted at 1550 °C at a heating rate of 5°C min^{-1} in a programmable electric furnace. Furthermore, the remaining steps were carried out in the same manner as for the glasses prepared using agro-food waste/ashes. The nomenclature of the samples and processing conditions are also given in Table 3.2.

3.2 Characterization methods

3.2.1 Density measurement

The density of the as-prepared glasses was determined using standard Archimedes' principle with xylene as a buoyant medium as follows:

$$\rho_{sample} = \frac{w_a}{w_a - w_x} \times \rho_x \quad (3.1)$$

Where, ρ_{sample} the density of the sample, ρ_x is the density of xylene at room temperature, w_a is the weight of the sample in air and w_x is the weight of xylene. The density of xylene is 0.863 g/cc at room temperature (30 ^oC).

3.2.2 X-ray diffraction (XRD)

XRD is a versatile and non-destructive technique most widely used for detecting the amorphousness or crystallinity of the present samples. The X-rays are produced by the cathode ray tube, are filtered by crystal monochromators, and are required to generate monochromatic X-rays. The X-rays are collimated to concentrate and directed onto the sample. The intensity of the reflected X-rays is recorded as the sample and detector are rotated. When the geometry of the incident X-rays impinging on the sample satisfies Bragg's law equation ($2d \sin\theta = n\lambda$), constructive interference occurs, resulting in a peak in intensity. Here, n is the order of reflection, and λ represents the wavelength of X-rays ranging from 0.1- 4 Å, which is the same order as the inter-planar spacing (d) of the crystals. As a result, the interaction of X-rays and crystals would result in diffraction patterns according to Bragg's

law [1]. The X-ray signals are recorded and processed by a detector, which converts it to counts per second. Further, the output is obtained on a device such as a computer monitor as shown in Figure 3.2. XRD can use to calculate structure details such as crystalline phases, the volume of crystalline phases, crystallite size, and type of strain (compressive or tensile) within the sample, etc. [1]. Glass is an amorphous material, that lacks diffraction peaks. A broad halo or more is observed in spite of diffraction peaks.

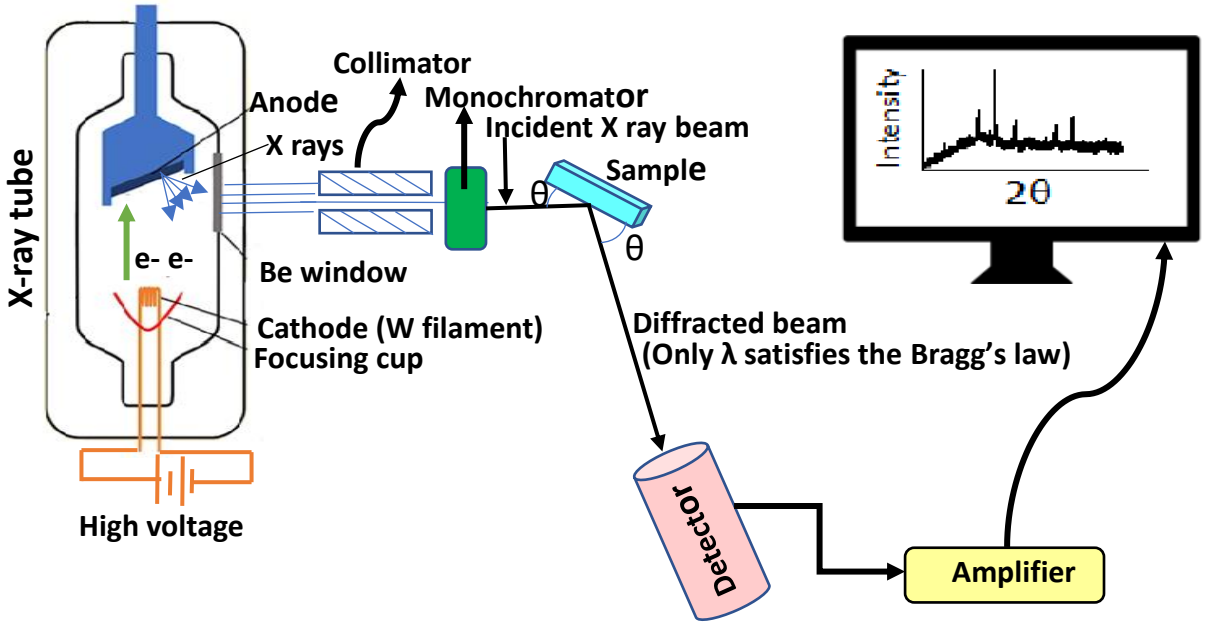

Figure 3.2 Schematic diagram of obtaining X-ray Bragg's diffraction pattern

The position of the broad halo is obtained according to the composition of the glasses. XRD patterns sometimes show more than one broad halo, indicating that the glasses are phase-separated or inhomogeneous. The phase-separated glasses form when immiscible contents are present in melted compositions [2]. The phenomenon of phase separation is caused by a decrease in the overall energy. If the separation of the mixture of two components favors the lowering of free energy, then glass becomes phase-separated, sometimes homogeneous melt with no phase separation leads to a reduction of free energy [3]. On the other hand, the glass-ceramics possess some crystalline peaks which are embedded in the glass matrix via heat treatment or development of hydroxyapatite layer after soaking in SBF solution. XRD also

gives sufficient information about the crystalline phase (s) that formed on the glasses. In the present study, the XRD patterns of the as-quenched samples before and after soaking in SBF were evaluated using a PANalytical's X'pert Pro X-ray diffractometer using CuKα radiation with a wavelength (λ)=1.54 Å operated at 30 kV and 15mA. The measurements were conducted in the air between the 2θ ranges of 20-90°. The scanning speed and step size were kept at ~ 4° min^{-1} and 0.02°, respectively, during the experiment. For phase identification, the X'pert high score plus software was used.

3.2.3 Fourier transforms infrared spectroscopy (FTIR)

FTIR is a very useful technique used to find the functional groups present in the glasses and other materials. When a material interacts with infrared radiation, absorbed IR radiation usually excites molecules into a higher vibrational state. The energy difference between the ground and excited vibrational states determines the wavelength of light absorbed by a specific molecule. The wavelengths absorbed by the sample provide information about its molecular structure. It is concerned with molecular bonds vibrating at different frequencies depending on the elements and the type of bonds. There are several particular frequencies at which bonds can vibrate in various modes such as stretching, bending, rocking, etc. also depending on the degree of freedom [4]. Shifting of IR bands is very useful in determining the weakening and strengthening of material bonds. It is also used to determine the range of bond lengths and bond strengths of the functional groups present in the materials [5]. The broadening of FTIR bands is due to the presence of the same group of vibrational frequencies that are difficult to resolve. Formation of HAp or change in the local structure of glasses/glass-ceramics and any materials after soaking/dipping in the SBF solution can be confirmed by this technique. It aids in understanding any structural changes caused due to interaction with SBF. In the present study, FTIR analysis of the powder samples before and after soaking in SBF was carried out in a Perkin Elmer Spectrum RX (1) spectrometer. The spectral resolution

was 0.8 cm^{-1}. Approximately 0.5 mg of each sample was mixed with 20 mg of KBr in an agate mortar and then pelletized using a hydraulic press of a pressure (0.63 kN/mm^2). This powder was used for recording the transmission spectra in the infrared frequency range i.e., 400-4000 cm^{-1}.

3.2.4 Differential scanning calorimetry (DSC)

DSC determines temperature and heat flows related to the thermal transitions in a material. In this thermal analytical technique, the difference in the amount of heat required to raise the temperatures of a sample and a reference is measured as a function of temperature. The temperature program for a DSC analysis is typically designed so that the sample holder temperature increases linearly as a function of time. Only a few milligrams of material are required to run the analysis. When a sample goes through a physical change, such as a phase transition, more or less heat will need to flow to it than to the reference to maintain both at the same temperature. The amount of heat that must be transferred/taken to the sample depends on whether the process is exothermic or endothermic.

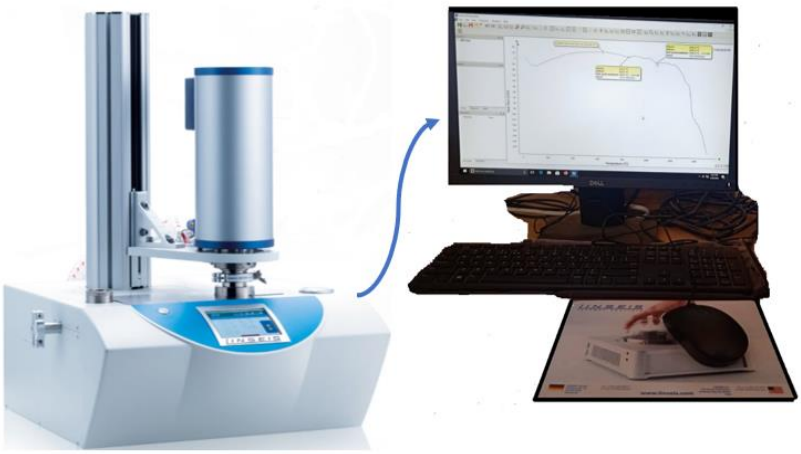

Figure 3.3 Differential scanning calorimetry setup

DSC can also be used to detect more-subtle phase changes, such as glass transition. DSC is commonly used to measure a wide range of properties in both organic and inorganic materials, from metals and simple compounds to polymers, etc. In the present study, DSC scans were

obtained with a model Linseis DSC PT 1600 thermal analyzer as shown in Figure 3.3. The DSC experiment was performed on as-prepared samples in the presence of commercial air. During the experiment, the heating rate was 10 $^{o}C\ min^{-1}$ using Al_2O_3 as a reference in the platinum crucible.

3.2.5 Vickers microhardness

Micro-indentations were done on the surfaces of the as-quenched samples using a diamond Vickers indenter on a micro hardness testing machine (Mitutoyo MVK-HO, Japan) to measure microhardness. The indentations using an applied load of 500 g for 15 seconds were made at four different points on the samples. The average diagonal of the pyramidal shape indentations was taken. The micro hardness was calculated using the following equation [6]:

$$H = 1.854\frac{L}{d^2} \qquad (3.2)$$

Where L is the applied load and *d* is the diagonal length of the square indentation in mm.

3.3 Bioactivity tests

In-vitro bioactivity and degradation of the prepared glasses in powdered form were determined using simulated body fluid (SBF) solution. The SBF solution used in this work was prepared as directed in Kokubo's protocol i.e., using high-purity chemicals i.e., NaCl, $NaHCO_3$, KCl, $K_2HPO_4 \cdot 3H_2O$, $MgCl_2 \cdot 6H_2O$, $CaCl_2$, Na_2SO_4 dissolved in de-ionized water [7]. The pH of the SBF solution was maintained at ~7.4 using 50 mM tris-hydroxymethyl aminomethane ($(CH_2OH)_3CNH_2$) and 45 mM HCl. The initial pH value 7.4 was taken, within the normal range of human blood plasma. The weight (powder sample)/volume (SBF solution) ratio was maintained to be 0.02 g/ml [10]. 1 g (gram) of powder was taken from each sample and put into the 50 ml of SBF into polyethylene bottles, then incubated at 37 °C for 7, 14, 21, and 28 days of soaking. After soaking the powder samples, the pH of the SBF solution was monitored every day using a digital pH meter (P Hep model HI96107). The least count of the pH meter was 0.1. For characterization, these samples were filtered from SBF and dried at room

temperature. A precision microbalance (Mettler Toledo) was used to monitor the weight loss of the dried samples after every 7 days of soaking. The weight measurements were calculated using formulae.

$$W_c\ \% \ = \left(\frac{W_o - W_f}{W_o}\right) \qquad (3.3)$$

Where, W_c refers to the weight change, W_o and W_f correspond to the weight of the sample before and after soaking in SBF, respectively.

Based on changes in the pH and weight loss of the soaked samples were characterized using XRD, FTIR, and SEM-EDS and compared with respect to pristine (unsoaked) samples. The residual SBF was characterized by microwave plasma atomic emission spectroscopy (MP-AES) to see the elemental release profile.

3.4 Characterizations for bioactive properties

In addition to the above-mentioned characterization techniques, some important characterizations are required to explicitly confirm the phenomenon of bioactivity as discussed in this section.

3.4.1 Microwave plasma-atomic emission spectroscopy (MP-AES)

MP-AES is a highly sensitive elemental analysis technique. It has proven valuable in a variety of applications. It is a complementary technique in the present bioactivity study, where the MPAES data confirm the pH change and overall weight change of the soaked sample. A magnetron and a waveguide are major components of the instrument. Electromagnetic energy in the range of 3.5 GHz is created by Magnetron [8]. The microwave energy is used to generate plasma discharge with nitrogen from a gas cylinder or extracted from ambient air. The samples are typically nebulized before interacting with plasma. The atomized samples are passed through the plasma, and the electrons are excited. When light emitted by the electron returns to the ground state, it is separated into a spectrum and the intensity of each emission line is

measured by the solid-state charge-coupled device (CCD) detector. The most commonly determined elements provide information up to the parts per billion (PPB) level.

In the present study, the concentration of ions leached out into the SBF solution from the sample surface was evaluated by an MP-AES system (Agilent 4100) with a spectral resolution of 25-40 pm. All the samples are prepared in 1 Normal nitric acid (HNO_3) solution. 0.1 g sample powder is added to a solution of 10 ml nitric acid and 25 ml water. The prepared solution is heated to a 50 % reduction of volume. The residual solution is further diluted by adding 100 ml of water. All the measurements are recorded and repeated in triplicate. For the final analysis, the averaged values are used.

3.4.2 Scanning electron microscopy (SEM) and Field emission scanning electron microscopy (FESEM) with energy dispersive spectroscopy (EDS)

SEM generates images of a sample by scanning the surfaces with a focused beam of electrons as shown in Figure 3.4 [9]. Electrons in the beam collide with an atom of the sample and produce a variety of signals.

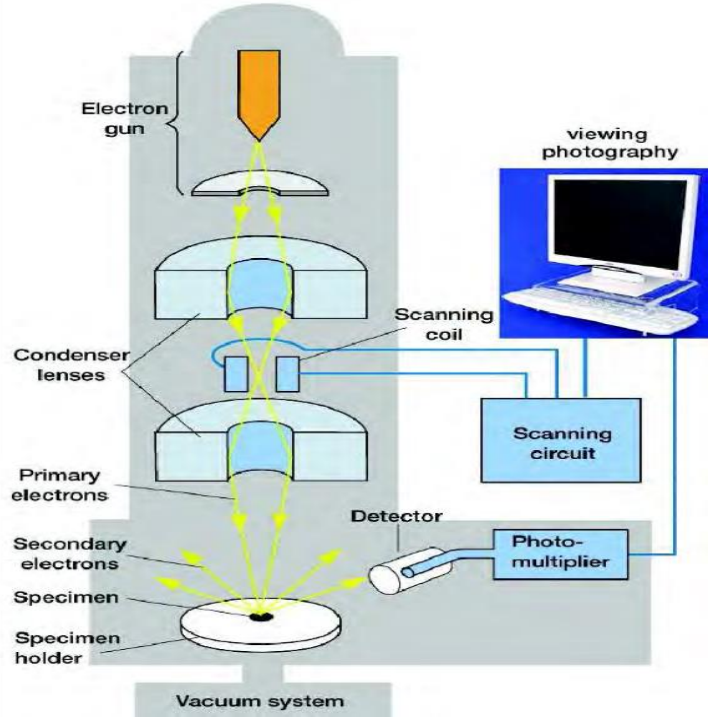

Figure 3.4 Schematic diagram of scanning electron microscope [11]

These signals are produced through secondary electrons, backscattered electrons, and characteristic X-rays. The secondary electrons (SE) provide information about the topographical region of the sample. These secondary electrons have lower energy and resolving power <10 nm. Backscattered electrons which are deflected in the back direction of the beam used to determine the spatial distribution of elements or compounds within the top micron of the sample. These electrons are of higher energy and resolution to the level of 1000 nm [10]. Characteristic X-rays are used to determine the composition of the sample. In addition to this, SEM equipped with energy dispersive spectroscopy (EDS) was used to determine the elemental composition of the selected sample surface. The working of EDS is also based on electron focusing same as in SEM [11]. When high-energy beam electrons interact with the shell electrons of the sample atoms an inner shell electron is ejected as shown in Figure 3.5.

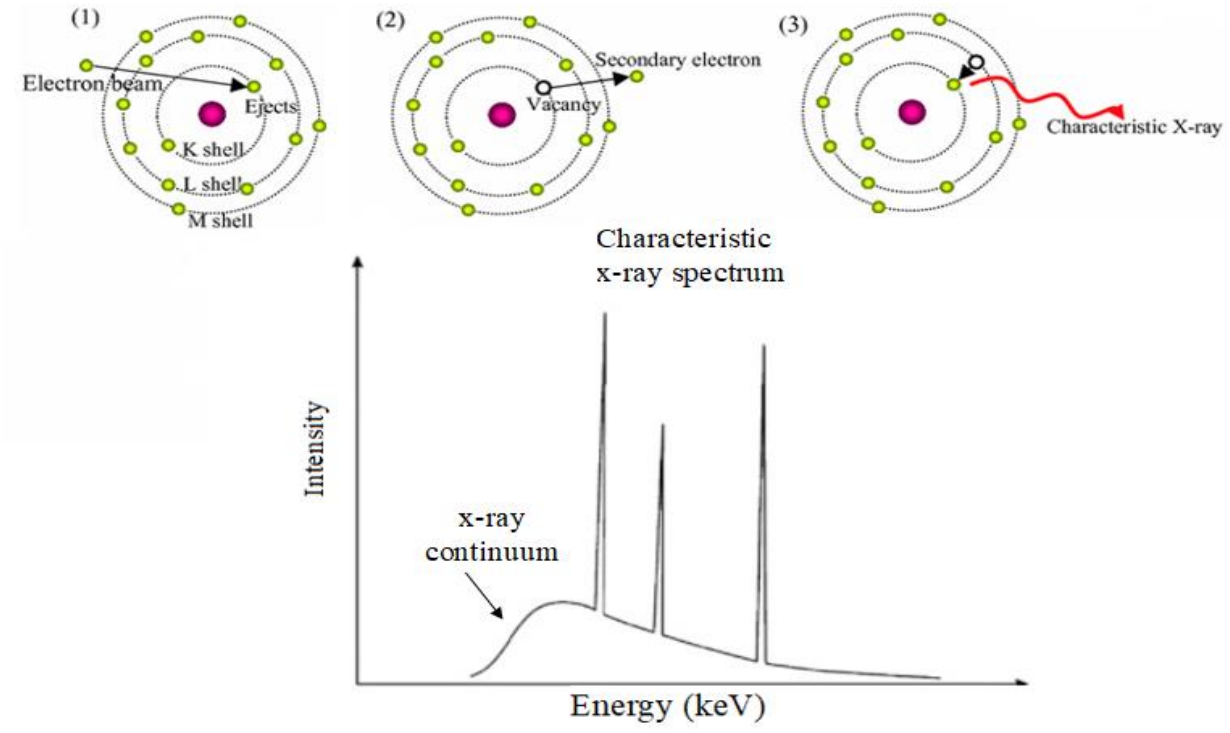

Figure 3.5 Working diagram of energy dispersive spectroscopy and schematic diagram of characteristic X-ray spectrum [12]

The removal of this electron temporarily ionizes the atom until an outer shell electron fills the vacancy and stabilizes it. Because this electron originates from a higher energy level, it must

expend a certain amount of energy before it can be accommodated in the inner shell. The energy difference between the higher and lower energy shells may be released in the form of X-rays. These are characteristic X-rays (discrete energy level), rather than continuous ones. Various elements will fill the voids in shells in different ways. Because each element produces a distinct set of peaks, the spectra may be used to identify the elements, these discrete X-rays are referred to as characteristic X-rays. The equipment for the detection of X-rays is known as an energy dispersive X-ray (EDX) detector.

The FESEM is a similar instrument to SEM, providing a wide variety of information from the sample surface, but with higher resolution and a much greater energy range [13]. In comparison with conventional scanning electron microscopy (SEM) field emission SEM (FESEM) produces clearer, less electrostatically distorted images with spatial resolution down to one and a half nanometres which are three to six times better. SEM images of the samples before and after soaking in the SBF solution provide valuable information about the changes on the surface of the samples. It occurs due to a chemical reaction between glasses, and SBF solution. SEM micrographs of all the samples were taken using SEM JEOL/EO (version 1.0). The samples are coated with platinum (Pt) on auto fine coater-JEOL (JEC-3000 FC) under an operating current of 20 mA for 60 seconds. EDS spectra of all the samples were recorded at appropriate voltages up to 10 keV.

3.5 Biocompatibility test

3.5.1 MTT Assay

To check the biocompatibility of the samples, osteoblast-like human cell lines, i.e., MG-63 have been utilized. The MG-63 cell lines were obtained from the National Center for Cell Science (NCCS), Pune, India. The cells were propagated in Dulbecco's modified Eagle's medium (DMEM) (Himedia), comprising 10 % (v/v) fetal bovine serum (Himedia), 100 IU ml^{-1} penicillin, 100 µg/ml streptomycin, and 2.5 µg/ml amphotericin (Himedia). In a humidified

chamber, cells were held at 37 °C, along with a 5% CO_2 level. Sample response was evaluated using 3-(4,5-dimethylthiazol-2-yl) 2,5-diphenyl tetrazolium bromide (MTT) cell proliferation assay on MG-63 as shown in Figure 3.6 [14, 15]. The cells were trypsinized, and 1×10^4 cell suspension was added to 96 well plates and kept in a CO_2 incubator overnight. Cells cultured in DMEM seeded in wells without any glass powder were used as control. After that, the cells were exposed to the powder sample at concentrations of 1, 2, 5, and 10 mg/ml overnight.

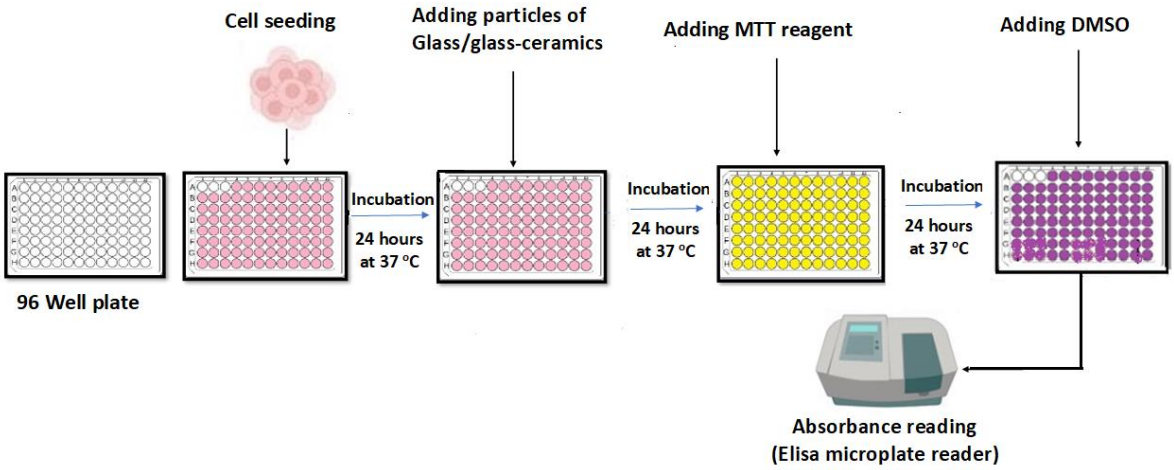

Figure 3.6 MTT assay used to check viability via yellow MTT reduced to purple color

Following 24 h of incubation, 20 µL of MTT reagent (Sigma, St. Louis, MO, 5 mg/ml) was put in all wells and again kept the plate for 4 h in a humidified chamber After that period, 170 µL medium was discarded. The formed formazan crystals were dissolved in a 100 µL organic solvent, i.e., dimethyl sulfoxide (DMSO) (Merck, Darmstadt, Germany). Finally, each well's Infinite Pro ELISA reader) where 630 nm was used as the reference wavelength. The experiments were carried out thrice using sample triplicates. The cell viability was measured by applying the given formula:

$$\text{Viability (\%)} = (\text{OD of treated cells}) / (\text{OD of control}) \times 100 \qquad (3.4)$$

Three independent analyses were shown as the mean ± standard deviation. The outcomes were analyzed by one-way variance analysis (ANOVA), accompanied by Tukey's multiple comparison test using Graph Pad Prism (GraphPad Software, Inc., San Diego, CA).

References

[1] B.D. Cullity, Elements of X-ray Diffraction, Addison-Wesley Publishing Company Inc. (1956).

[2] Y.-M. Sung, S.A. Dunn, J.A. Koutsky, J. Europ. Ceram. Soc. 14 (1994) 455.

[3] J.E. Shelby, Introduction to Glass Science and Technology, 2nd ed. The Royal Society of Chemistry, UK (2005).

[4] B.Schrader (ed.), Infrared and Raman spectroscopy: Methods and applications, VCH Publishers, Inc., New York (1995).

[5] R.P. Smith, J. Phys. Chem. A. 60 (1956) 1293.

[6] S.A. Shahdad, S. Bull, S. Rusby, R.W. Wassell, Dent. Mater. 23 (2007) 1079.

[7] T. Kokubo, T. Kitsugi, T. Yamamuro, J. Biomed. Mater. Res. Part B. 24 (1990) 721.

[8] K.J. Jankowski, A.P. Ramsza, E. Reszke, M. Strzelec, Microwave Induced Plasma Analytical Spectromerty, 1st ed. Royal Society of Chemistry, Warsaw, Poland (2010).

[9] K. Shimizu, T. Mitani, New Horizons of Applied Scanning Electron Microscopy, Springer Science & Business Media (2009).

[10] N. Jain, P. K. Jain, R. K. Singh, A. Srivastava, Fundam. Appl. 15 (2022) 67.

[11] J.C. Russ, Fundamentals of energy dispersive X-ray analysis: Butterworths monographs in materials, Butterworth-Heinemann 1st ed. (1984).

[12] K. Shimizu,T.Mitani, New Horizons of Applied Scanning Electron Microscopy, Sringer Berlin Heidelberg, Germany (2010).

[13] A. Alyamani, O. Lemine, FE-SEM Characterization of some nanomaterial, Scanning electron microscopy, Intech Open (2012).

[14] P. Singh, M. Baranwal, S.M. Reddy, Pharm. Biol. 54 (2016) 2269.

[15] M. Goyal, M. Baranwal, S.K. Pandey, M.S. Reddy, Indian J. Microbiol. 59 (2019) 428.

4. Effect of SCLA and ESP variations

In this chapter, the results of three different compositions are discussed in which SCLA varies by ESP with fixed CHA. The ESP contents increase in glass composition increase the bioactivity of the glasses.

4.1 Chemical analysis of as-prepared samples

The EDS analysis was done on the as-quenched samples to find out the chemical compositions. The chemical compositions of as-quenched samples were done at different particles as shown in Figure 4.1. A representative SEM with the EDS spectrum of the CSE-1 sample is given in Figure 4.1. Si, Ca, P, K, Mg, and some trace elements are present as shown in Table 4.1.

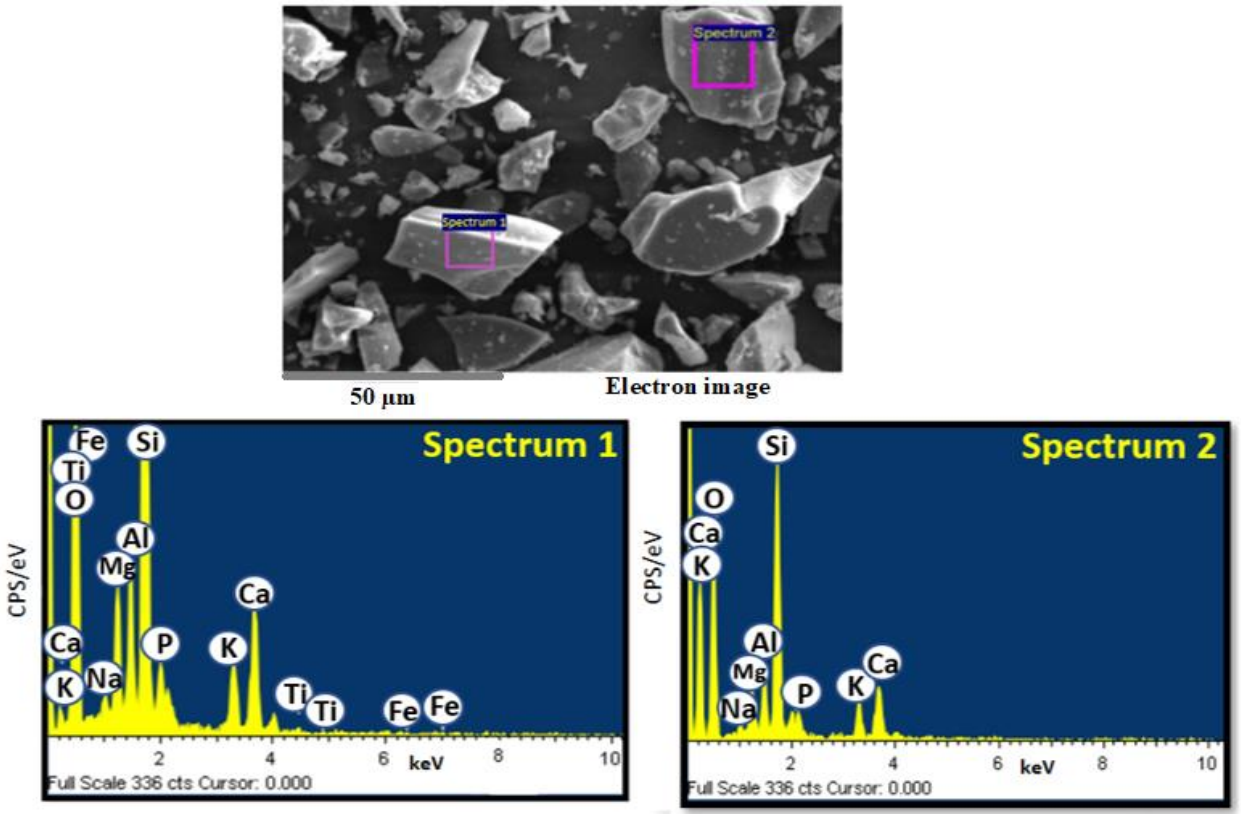

Figure 4.1 Representative SEM with EDS spectrum of CSE-1 sample taken at two different places

As ESP is added to the cost of SCLA, glass former elements like Si and P decrease in CSE-2 and CSE-3 glasses in comparison to CSE-1. On the other hand, Ca, K, and Fe increase, whereas, Na and Mg decrease in CSE-2 and CSE-3 glasses. The content of Ti and Al did not show any trend in the present glasses. However, a good amount of Al is present as shown in Table 4.1. It is possible that the Al might be picked up from the Al_2O_3 crucible since samples are melted in recrystallized alumina crucible as also reported by other researchers [1-3].

Table 4.1 The EDS analysis (wt %) of CSE-1, CSE-2, and CSE-3 samples with an indication of mean ± standard deviation (n=3)

Sample label	Si	Ca	P	Mg	K	Al	Na	Fe	Ti	O
CSE-1	25.72 ±0.80	9.94 ±0.63	2.31 ±0.74	4.38 ±0.23	5.28 ±0.24	5.27 ±0.61	1.1 ±0.28	0.54 ± 0.16	0.16 ±0.17	45.30 ±0.16
CSE-2	24.04 ±0.71	11.72 ±1.13	2.27 ±0.37	4.21 ±0.60	5.44 ±0.70	6.01 ±0.18	0.72 ±0.16	0.51 ± 0.21	0.17 ±0.06	44.91 ±0.61
CSE-3	22.37 ±0.40	17.79 ±0.68	1.99 ±0.53	2.86 ±0.43	5.81 ±0.63	4.26 ±0.43	0.61 ±0.17	1.10 ±0.57	0.11 ±0.10	43.10 ±0.57

4.2 Physical properties

The as-quenched samples were appeared in light greenish color. It clearly indicates that the agro-food wastes derived samples may have some transition elements like iron, copper, titanium, etc [4, 5]. The apparent density of CSE-1, CSE-2 and CSE-3 is 2.46, 2.57, and 2.70 g/cc, respectively. The density of the samples increases with egg shell powder (ESP) contents in glasses. As the network modifier increases, the modifier ions occupy the interstitial sites within the glass network and break the network that leading to an increase in the compactness of the glasses [6]. Because of this, the density of the glasses is increased with the replacement of SCLA with ESP. The density of present samples is comparable to earlier reported

conventional glasses, such as $45SiO_2$-$25CaO$-$10Na_2O$-$5P_2O_5$-15TO, doped with TO = TiO_2, MnO_2, Fe_2O_3, and ZnO [6]. However, the density of conventional bioglasses (CBG) has higher values, than present glasses. The reason for the lower density of present glasses may be due to the presence of various inherent trace elements in the agro-food wastes which could be responsible for the lower density of the present samples.

4.3 X-ray diffraction (XRD)

The amorphous nature of as-prepared samples was confirmed by X-ray diffraction (XRD).

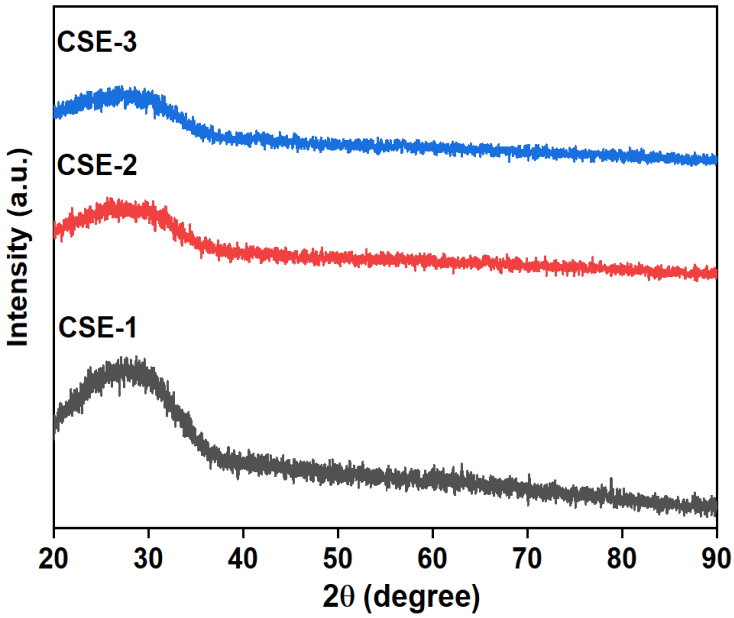

Figure 4.2 XRD patterns of as-quenched CSE-1, CSE-2 and CSE-3 samples

XRD patterns exhibit broad hump (2θ) ~20-35^o as shown in Figure 4.2. This indicates that all three samples are amorphous in nature. The position of broad humps depends on the initial constitutes of the samples.

4.4 Fourier transforms infrared spectroscopy (FTIR) analysis

FTIR spectra of all three samples manifest the stretching and bending bonds of the sample's constituents. All spectra normalized to the bands located at ~1035 cm^{-1}. The FTIR spectra (Figure 4.3) show the bands at 3624, 1802, 1035, 764, 560, and 470 cm^{-1}. The band around

3624 cm^{-1} corresponds to the H-O-H attributed to the stretching vibrations of absorbed water molecules [7]. It is assumed that the samples absorbed atmospheric moisture during the sample preparation for FTIR measurement. This band becomes prominent as an ESP content is increased in the samples. It indicates that ESP addition increases the tendency of water absorption in the present samples. It is particularly good for bioceramic materials used for getting and replacement of bones since their glass surface enhances the tendency to form the silanol group which is responsible for the HAp formation [8]. Another broad band centered at 1802 cm^{-1} corresponds to the stretching mode of the Si-OH group [9]. The most intense and broad IR bands occur at 1035 cm^{-1} corresponding to the vibrations of $[SiO_4]^{4-}$ and $[PO_4]^{3-}$ which may overlap one another. Similar results have also been reported by Singh et al. [10] for CBG. The reason for the broadness of this band is due to the presence of different silicate units having different coordination numbers. The band at 764 cm^{-1} has shown a combined effect for Si-O-Si bending vibration and Si-O-Al stretching mode. This band is more prominent in the CSE-3 sample than in the other two samples. It is confirmed that these samples exhibit some contents of Al (Table 4.1). It can be seen that with increasing ESP contents on replacing SCLA, the concentration of SiO_2 in the glasses and position of these band shifts towards lower wavenumber. The shifting of this band at the lower wavenumber could associate with the formation of non-bridging oxygens (NBOs). Bands at 470 cm^{-1} correspond to bending vibrations of SiO_4 tetrahedra. It indicated that silica has formed the glass network [11]. Another band at 560 cm^{-1} is related to asymmetric bending vibrations of P-O bonds. The FTIR spectra and EDS results are consistent to confirm that P is also present in the samples. By increasing the contents of ESP in the glass structures the intensity of the P-O-P bending band has also decreased. The content of P is also decreased as observed in the EDS analysis (Table 4.1). This may be associated with network modifications, ESP containing higher CaO than SCLA. It is also a

modified glass network, this increases the number of NBOs, which changes the glass structure. So, decreasing the content of P in CSE-2 and CSE-3 than in CSE-1 and modifications in structural units lead to a change the nature of the P-O-P band as shown in Figure 4.3. The deconvolution was done on broad spectra of the samples to distinguish among various silicate units. The deconvolution spectra of the samples are showing six bands i.e., 733-724 cm^{-1}, 870-861 cm^{-1} (Q^0), 915-906 cm^{-1} (Q^1), 1035-1012 cm^{-1} (Q^2), 1173-1153 cm^{-1} (Q^3), and 1208-1205 cm^{-1} (Q^4). These bands are corresponded to the discrete anionic structural units such as 3D networks; sheets, infinite chains, dimmers and monomers with NBOs versus silicon ratio of Q^0, Q^1, Q^2, Q^3 and Q^4, respectively [12]. All bands mentioned in the spectra are slightly different to each other as shown in Figure 4.4. The bands 870-861 cm^{-1} are corresponding to $Si\text{-}O^-$ stretching vibrations mode in Q^0 units in the silicon-oxygen sub-networks. The band near 915-906 cm^{-1} is corresponding to asymmetric stretching vibrations Si-O-Si and P-O-P mode. Broad band at 1035-1012 cm^{-1} corresponds to stretching vibrations of $Si\text{-}O^-$ bond in the Q^2 structure of the silica network [13]. The band at 1173-1153 cm^{-1} is related to asymmetric stretching vibrations of Si-O-Si and P-O to Q^3 units [14]. A band at range 1208-1205 cm^{-1} is of Q^4 unit corresponding to stretching vibration mode of Si-O-Si and O-P-O bridging unit. The deconvolution fitting indicates that the intensities of all bands in the CSE-2 sample decrease as compared to other samples. This may be due to the presence of higher contents of intermediate oxide i.e., Al as compared to Na, Mg, and K. With the increase in Al content, there may have more Al-O-Si or Al-O-P linkages in the glass. The relative area of the bands is decreasing in the range of 866-912 cm^{-1} and 1153-1205 cm^{-1}. On the other hand, the relative area corresponding to band 1034 cm^{-1} increased in the CSE-2 sample. In the case of a CSE-3 sample, the band occurs at around 1153 cm^{-1} due to asymmetric stretching of Si-O-Si and P-O units. It showed maximum intensity as compared to CSE-1 and CSE-2 samples.

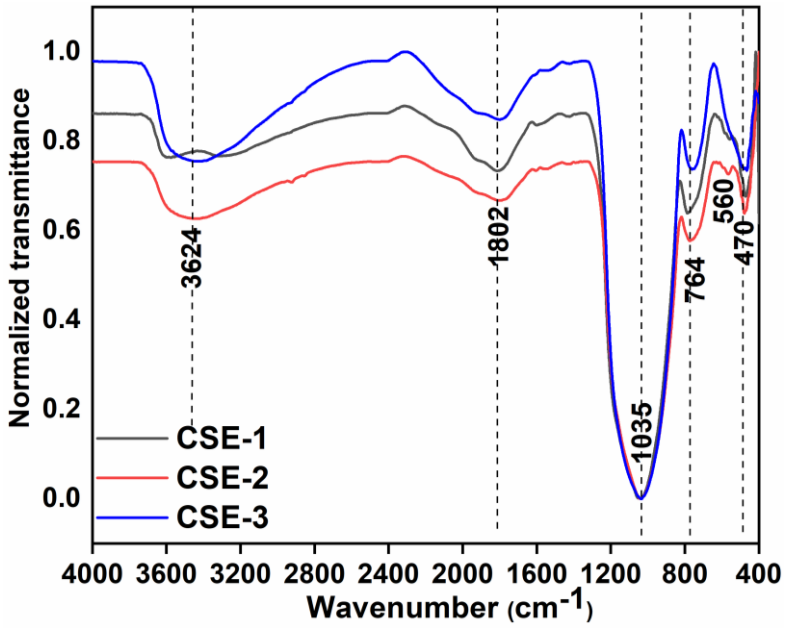

Figure 4.3 Normalized FTIR transmission spectra of all three samples

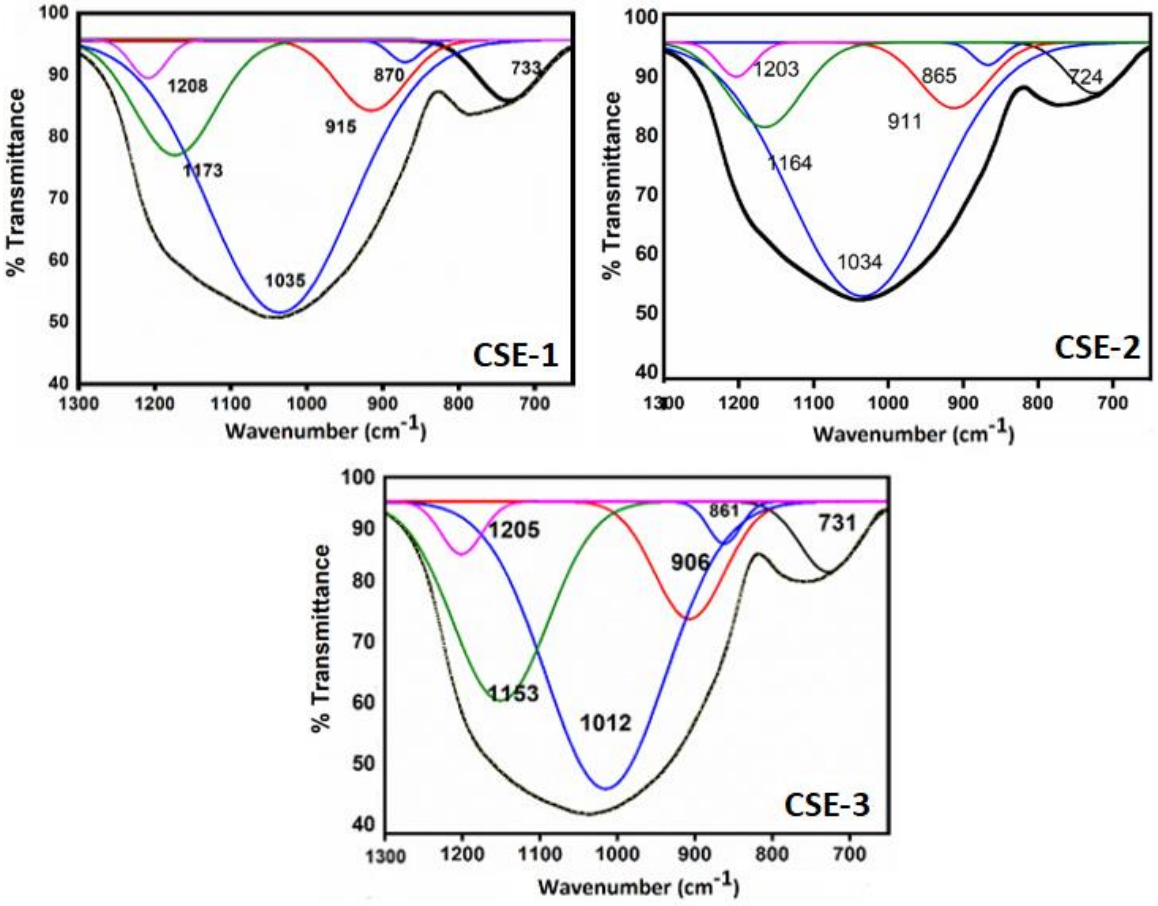

Figure 4.4 Deconvolution spectra by peak fitting method using Gaussian curves of all three samples in the wave number of 700-1300 cm^{-1}

This band corresponds to the Q^3 unit that forms the inter linkage of one SiO_4 group with another SiO_4 tetrahedron. It may also relate to SiO_4 tetrahedron with an AlO_4 group. All these SiO_4 and AlO_4 tetrahedral form the glass network in alumina silicate glasses due to the presence of Al^{3+} in four-fold coordination [15]. The AlO_4 needs charge balancing despite SiO_4 tetrahedral. In this case, Ca^{2+} may play a dual role as modifiers and charge balancing in AlO_4 units [16]. So, Ca^{2+} plays the role of network modifiers to form more NBOs. Similarly, the presence of some other network, modifying oxides can also disrupt the bridging oxygens (BOs) of the Si-O^- (Si, Al) bond leads the formation of NBOs. The intensity of all bands in the CSE-3 sample is increased due to the breaking of Si-O-Si and P-O-P bonds in the glass network. It is taken place due to the increase of Ca contents and some other modifiers. The NBOs may be increased due to Si-O-Ca, and Al-O-Ca bonds in the glasses. So, the relative area of these bands is increased. The full width at half maxima (FWHM) in the CSE-3 sample is also increased as compared to two other samples (Table 4.2). The FWHM increases due to the presence of modifiers with higher cation field strength [17]. This indicates that the degree of disorderness increases due to changes in the distributions of the Si-O^- and P-O bonds.

Table 4.2 Deconvolution parameters of glasses in wavenumber of 700-1300 cm^{-1}. The band center (cm^{-1}) of the component bands, relative area, and FWHM is full-width at half maxima

CSE-1			CSE-2			CSE-3		
Band centers	Relative area	FWHM	Band centers	Relative area	FWHM	Band centers	Relative area	FWHM
733	6.1	94.9	724	5.1	85.68	731	5.7	86.9
870	1.1	47.2	866	1.2	45.9	861	1.9	49.4
915	7.9	105.5	912	8.3	106.2	906	11.6	107.3
1035	64.9	222.2	1034	68.7	227.2	1012	48.5	181.9
1173	15.3	123.9	1165	11.6	114.6	1153	26.6	143.9
1208	2.2	53.4	1203	2.3	55.4	1205	3.0	62.0

The vibrational frequency of molecular units is directly related to the force constant which is associated with cation-anion bonds [18].

The bond length of Si-O^- can be calculated by using stretching vibrational modes and the force constant, K. The K is correlated to the average bond distance (*r*) by the following relation [19]:

$$K = \frac{17}{r^3} \quad (4.1)$$

$$K \text{ is determined by using } \nu = \frac{1}{2\Pi c}\sqrt{\frac{k}{u}} \quad (4.2)$$

Where *v* is the frequency of vibration, *c* is the velocity of light, and μ is the effective mass of the units.

$$\text{Two body reduced mass is } \frac{M_{Si}M_O}{M_{Si}+M_O} \quad (4.3)$$

Where M_{Si} and M_O are the atomic weights of Si and O [19]. The calculated force constant for SiO_2 units and bond distance values is given in Table 4.3. The change in force constant confirmed that BOs converted into NBOs with increasing contents of ESP in the glasses. The decrease in intensity of deconvoluted bands is probably related to the lowering of the network dimensionality. This is caused by the addition of modifiers and intermediate oxides like Al_2O_3. The increase in intensity is related to a breaking of Si-O-Si and P-O-P bonds in the glass network. It is concluded that the changes in their peak positions shifts towards lower wavenumber due to change among Q^0, Q^1, Q^2, Q^3, and Q^4 units and their amount in the glasses.

Table 4.3 Calculated force constant and bond distance of glasses using the most intense bands along with micro hardness

Sample ID	**Wavenumber (cm^{-1})**	**K (N/m)**	**R (Å)**	**Micro hardness (GPa)**
CSE-1	1035	387.5	3.52	5.64
CSE-2	1034	386.8	3.53	5.71
CSE-3	1012	370.5	3.57	6.26

4.5 Hardness analysis

The hardness is a very complex property that depends upon different factors such as bond strength, porosity, degree of polymerization, and fictive temperature [20]. When SCLA is replaced by ESP, the micro hardness value of the glass samples showed an increasing trend. It lies in the range 5.64-6.26 GPa as shown in Table 4.3. The Vickers's hardness of the oxide glasses is ~ 2-8 GPa [12]. Researchers have earlier reported the value of micro hardness in the range of 5.32 GPa to 5.74 GPa using peanut shell powder and ESP in soda-lime silicate glasses [21, 22]. In the present study, the maximum hardness is 6.26 GPa. The higher contents of the ESP (CaO) can increase the NBOs by disrupting the silica and phosphate network chains as also observed in FTIR spectra. This leads to compacting of the local glass structure. It can also be said that with the increasing concentration of the modifiers the packing of the molecules becomes denser. Another reason may be the presence of CaO (3.35 g/cc) has a high density as compared to Si (2.65 g/cc). The higher ESP (CaO) contents make the glass structure more rigid, resulting in higher hardness. This results in an increase in microhardness with the increase of CaO contents due to glass densification. Conventional phosphate-soda glasses containing Li_2O or K_2O as modifiers showed the maximum value of Vickers hardness i.e., 6.18 GPa [23]. It was observed that glasses with higher contents of CaO and lowest contents of Na_2O have the highest value of hardness in these glasses. Jha et al.[24] reported the hardness in the range of 4.55-4.92 GPa for $55SiO_2$-$10K_2O$-(35-x)CaO-xMgO conventional chemical-derived glasses. The value of hardness increases with the replacement of CaO by MgO due to the higher field strength of Mg^{2+} $(0.45Å)^{-2}$ than Ca^{2+} $(0.33Å)^{-2}$. Thus, it is concluded that the increase in the compactness of the glass structure is due to modifications in the glass network by CaO and other trace elements.

4.6 Differential scanning calorimetry (DSC)

Initially the DTA/TGA perform on CSE-1, CSE-2, and CSE-3 samples. In DTA/ TGA, the characteristics of the glass were not observed. After that, all the samples were investigated by DSC. Because DSC sensitivity was higher than DTA/TGA.

All glasses show endothermic peaks in the range 698-723 ^{o}C as shown in Figure 4.5. These peaks correspond to the glass transition temperature (T_g).

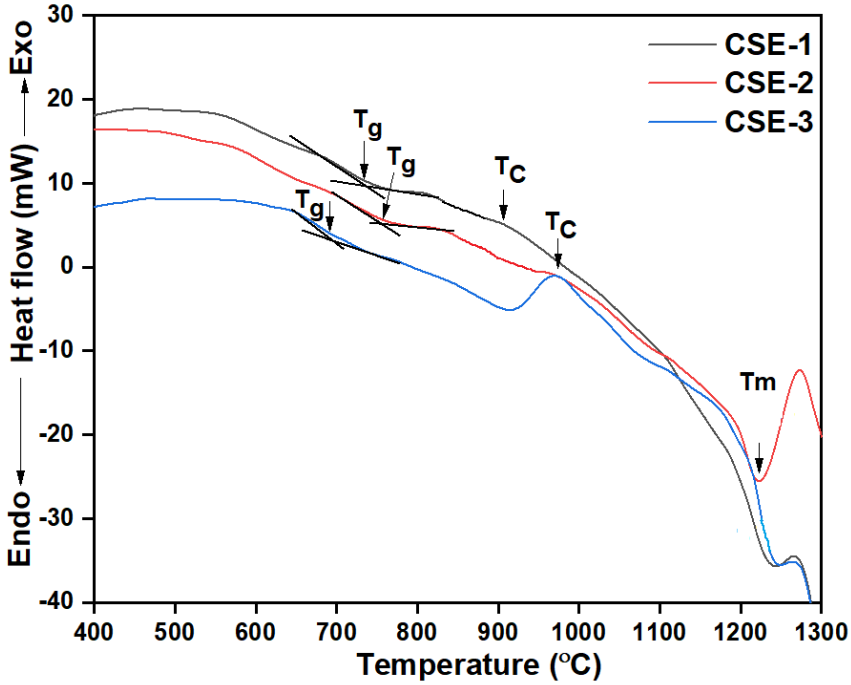

Figure 4.5 (a) DSC curves for glasses CSE-1, CSE-2, and CSE-3, thermal signals showing the glass transition (T_g), crystallization temperature (T_c), and melting temperature (T_m)

The glass transition temperature (T_g) has been measured from the peak of the derivative curve of DSC. It has been observed that decrease in T_g for glass CSE-3 in comparison to glass CSE-1 and CSE-2. It might be related to the decrease in Si content from 25.72 to 22.37 wt %, which results from depolymerization of the silica network as the calcium contents increase which acts as a modifier. T_g has directly correlated with a coordination number of the glass former and the formation of NBOs, which supports the depolymerization of the network structure [25]. On

the other hand, glass CSE-2 exhibits higher T_g than other glasses. It might be due to the formation of higher glass network connectivity of Si-O-Al or Al-O-P units [26]. These results also agreed with the results of FTIR results. After this temperature exothermic peak corresponds to the crystallization temperature (T_c). Here, a single exothermic peak has been observed for the glass CSE-1, CSE-2, and CSE-3. The glass CSE-1 has shown broad and non-distinctive T_c. The value of T_c is also lower (904 ^oC) for glass CSE-1 in comparison to the other glasses. This might be due to lower Ca or modifier contents [27]. Usually, higher modifiers content decreases T_c of the glass [28]. In the present glasses, many constituents are present that play an important role in these anomalies. It has been noticed that T_c become more pronounced in glass CSE-3, with an increase of ESP (Ca) content up to 30 wt %. It indicated that the less Ca contents decrease the tendency of glass formation, also given in Table 4.4. But it is opposite to conventional chemical-derived glasses [29]. For instance, ZnO also acts as a modifier that improves the glass-forming ability of glass ($31.92SiO_2$-39.81CaO-8.54 MgO-$0.12BaO$-$0.39Na_2O$-$0.58K_2O$-$15.12Al_2O_3$) when the ZnO content is low (2 wt %) but weakens the glass-forming ability as the ZnO contents increases (6 wt %) [29]. Further, a single endothermic peak ascribed to the melting of crystalline phases T_m precipitated heating of glasses. Additionally, Hruby's parameter (K_H) is used to determine the glass-forming tendencies of the materials using the following equation [30]:

$$K_H = \frac{T_c - T_g}{T_{m-T_c}} \qquad (4.4)$$

Here T_c-T_g is proportional to glass-forming ability, and T_m-T_c is inversely proportional to glass-forming ability. The calculated data in Table 4.4 indicate that the glass-forming ability increases in the following order: CSE-2, CSE-3, and CSE-1

Table 4.4 T_g, $T_{c,}$ and T_m of the CSE-1, CSE-2 and CSE-3 glasses

Sample	T_g (°C)	T_c (°C)	T_m (°C)	K_H Parameter
CSE-1	718	904	1242	0.55
CSE-2	723	967	1216	0.97
CSE-3	698	967	1245	0.96

The lowest value of K_H is characterized for CSE-1 (0.55) in comparison with the K_H value for glass CSE-2 and CSE-3.

4.7 Assessment of bioactivity (*In-vitro*)

4.7.1 Durability of the glasses

The glass durability test aims to evaluate the dissolution rate of the glasses after being soaked in simulated body fluid (SBF). Higher dissolution of the glass in a medium (SBF) result in more weight loss of glass, which indicates the low durability of the glass and the fast generation of HAp. Thus, moderate weight loss is important for good bioactive materials. The percentage of weight loss of all the prepared glasses soaked in SBF at 37 °C as a function of time is given in Figure 4.6. The glass CSE-3 has shown a maximum weight loss (9 %) after 7 days of soaking in SBF as compared to the other two glasses i.e., CSE-1 (7 %) and CSE-2 (5.3 %). It is due to leaching out of more alkali and alkaline earth metal ions from the glass CSE-3, in comparison to the other two glasses. Initially, the higher weight loss of the glasses is associated with a faster rate of formation of the apatite layer on the glass surfaces [31]. A slight weight gain is observed for the CSE-1, CSE-2, and CSE-3 glasses after 14 days of soaking in SBF, respectively. This is related to the migration of some ions such as HPO_4^{3-}, Cl^-, OH^-, and CO_3^{2-} from SBF to the glass surfaces as confirmed by MP-AES analysis of SBF after soaking of glasses (discussed in section 4.7.3). The same results were also observed for conventional chemicals-derived mesoporous bioactive glasses [32].

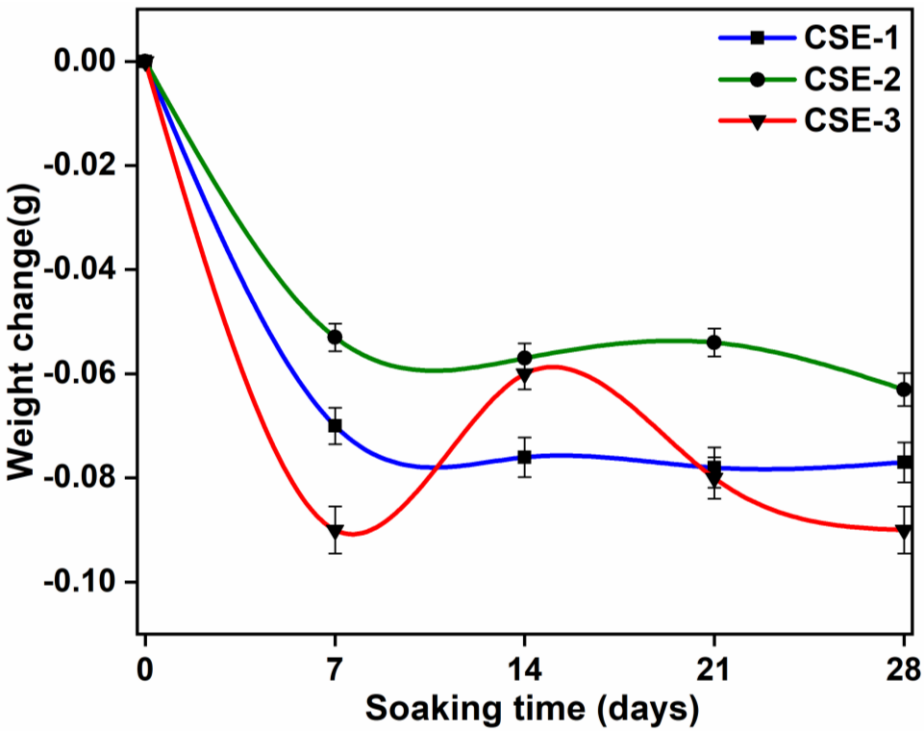

Figure 4.6 Weight loss of CSE-1, CSE-2, and CSE-3 glasses before (0 day) and after 7, 14, 21, and 28 days of soaking in SBF. The error bar in the figure indicates the standard deviation

However, weight loss in the present glasses is more than in the reported mesoporous glasses due to the release of more Si ions from the present glasses. It could also be associated with the presence of trace elements in present glasses that modify the silica glass network and the weakening of the connectivity of the glass network. It indicates that, after 14 days of soaking in the SBF solution, the deposition of the carbonated Ca-P layer on the surface of the glasses leads to weight gain. Furthermore, all the glasses again showed weight loss after 28 days of soaking. However, the dissolution rate is comparatively slower than the initial days of soaking. The present results are also similar to the results of the conventional chemicals used in glass composition (48-x) SiO_2-36CaO-4P_2O_5-12Na_2O-xTiO_2 of titania doped bio-ceramics [33]. The dissolution rate of the present glasses depends on their local glass structure, which might be influenced by different modifiers presented in agro-food wastes derived glasses.

4.7.2 Variation in pH of SBF

The variation in pH of the SBF is determined during the *in-vitro* test. The changes in the pH of the SBF also provide a fair idea of glass dissolution in SBF. It is observed that the pH variation does not follow any trend. The maximum dissolution of the glasses is attributed to the maximum change in the pH of the SBF. The pH variation in SBF for all the glasses is given in Figure 4.7. The pH variation occurs in consecutive steps associated with the formation of a HAp layer on the glass surfaces [34, 35]. In the present glasses, the pH value increases by around 0.5-0.6 after 7 days of soaking all glasses. After 7 days of immersion, more pH change is found for glass CSE-3, relative to other glasses. It is due to more ions leaching out from this glass. This particular glass also showed the highest change in weight after soaking in SBF, as discussed in the previous section. The pH change at a slower rate is observed (Figure 4.7) after 7 days of glass soaking. The pH value in SBF after 28 days of soaking attain a maximum value of 8.4, 8.3, and 8.6 for glasses CSE-1, CSE-2, and CSE-3, respectively. In the present glasses, the presence of different modifiers with the different bond strength and their chemical character, affect the dissolution rate of the glasses in SBF. The release of modifiers was exchanged with the H^+ ions of the SBF solution. It leads to raising the hydroxyl concentration (OH^-), i.e., an increase in the pH of the SBF. In the HAp forming mechanism, the glasses release silica into the SBF and formed silicic acid ($Si(OH)_4$). Polycondensation of the Si-OH groups occurred near the glass surface. When further pH rises, signify the reabsorption of Ca^{2+} and P^{5+} from the SBF onto the glass surface to form HAp on the surface of the glasses. Thus, with time, the rise in pH was slower as the solution was over-saturated and the reaction to ion exchange stopped further. These results are supported by the results of weight change in glasses. Similar results were also reported for conventional chemical-based glasses ($45SiO_2$-$24.5CaO$-$24.5Na_2O$-$6P_2O_5$ in wt % prepared by substituted Li_2O, K_2O, MgO, and ZnO) that

have more ionic bonds, maybe resulting in a faster release of ions in the early stage of soaking [36].

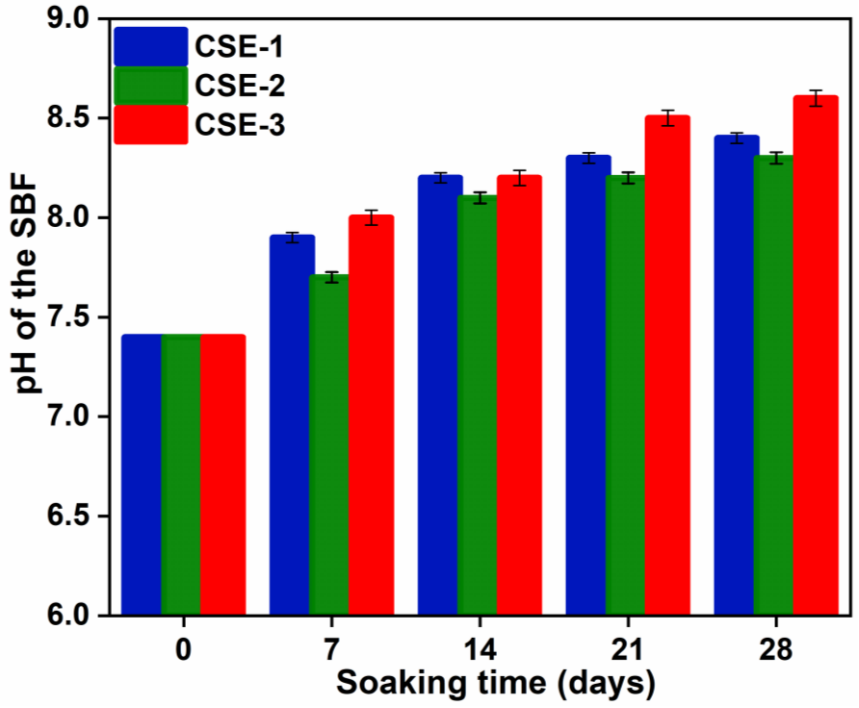

Figure 4.7 Variation in pH of the SBF with soaked glasses CSE-1, CSE-2, and CSE-3 for 0, 7, 14, 21, and 28 days, with error bars, indicates the standard deviation

In that case, the pH value is increased rapidly. Further to the increase in soaking time, the rate of dissolution became slower as also reported by other researchers [37]. The Ca-P ions leached out from the glass as well as from SBF to form a Ca-P rich layer on the glass surface during the precipitation processes. Slowly, it forms carbonated hydroxyapatite (c-HAp) by absorbing CO_3^{2-} ions from the solution [38].

4.7.3 MP-AES analysis of SBF

MP-AES provides valuable information about the changes in pH and the dissolution of glasses when glasses are soaked in the SBF. MP-AES data has been observed after soaking the glass powder for 28 days. It shows the release of ions in the SBF with respect to the original SBF as given in Table 4.5. However, the amount of leached trace elements was too small for all the

glasses which is insignificant to change the pH of the SBF. The network modifier Na^+ ions leached out in a higher percentage than any other ions. The leaching of alkali ions and their substitution with H^+ ions are important phenomenon in the bone-bonding process and regeneration of bones. The K^+ ions are also released from the glasses. It shows the increasing trend such as CSE-3 > CSE-2 > CSE-1. This helps to increase the solubility of the glasses because the ionic radius of K^+ is larger than Na^+ ions [38]. Moreover, it has also a higher effect on glass network modification than Na^+ ions [39]. The network former Si^{4+} cations have also been released in the SBF for all the glasses. However, the leaching value of Si^{4+} cations is the highest for CSE-3 glass as compared to other glasses.

Table 4.5. Si, Ca, Mg, K, Na, Al, Ti, and Fe ions concentration in SBF after 28 days of soaking. The results are taken by mean ± standard deviation (mg/l, n=3). Here, n represents an experiment performed three times

Label	Si	Ca	Mg	K	Na	Al	Ti	Fe
Reference SBF	-	113.5 ±1.5	62.5 ±3.5	351 ±2	2980 ±10	-	-	-
CSE-1	43.6 ±0.9	191 ±2	410 ±2	376 ±4	3420 ±14	< 0.01 ± 0.00	0.70 ±0.05	0.22 ±0.01
CSE-2	44.4 ±0.8	139 ±4	150 ±1	495 ±2	3520 ±14	< 0.01 ± 0.00	0.69 ±0.01	0.19 ±0.01
CSE-3	63.2 ±1.1	110 ±1	136 ±3	504 ±3	3947 ±13	< 0.01 ± 0.00	0.68 ±0.02	0.16 ±0.02

Since it has the highest number of modifiers (Ca and K). The breaking up of the network's outer silica layers by these modifiers results in the release of Si^{4+} ions during the first phase of dissolution and the formation of silanols (Si-OH) at the bioactive glass solution interface results in the dissolves in the form of $(Si(OH)_4$ to the SBF solution [40]. These silanol groups in the SBF played an essential role to make Ca-P precipitation [41]. On the other hand, modifier/former Mg^{2+} ions were also released in all glasses for up to 28 days in different

concentrations. As can be observed, the content of Mg in the composition (30 wt % SCLA and 10 wt % of ESP) of glass CSE-1 is increased, and a higher amount of Mg^{2+} ions leached out into the solution as compared to two other glasses. Based on previous studies, found that when more Mg^{2+} ions leach out from the glass surface to SBF, would further slowdown the rate of ion exchange. Because of this, the bond energy of Mg-O is higher than Ca-O. Due to this, the rate of formation of the apatite layer on the glass surface becomes lower [42]. The Ca^{2+} ions were also released as compared to the original SBF. The glass CSE-3 found that Ca^{2+} ions decreased slightly below the value originally present in the SBF solution, relative to the other two glasses. It can be concluded from the above results that poor precipitation occurred on CSE-1 and CSE-2 glasses. Only glass CSE-3 has shown that some of the Ca^{2+} ions remove from the solution and deposited on the glass surface.

4.7.4 XRD analysis

Figure 4.8 (a-c) depicts XRD patterns for all the glass samples, before and after soaking in SBF for 7, 14, 21, and 28 days. XRD patterns of all the glasses didn't show any remarkable changes after soaking for a different time period in SBF. However, few very weak and sluggish diffraction peaks (indexed with ICDD card no.09-432) are observed for CSE-2 and CSE-3 glasses after soaking in SBF. These peaks could be associated with amorphous HAp. In the later stage of soaking, these XRD peaks are disappeared as shown in Figures 4.8 (b) and 4.8 (c). It is the manifestation that a metastable HAp formed on the surface of these glasses. It could be related to the leaching of Mg, in the later stage of soaking, may retarded the precipitation of the amorphous Ca-P layer. Mg also reduces the rate of formation of a more stable apatite layer when leached to the SBF solution [43]. It is also stated in earlier studies, that higher magnesium contents in glasses are required greater time for apatite layer formation and its crystallization [44].

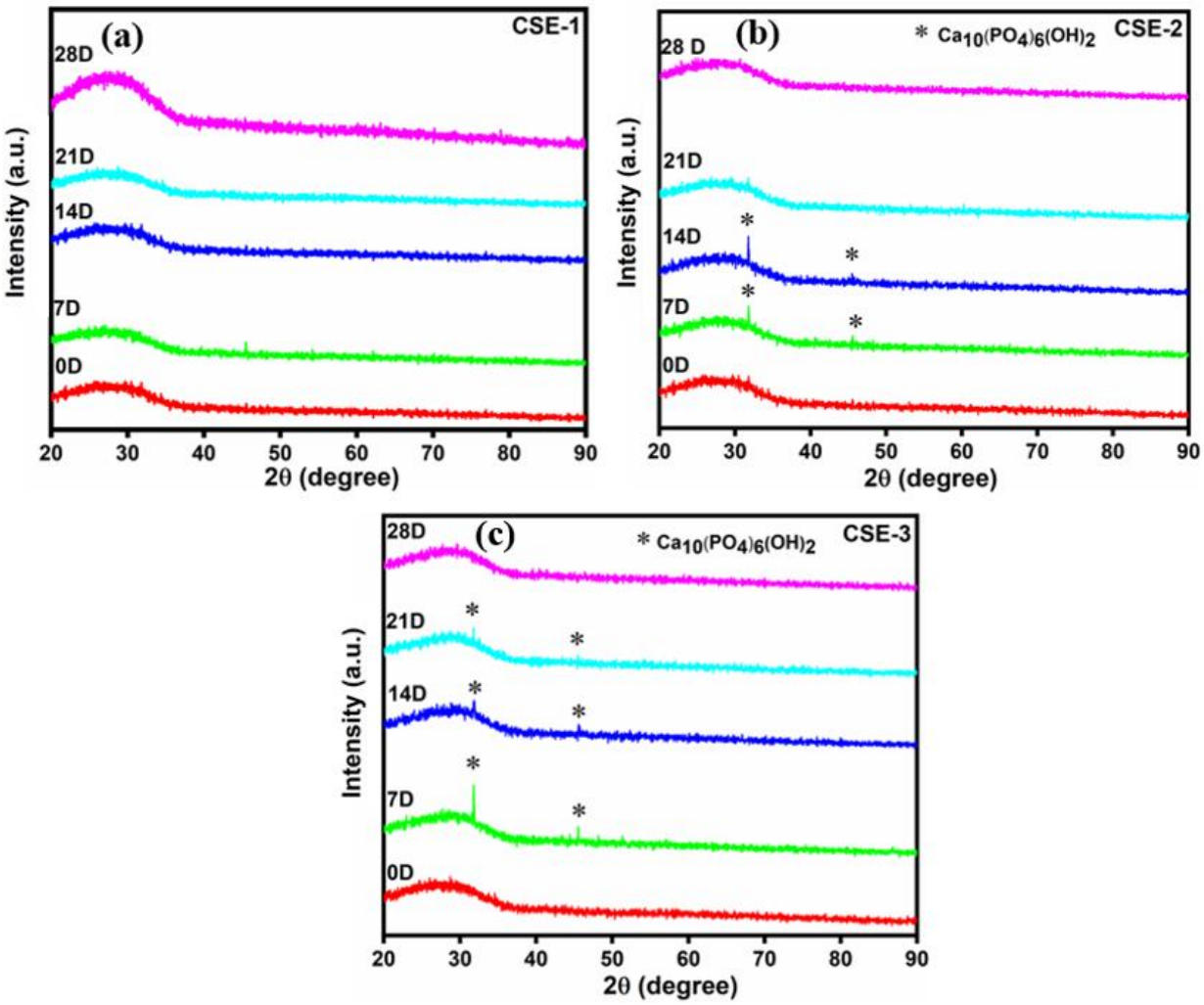

Figure 4.8 XRD patterns of (a) CSE-1, (b) CSE-2 and (c) CSE-3 glasses before (0 day) and after soaking in SBF for 7,14, 21 and 28 days

The release of higher Mg^{2+} ions on the glass surface inhibits the crystallinity of the apatite. Thus, in the present glasses, the amorphous apatite layer is formed. A similar result has been reported for conventional chemicals derived SiO_2-K_2O-CaO-MgO glass [24]. The study also showed the release of Mg^{2+} ions on the glass surface inhibits the crystallinity of the apatite.

4.7.5 FTIR analysis

FTIR spectra of CSE-1 to CSE-3 glasses are measured before and after immersion in SBF solution for 7, 14, 21, and 28 days as given in Figure 4.9 (a-f). All spectra are normalized to the bands located at ~1035 cm^{-1}.

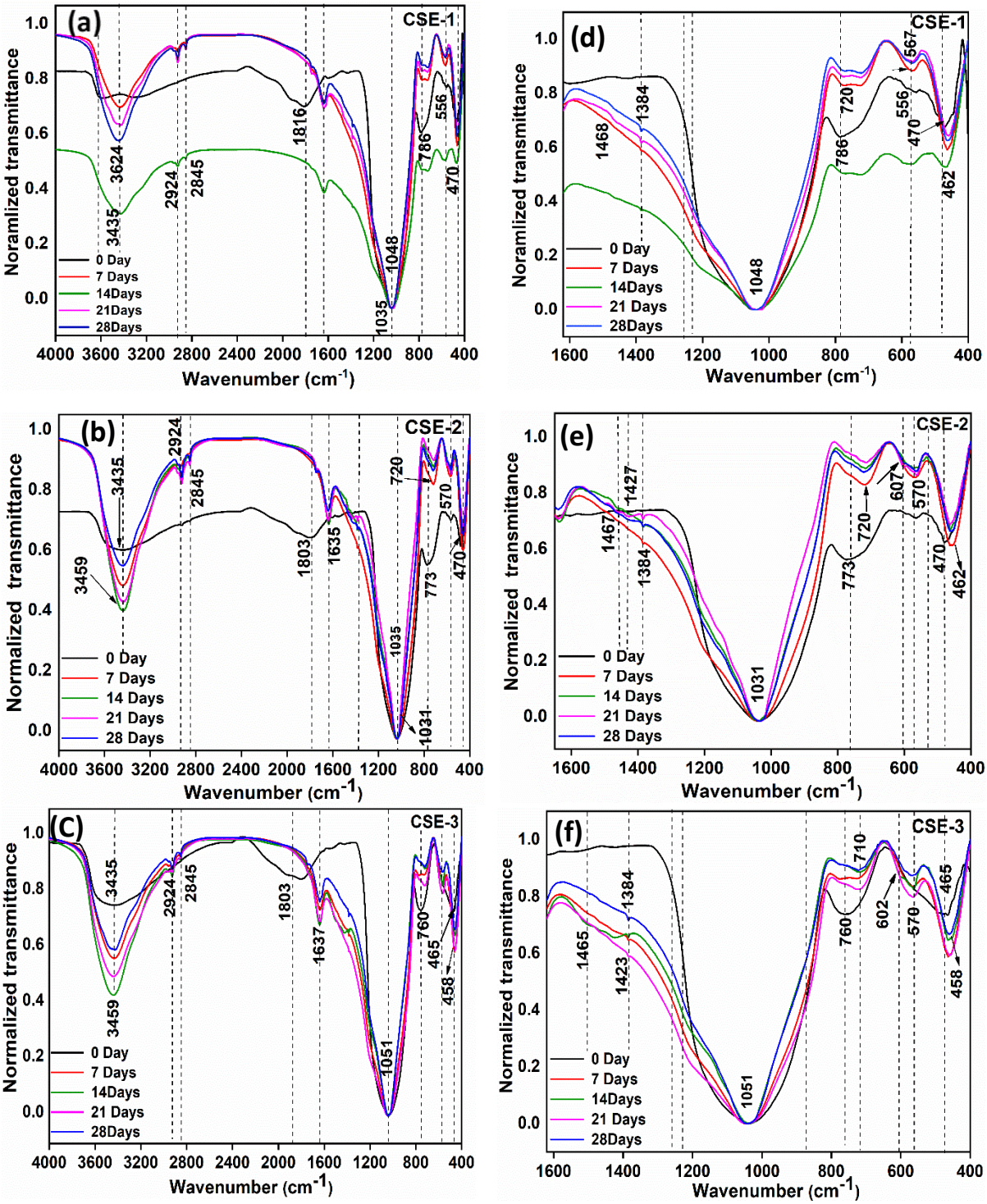

Figure 4.9 Normalized FTIR spectra of (a) CSE-1, (b) CSE-2, (c) CSE-3 glasses before and after soaking in SBF for 7,14, 21 and 28 days. The figures (d to f) are the magnified images of (a to c) which show the proper shifting and appearance of new bands

The IR band at 472 cm^{-1} and 786-760 cm^{-1} attributed to bending and stretching vibrations of Si-O-Si tetrahedra shifted towards lower wavenumber as compared to all unsoaked glasses. It showed the weakening of the glass structure due to physicochemical reactions that are taken place between the glasses and SBF. It also confirmed the formation of the silica-rich layer [45]. These results also confirmed the results of MP-AES. Another band located at ~556-570 cm^{-1} is attributed to the antisymmetric vibration of the P-O bond for unsoaked glasses CSE-1 and CSE-2. This band shifted towards higher wavenumber in comparison to unsoaked samples. Such a band does not appear in unsoaked glass CSE-3. The IR spectra of glass CSE-3 showed additional bands at 560 cm^{-1} after 7 days of soaking in SBF. It is also observed that the intensity of this band after soaking in SBF increases as compared to unsoaked samples. Two new bands at 562 cm^{-1} and ~ 602 cm^{-1} tend due to PO_4^{3-} bending vibrations after 14 days of soaking for CSE-2 and CSE-3 glasses, respectively, as shown in Figure 4.9. The cause might be the weak crystallinity of the amorphous Ca-P layer [46]. However, the above-mentioned ~ 602 cm^{-1} band is not found in CSE-1 glass after soaking in SBF solution for up to 28 days. These results agreed with the results of weight gain after 14 days of soaking in SBF. The most intense and broadband ~1035 cm^{-1} ascribed to the stretching vibrations of both Si-O-Si and P-O bonds observed in all glasses before soaking in SBF [47]. The most intense and broadband glasses CSE-1 showed blue shifts (~1035 to 1048 cm^{-1}) after 7 to 28 days of soaking in SBF. The glass CSE-2 showed the broadband ~1035 shifts towards the lower wavenumber side (~1035 to 1031 cm^{-1}) from 7 to 28 days of soaking in SBF. This also showed the weakening of the structure due to a physicochemical reaction that occurred in glass and SBF. According to the literature, the phosphate group of vibrational bands appeared at ~1032 and ~1050 cm^{-1} [48]. The glass CSE-3 showed the broad band ~1035 shifts towards the higher wavenumber side (~1035 to 1051 cm^{-1}) from 7 to 28 days of soaking in SBF. The transition of the bands to higher

wavenumbers correlates with the release of modifiers such as Ca^{2+}, Mg^{2+}, K^{+}, Na^{+}, and cations of some trace elements from the glass. It confirmed the precipitation of Ca-P onto the surface of the glasses [45]. It can be related to the bioactivity of these glasses. The new weak vibration bands 1384 cm^{-1}, 1423, and 1465 cm^{-1} ascribed to stretching of the carbonate group (C-O) that is found in all glasses after soaking in SBF. The glass CSE-1 showed this (C-O) band after 21 days of soaking in SBF. The glasses CSE-2 and CSE-3 showed C-O bands after 14 days of soaking in SBF. The other band ~1637 cm^{-1} after soaking in SBF indicated the existence of H_2O in the HAp layer [33]. The broad band at 3435 cm^{-1} and weak bands at ~ 2845 to 2924 cm^{-1} correspond to the O-H stretching vibrations in all the soaked glasses. These are in accordance with the results for bioactive conventional chemical-based glasses [41]. The intensity of the band at 3435 cm^{-1} increases has been observed for all glasses compared with unsoaked glasses. It indicated that the presence of the ESP constituents increased the propensity of the present glasses to adsorb water. It is a strong indication that the present glasses are able to shape the group of silanol which is the prerequisite for the formation of a HAp layer [16].

4.7.6 SEM with EDS analysis

The SEM micrograph of unsoaked glass powder in SBF showed irregular particles on the surface of the glasses. For comparison, the SEM images of CSE-1, CSE-2 and CSE-3 glasses (unsoaked) also depicts in Figure 4.10 (a), 4.10 (d) and 4.10 (g), respectively. The SEM micrographs have shown the different morphology of the HAp layer on all glass surfaces after soaking in the SBF solution for 7 and 28 days in Figure 4.10 (b-i). The SEM images of all the glasses, taken at 25000 X magnification, showed the presence of tiny particles with a diameter below 1µm covering the whole surface of the glasses just after 7 days of soaking in SBF, except for CSE-1 glass. It might be due to the lower contents of the ESP (CaO) and higher contents of SCLA (SiO_2) in CSE-1 glass.

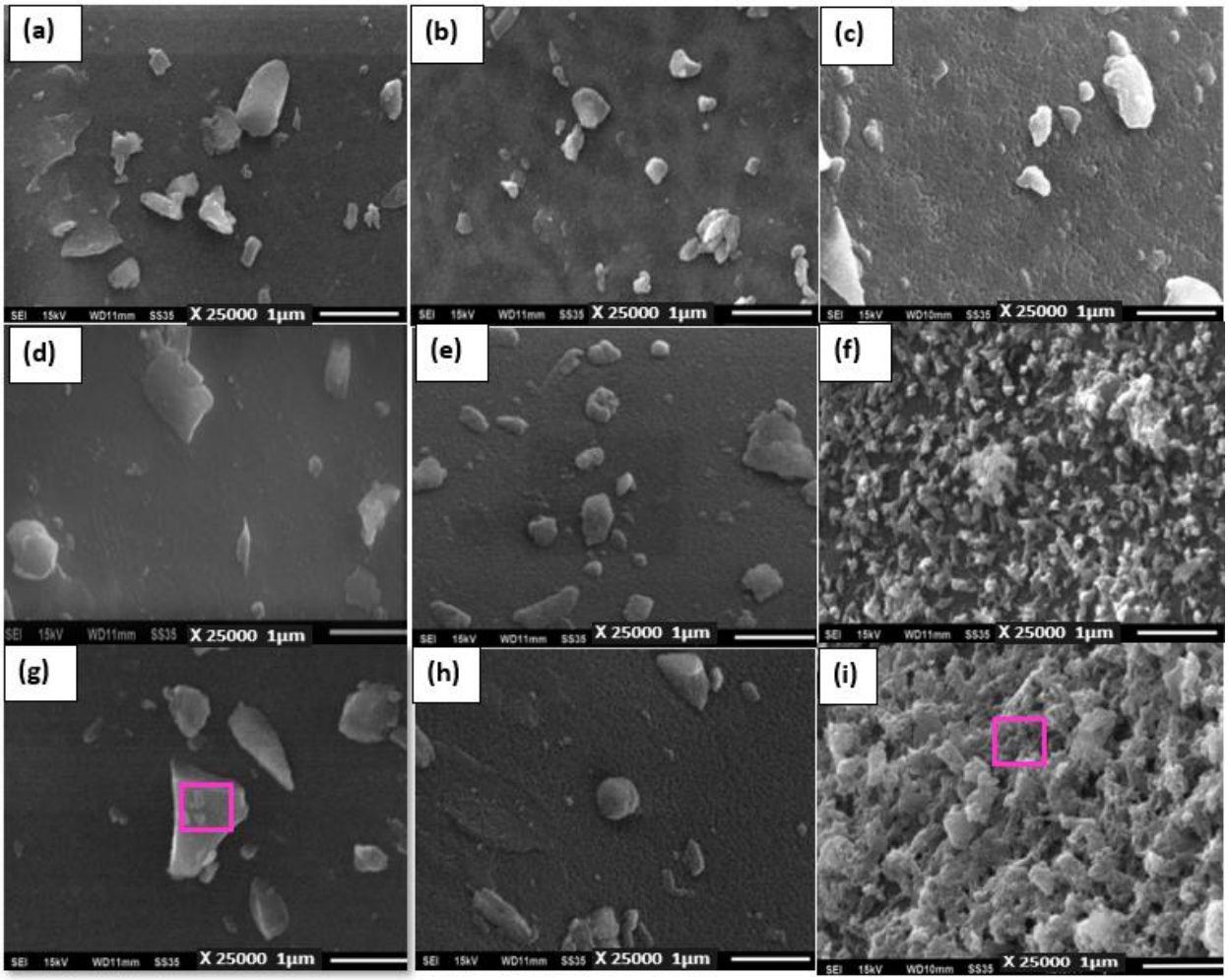

Figure 4.10 SEM images showing the development of the hydroxyapatite layer on the surface of bioactive glasses at a different soaking time in SBF. Representative SEM images of unsoaked glasses (a) CSE-1, (d) CSE-2, (g) CSE-3 and for soaked glasses (b) 7 days of CSE-1, (c) 28 days of CSE-1, (e) 7 days of CSE-2, (f) 28 days of CSE-2, (h) 7 days of CSE-3 and (i) 28 days of CSE-3

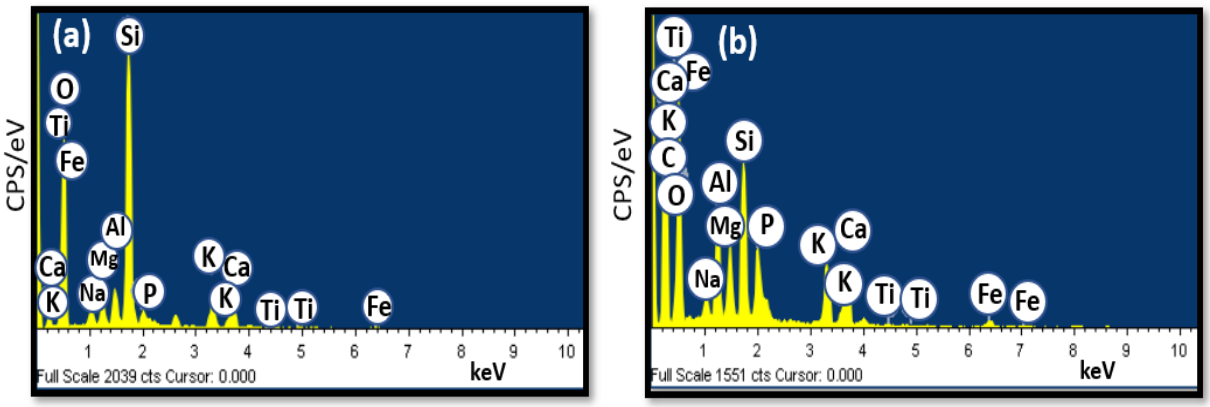

Figure 4.11 Representative EDS spectra of (a) unsoaked glass CSE-3 and (b) soaked glass CSE-3 after 28 days of soaking in SBF

Table 4.6 The glasses CSE-1, CSE-2, and CSE-3 after soaking in SBF for 7,14, 21 and 28 days show the values of Ca and P (wt %) and Ca/P (molar ratio) with an indication of mean ± standard deviation (n=3)

Days of soaking in SBF	CSE-1			CSE-2			CSE-3		
	Ca	**P**	**Ca/P**	**Ca**	**P**	**Ca/P**	**Ca**	**P**	**Ca/P**
7 days	7.37 ± 0.46	2.47 ± 0.39	2.33 ± 0.09	8.82 ± 0.80	2.45 ± 0.09	2.78 ± 0.50	14.58 ±1.82	2.80 ± 0.69	4.10 ± 0.79
14 days	9.25 ± 0.63	3.25 ± 0.46	2.22 ± 0.12	9.10 ± 0.94	3.07 ±0.49	2.29 ± 0.31	10.33 ±1.33	3.10 ± 0.72	2.57 ± 0.43
21 days	8.61 ±1.33	3.08 ± 0.72	2.17 ± 0.43	9.26 ± 1.19	3.99 ±0.71	1.78 ± 0.34	11.15 ±0.87	3.12 ± 0.50	2.78 ± 0.26
28 days	9.30 ±1.18	2.79 ± 0.65	2.58 ± 0.37	9.58 ±1.68	3.11 ± 0.31	2.39 ± 0.96	12.04 ±0.76	3.43 ± 0.28	2.72 ± 0.33

So, the physicochemical reaction between CSE-1 and SBF is minimum due to a strong silicate glass network. Similar results were also reported for conventional chemical-based composition ($CaO\text{-}SiO_2$) of binary bioactive glasses [49]. With the increase of the soaking period in SBF for 28 days, the glass surface of CSE-1 was covered with micropores on the glass surface. The reason might be that the release of more Mg^{2+} ions cause a strong effect on the morphology, as earlier discussed in MP-AES results. Based on previous studies, the higher leaching of Mg^{2+} ions reduces the size and enhances the irregular structure of amorphous c-HAp [50]. The reason might be that the release of more Mg^{2+} ions cause a strong effect on the morphology, as earlier discussed in MP-AES results. Based on previous studies, the higher leaching of Mg^{2+} ions reduces the size and enhances the irregular structure of amorphous c-HAp [50]. Although, the porous surface of the implant could be advantageous, since, it provides a channel for bone growth and also improves microscopic bio-resorptions [51]. The glasses with increasing

calcium (ESP) contents in CSE-2 and CSE-3 also showed spherical particles of apatite after 7 days of soaking in SBF. By analyzing the surface of the glasses; it seems that small chunks of glass particles were also present on them. Further, with an increase of the soaking period in SBF, the glasses CSE-2 and CSE-3 showed different morphology. The glasses CSE-2 and CSE-3 clearly showed the formation of the HAp layer which is more compact and sponge-like in appearance, covered the whole surface as observed in Figure 4.10 (f) and (i), respectively. This corresponds to the introduction of CO_3^{2-} ions from SBF to the glass surface. The same morphology of the amorphous c-HAp layer has also been reported for conventional chemical-based bioglasses [52]. The presence of carbon (%) 0.10 %, 0.24 %, and 0.33 % in CSE-1, CSE-2, and CSE-3 glasses for 28, 21, and 14 days of soaking in SBF, respectively, are confirmed by carbon hydrogen nitrogen sulfur and oxygen elemental (CHNSO) analysis. The representative EDS graphs of unsoaked and soaked glasses were given in Figure 4.11. The EDS graphs show the occurrence of Ca, P, C, Cl, and O after soaking in SBF. It also showed the other elements (Si, Na, Mg, K, Al, Ti, and Fe) which were inherited in glasses derived from agro-food wastes. The comparison of the Ca//P molar ratio for all glasses after 7-28 days of soaking in SBF is shown in Table 4.6. The Ca/P ratio is determined based on the peak intensity of the EDS spectra. The observed Ca/P molar ratio for all the glasses is greater (lie in the range of 1.78 to 4.10) than the standard stoichiometric Ca/P ratio of HAp (1.67) [37]. Based on an earlier *in-vitro* study using rice husk as a silica source reported the Ca/P molar ratio was as high as 2.8 for c-HAp [53]. It can be concluded that, due to the presence of Ca, other alkalies, alkaline earth metal oxides, and inherent trace elements in CHA, SCLA, and ESP increase the Ca/P ratio as compared to the standard stoichiometric ratio of Ca/P i.e., 1.67 reported for bioactive glasses.

4.7.7 Biocompatibility test

The biocompatibility assessment of the bioglasses CSE-1, CSE-2, and CSE-3 was performed by evaluating the viability of MG-63 osteoblast-like cell lines with MTT colorimetric assay. The MG-63 cell lines were exposed to various concentrations such as 1, 2, 5, and 10 mg/ml followed by 24 h incubation as shown in Figure 4.12. All bioglasses have shown cell proliferation in comparison to control (0 mg/ml) up to 5 mg/ml. The maximum viability has been observed at a lower concentration of 1 mg/ml (127.48 %) followed by 2, 5 mg/ml concentrations. However, at 10 mg/ml concentration, there has a reduction in the cell viability compared to other concentrations. However, cell viability is > 90 %, even at a higher concentration of bioglass. The International Organization for Standardization (ISO10993-5) suggests that the substance can be identified as cytotoxic when more than 30 % of the cell viability is lost [54].

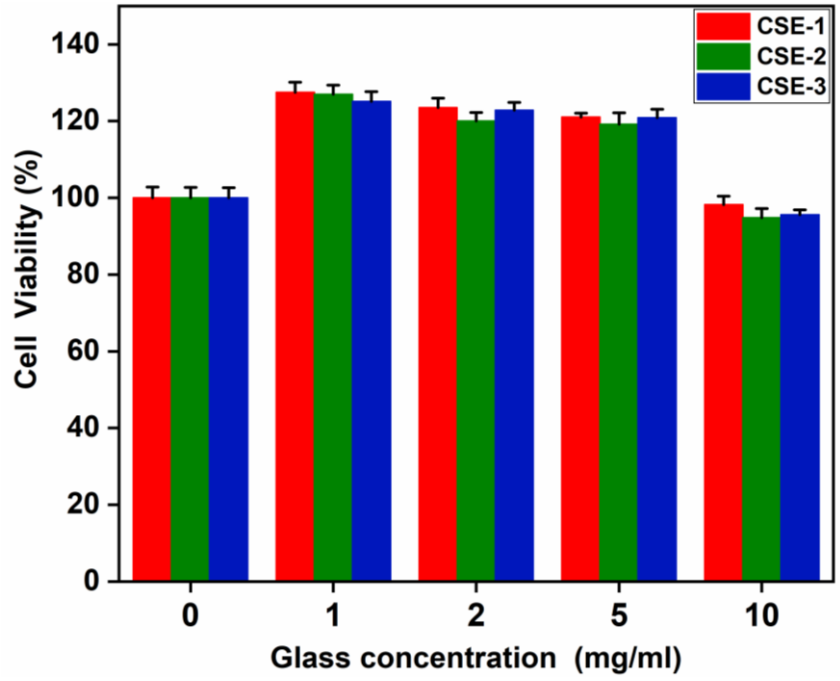

Figure 4.12 Cell growth effect of CSE-1, CSE-2, and CSE-3 glasses on human osteoblast-like (MG-63) cell lines. Cells without any treatment represent 0 mg/ml. Each experiment was performed in triplicate. The bar shows the treatments on MG-63 cells are not significantly different at $P<0.05$

Thus, it is obvious that the bioglasses CSE-1, CSE-2, and CSE-3 are non-toxic. These results agreed with earlier reported results for conventional chemical-derived mesoporous nano bioactive glasses via the MTT test [55, 56].

4.8 Effect of WSA on various properties

As discussed above, the SCLA is replaced by WSA in the glass composition to study the effect of WSA on various properties of glasses.

4.8.1 Chemical analysis of as-prepared samples

EDS analysis was carried out to determine the elemental composition in wt % of as-prepared samples from CHA, WSA, and ESP as shown in Table 4.7. When WSA is replaced instead of ESP, the glass former Si decreases and the Ca content increases demonstrating systemic variation as observed for the base glass. Another glass former P has not shown much variation with respect to ESP. The modifiers K, Mg, and Na exhibit a decreasing trend in chemical composition. But, the concentration of K increased from ~ 5 to 12.55 wt % when WSA replaced the SCLA in the base glass. Other transition metals such as Ti and Fe are also present. But, the presence of these elements in the glass composition is not showing any trend.

Table 4.7 The EDS analysis (wt %) of CWE-1, CWE-2, and CWE-3 samples with an indication of mean ± standard deviation (n=3)

Sample label	Si	Ca	P	Mg	K	Al	Na	Fe	Ti	O
CWE-1	22.52	8.43	1.50	4.80	12.55	5.29	1.12	1.25	0.63	41.90
	±0.72	±0.63	±0.61	±0.39	±0.48	±0.55	±0.15	±0.14	±0.17	±0.12
CWE-2	20.86	14.58	1.37	4.20	10.24	6.34	0.98	0.34	0.15	40.94
	±0.48	±0.86	±0.60	±0.56	±0.74	±0.11	±0.19	±0.61	±0.02	±0.21
CWE-3	17.68	16.48	1.07	3.60	8.10	10.76	0.64	0.59	0.28	40.80
	±0.56	±0.58	±0.72	±0.62	±0.21	±0.33	±0.21	±0.41	±0.06	±0.24

Surprisingly, Al has also present in all the samples same as base glass and CSE glasses. The CWE-3 sample has the largest concentration of Al. It has been observed that the propensity of Al diffusion from the crucible increases as the ESP content increases. It has been observed that Al_2O_3 tends to be more reactive than typical oxides of SiO_2 and CaO [45]. It might be due to the lower particle size of agro-food waste ashes than used minerals for glass formation [1]. Here, Al contents also show an increasing trend. In comparison to CSE glasses, the WSA glasses are more reactive towards the alumina crucible.

4.8.2 Physical properties

The value of apparent density for samples CWE-1, CWE-2, and CWE-3 is 2.39, 2.73, and 2.81 g/cc, respectively. The density of the present samples has shown a higher value for samples CWE-2 and CWE-3 than the sample CWE-1. It indicates that on replacing SCLA with WSA, the network becomes more closely packed that increase the density. However, density has decreased for sample CWE-1 in comparison to glass CSE-1. In sample CWE-1, K contents > Ca contents in comparison to base glass (Table 4.7). This might be due to the presence of higher K contents, which also acted as a modifier. It shortens the bond chain length and formed NBOs. However, K has a higher ionic radius and lower field strength than Ca. Therefore, K contents lead to an increase in the size of the interstices of the glass network and increase the free volume of the network which decreases the density [57]. The similar results have also been reported for composition $(20\text{-}x)Na_2O\text{-}xK_2O\text{-}10CaO\text{-}70SiO_2$ (where, x= 0, 5,10, and 20 in mol %) of conventional chemical derived glasses [58]. The density of conventional glasses decreases from 2.52 to 2.49 g/cc with an increase of K_2O contents. On the other hand, $20Na_2O\text{-}(10\text{-}x)$ $CaO\text{-}xBaO\text{-}70SiO_2$ (x= 0, 5, 10 in mol%), the values of density increases from 2.52 to 2.84 g/cc with increase of CaO contents [58]. The results indicate that the agro-food wastes derived

(SCLA and WSA) samples have shown lower values of density in comparison to conventional chemical-derived glasses.

4.8.3 XRD analysis

Figure 4.13 shows the XRD patterns of all as-prepared samples. After replacing SCLA with WSA, the amorphous nature in similar conditions show a better and well-resolved one halo. The absence of sharp diffraction peaks and the presence of a broad hump confirmed the amorphous nature of these samples.

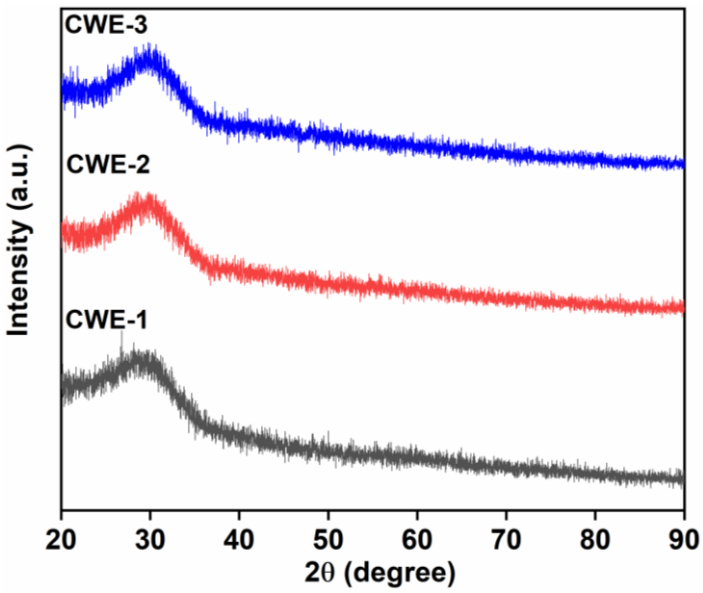

Figure 4.13 XRD patterns of as-quenched samples in which WSA used as a major component

4.8.4 FTIR analysis

FTIR spectra of all the samples showed transmittance bands in the wavenumber region from 458-3434 cm^{-1} given in Figure 4.14. The bands appeared at 3434 cm^{-1}, 1732 cm^{-1}, and 1624 cm^{-1} that may be due to the H_2O molecules and bending vibrations of OH bonds [59]. The most intense and broad band at 1014 cm^{-1} corresponds to stretching vibrations of $Si\text{-}O^-$ the bond of the silica network observed for sample CWE-1. This band shifts toward the lower wavenumber side at 1011 cm^{-1}, and 987 cm^{-1} for samples CWE-2 and CWE-3 on replacing ESP at the cost of WSA. This is due to the presence of network modifiers that depolymerize the glass network

and formed NBOs or terminal oxygens that change the glass structure. The sample CWE-3 has a band at 987 cm^{-1} corresponding to $Si\text{-}O^-$ asymmetric stretching vibrations at Q^2 sites that form Si-O-Al linkages. Another band 705 cm^{-1} attributed to bending vibrations of the Si-O-Si and Si-O-Al bond involving bridging oxygen (BO). This band also shifted towards lower wavenumbers 695 cm^{-1} for sample CWE-3 as shown in Figure 4.14 (b).

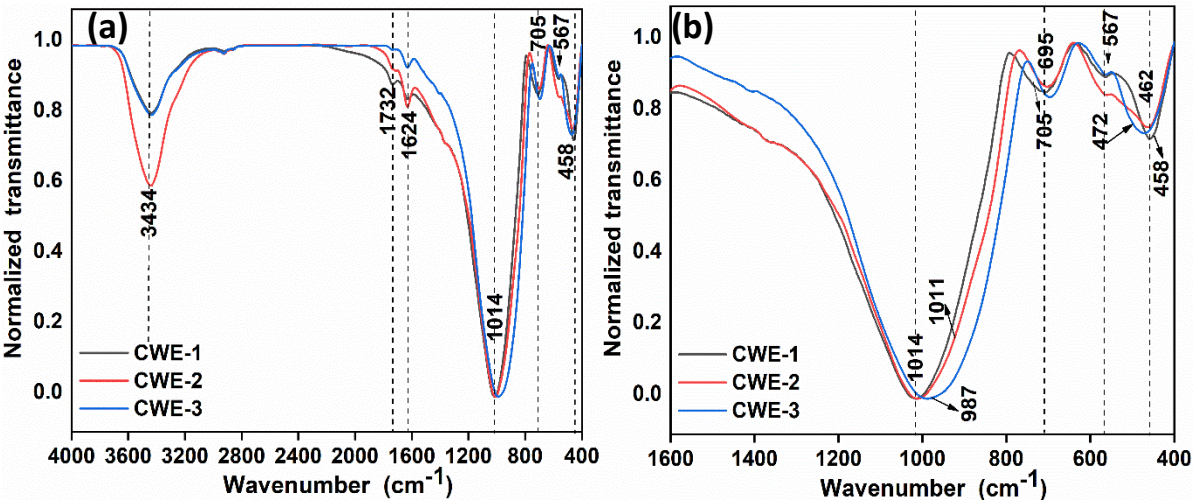

Figure 4.14 Normalized FTIR spectra of (a) CWE-1 to CWE-3 samples. Figure (b) is the magnified image of (a) which shows the proper shifting of bands

A similar band is observed at 695 cm^{-1} for a conventional chemical-derived glass composition ($39SiO_2$-$12Al_2O_3$-$10MgO$-$12K_2CO_3$-$6.6CaO$-$20MgF_2$-0.4 CNT in mol%) is attributed to the symmetric stretching vibration mode of Si-O-(Si-Al) in AlO_4 tetrahedra (4-fold coordination) [54]. It indicated the substantial formation of AlO_4 structural units [60]. Another band 567 cm^{-1} attributed to asymmetric bending vibrations of O-P-O bonds observed for all CWE samples [61]. However, in the CSE glasses, the P-O bonds diminished with an increase of Ca contents. However, in the WSA series, it has not been observed. It has also been supported by EDS analysis (Table 4.7). The band at 458 cm^{-1} corresponds to bending vibrations of silica tetrahedra that formed glass network shifted towards higher wavenumbers particularly bands at 462 cm^{-1} and 472 cm^{-1} for samples CWE-2 and CWE-3, respectively. This indicated that the silica

network strengthens in these samples in comparison to CSE glasses. According to literature, it has been reported that the lower frequency bands (400-600 cm^{-1}) shifted towards higher wavenumber with increasing Al contents in the conventional chemical-based composition of silver alumina phosphate glasses [62]. Here, Al plays the role of glass former (AlO_4). This also showed that some of the alumina oxides as a glass former can form BO with NBOs in the phosphate network and form Al-O-P bonds [63]. An increase of this type of bond may lead to shifting to a higher wavenumber side with decreasing NBOs concentration in the glasses. In the present study, a similar range of bands shifted towards the higher wavenumber side, is due to the relative change in the strength of the chemical bonds by the change in the glass composition in comparison to base glass. The results indicated that on replacing SCLA with WSA, the CWE-2 and CWE-3 samples are less depolymerized of silica-phosphate network in comparison to CSE glasses.

4.8.5 Hardness analysis

The microhardness of the samples was determined to check the change in their mechanical properties with the replacement of SCLA by WSA in the base glass. The microhardness of the samples CWE-1, CWE-2, and CWE-3 is 5.34, 6.39, and 6.47 GPa, respectively. The value of hardness shows an increasing trend. It might be due to the dominant formation of AlO_4 at a higher concentration of Al as discussed earlier in FTIR results. Similar results have also been observed for conventional chemical-derived calcium alumina phosphate glasses, the addition of a higher concentration of alumina acts as the former, leading to an increase in the degree of network connectivity and average bond strength. It increases the hardness, therefore hardness of sample CWE-3 is higher than CWE-2 and CWE-1 samples [62, 64]. However, in comparison to CSE glasses, the overall value of hardness has lower for CWE-1 and higher for CWE-2 and CWE-3 glasses. Conventional chemical-derived silica glasses containing K_2O or CaO as

modifiers have shown the value of Vickers hardness lies in the range of 5.49 GPa to 7.29 GPa, which is higher than the agro-food wastes derived samples [58].

4.8.6 DSC analysis

When WSA is replaced with ESP, it can observe from the graph (Figure 4.15) that the glass transition temperature (T_g) for the glass samples CWE-1, CWE-2, and CWE-3 increased with the increasing percentage of ESP content. It is in the range of 695 to 752 °C. It indicated that the increase of T_g means there is an increase in the strength of the glass network. The increase in T_g as the Si contents decrease (22.52 to 17.68 wt %) indicates that there is also the presence of alumina in a higher concentration that formed tetrahedral coordination [25]. It also plays a similar role to the silica part i.e., the network former. This result also supports the FTIR results. But, in comparison to base glass i.e., SCLA replaced by WSA, the value of T_g is lower for glass CWE-1 in comparison to CSE glasses and higher for CWE-2 and CWE-3 glasses. These results also agreed with the results of the hardness and density of these glasses. Further the single crystallization temperature (T_c) at 956 ^oC observed for the glass CWE-1. The value of T_c is higher than the CSE-1 glass. This might be due to the presence of higher K > Ca contents that promoted the formation of glass and suppressed the tendency of separation into immiscible phases. Similar, results have been reported for conventional chemical-derived Li_2O-SiO_2-K_2O glasses [65]. When further ESP is replaced at the cost of WSA, the K contents decrease, and Ca contents increases (Table 4.7). The DSC curves show two exothermic peaks for glass CWE-2 and CWE-3. Two exothermic peaks indicated that there might be heterogeneity in glass due to the separation exhibited by two matrices. The primary crystallization occurs at 903 ^oC and 896 ^oC for CWE-2 and CWE-3 followed by secondary crystallization at higher temperatures 1014 ^oC and 1010 ^oC (Table 4.8). Further two endothermic peaks around 1075-1190 ^oC ascribed to the melting of crystalline phases precipitated the heating of glasses. It has also been observed

that as the alumina contents increased in the glasses CWE-2 and CWE-3, the value of T_c and T_m decreases. Similar results have been reported for a conventional chemical-derived calcium alumina silicate glasses (44.6SiO_2-18.1Al_2O_3-13CaO-9.8MgO-2.1TiO_2-2.4K_2O-1.0 Na_2O) in wt % that show phase-separation when held at low temperature below its melting point <1600 ^oC and show a decrease of T_c and T_m with an increase of alumina contents (22 wt % Al_2O_3) [66]. Similar behavior can be suspected for WSA glasses as they are more reactive to alumina contents in comparison to SCLA glasses. The value of T_c and T_m decreases for CWE glasses in comparison to CSE glasses.

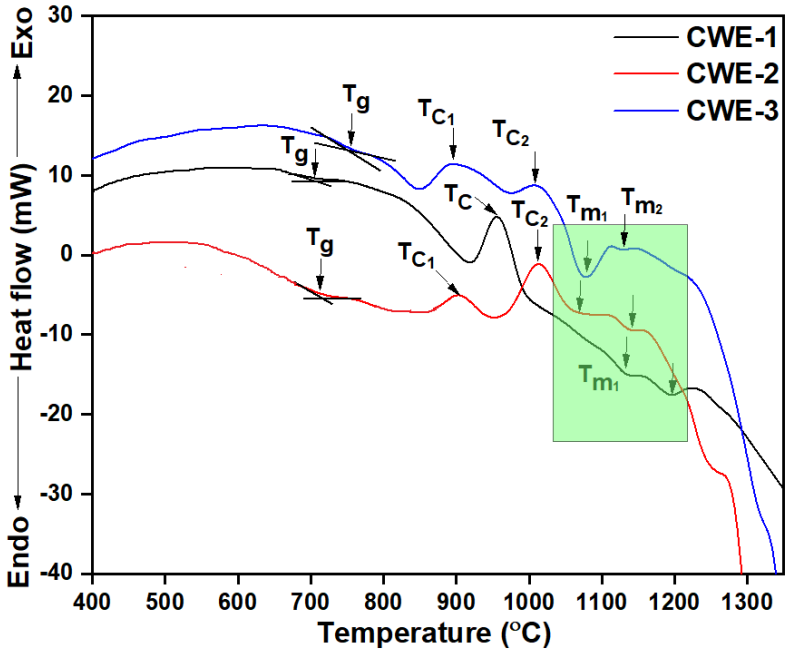

Figure 4.15 (a) DSC curves for glasses CWE-1, CWE-2, and CWE-3, thermal signals showing the glass transition (T_g), crystallization temperature (T_c), and melting temperature (T_m)

Table 4.8 T_g, T_c, and T_m of the CWE-1, CWE-2 and CWE-3 glasses

Sample	T_g (°C)	T_{c1} (°C)	T_{c2} (°C)	T_{m1} (°C)	T_{m2} (°C)	K_H Parameter
CWE-1	695	956	-	1133	1192	1.48
CWE-2	726	903	1014	1075	1140	1.09
CWE-3	752	896	1010	1078	1129	0.78

It may also be due to the presence of mixed modifiers that changes T_c values which also depend on the modifier concentrations [67]. Here, the lowest crystallization peaks of glasses CWE-2 and CWE-3 has considered for calculating the glass stability. Because once crystallization occurred, subsequent events at a higher temperature, glass stability is not affected [68]. The glass CWE-1 has shown more glass stability in comparison to other glasses as given in Table 4.8. Similar results have been reported for conventional chemicals-based silica-phosphate glasses that contain a higher amount of K_2O and exhibit higher stability [69]. It can be concluded from the above results that the CWE-based synthesized glasses become heterogenous and phase-separated with an increase of ESP contents at the cost of WSA in comparison to SCLA (CSE) glasses.

4.9 Assessment of bioactivity (*In-vitro*)

4.9.1 Weight change and pH variation of glasses soaking in SBF

The weight change of the glasses due to the release or gain of basic (Ca^{2+}, Mg^{2+}, Na^{+}, K^{+}) and acidic (Si^{4+}, P^{5+}) ions from soaked glasses to SBF is shown in Figure 4.16 (a). After soaking in SBF for 7 days, glasses have shown weight loss in the order of CWE-2 > CWE-1> CWE-3. Glass CWE-2 has released more ions such as Ca^{2+}, K^{+}, and Mg^{2+}, Na^{+} in SBF, causing more weight loss in the initial stage of soaking. However, CWE-based glasses have shown maximum weight loss of up to 7 % which is lower than the CSE glasses. The CWE glasses have also shown opposite order in weight loss in comparison to CSE glasses (CSE-3>CSE-1>CSE-2). After 14 days of soaking in SBF, the glasses CWE-1 and CWE-2 gained weight, due to the deposition of ions on the glass surface from SBF [70]. Furthermore, these glasses showed little variation in weight gain as observed for CSE glasses. On the other hand, the glass CWE-3 has shown fewer variations throughout the experiment. These results also agreed with the results

of pH variations that gave information on the exchange of ions between glass and SBF. Figure 4.16 (b) shows that after 7 days of soaking the glasses in SBF, the maximum pH of glasses CWE-1, CWE-2, and CWE-3, changes from 7.4 to 7.8, 8.1, and 7.5, respectively.

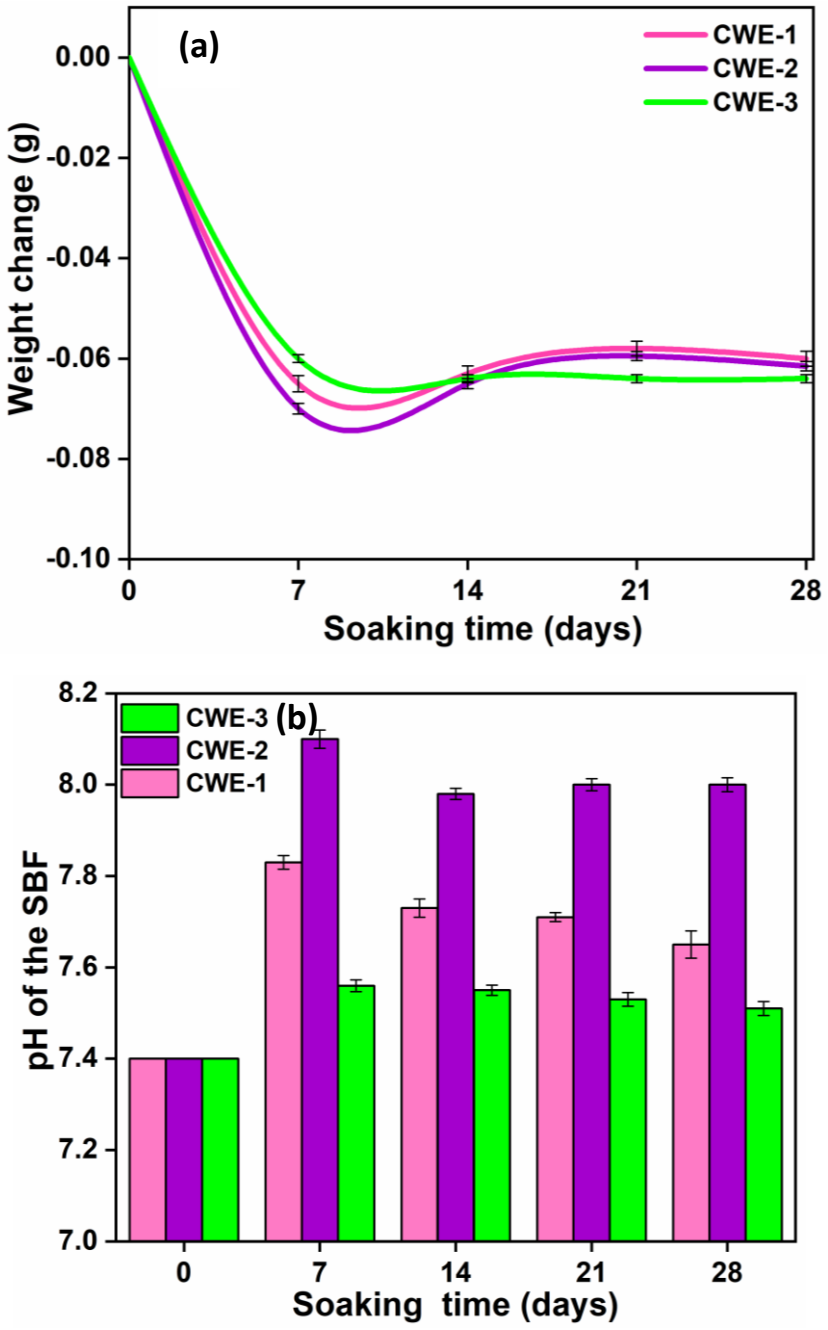

Figure 4.16 (a) The weight loss of CWE1, CWE-2, and CWE-3 glasses during soaking time (0, 7, 14, 21, and 28 days) in SBF solution (b) pH variations of SBF solution containing all glasses with different soaking times as the initial value of pH at 7.4. The error bars denoting the standard deviation (as mean ± SD, n=3)

But, the release of Al contents is slightly higher in the glass CWE-3 in comparison to CSE-3 glass. Furthermore, with an increase in soaking time, the values slightly decreased by 0.1-0.2 up to 28 days of soaking the glass in SBF. These results showed the opposite behavior to CSE glasses. This might be due to the increased acidic nature of SBF i.e. due to the incorporation of more phosphoric ions from SBF onto glass surfaces [8]. Tripathi et al. [71] reported similar pH behavior of SBF after soaking the CBG in SBF for up to 28 days. The results exhibited that the maximum pH value reached 9.72 after 3 days and then decreased for the next 28 days, confirming the formation of the HAp layer on the CBG. It can be concluded from the above results, that the pH change and weight loss in the CWE glasses are lower than in the CSE and conventional chemical-derived glasses due to the release of lesser ions from CWE samples to SBF.

4.9.2 MP-AES analysis

Table 4.9 compares the concentrations of Si^{4+}, Ca^{2+}, Mg^{2+}, K^{+}, Na^{+} ions, and other trace elements in the SBF solution before and after 28 days of sample soaking. After 28 days of soaking, the release of K^{+}, $Na^{+,}$ and Mg^{2+} ions in glass CWE-2 are higher in comparison to other glasses. The value of Si^{4+} ions in the SBF solution was observed for glasses in the order of CWE-2 > CWE-1 > CWE-3. These results are also in the same line as the results of weight loss and pH variations in the soaked glasses. However, the values of Si^{4+} and Mg^{2+} ions in the SBF are lower in comparison to the CSE glasses. It has been noted that Ca^{2+} ions are also released from all the glasses. Only glass CWE-1 has lower Ca^{2+} ions compared to other glasses. The decrease in the Ca^{2+} ions in SBF is attributed to the rapid growth of the apatite nuclei formed on the surface of the glass that overcame the release rate of Ca^{2+} ions to the solution [24]. From Table 4.9, it has also been observed that the leaching of other ions such as Ti, Fe, and Al from the samples into the SBF solution is negligible same as observed for CSE glasses.

Table 4.9 Si, Ca, Mg, K, Na, Al, Ti, and Fe ions concentration in SBF after 28 days of soaking. The results are taken by mean ± standard deviation (mg/l, n=3)

Label	Si	Ca	Mg	K	Na	Al	Ti	Fe
Reference SBF	-	117 ±1.5	61.8 ±2.2	207 ±2	2890 ±5	-	-	-
CWE-1	33.2 ±1.3	95.6 ±0.8	84.5 ±1.1	382 ±2	3519 ±4	<0.01 ±0.00	0.68 ±0.02	<0.01 ±0.00
CWE-2	38.8 ±1.1	245 ±1	148 ±3	488 ±3	3657 ±10	<0.01 ±0.00	0.65 ±0.02	<0.01 ±0.00
CWE-3	5.95 ±1.5	119 ±2	56.8 ±0.24	236 ±2	3256 ±8	0.78 ±0.11	0.62 ±1.1	<0.01 ±0.00

It also affects the leaching of the other ions into the SBF solution and improves the durability in neutral solution [12, 72]. Some studies also exhibited that the formation of Al-OH bonds on the conventional chemical-derived glass surface inhibits the apatite formation [67]. It reduces the concentration of silanol groups on the glass surface (which act as nucleating centers for apatite formation) [71, 73]. The lack of silanol (Si-OH) groups on the sample surface prevents HAp formation. It can be concluded that the effect of Al in the CWE-3 glass strengthens the glass network and induces enrichment of Al-OH groups at the surface of glass upon exposure to SBF, thus suppressing the HAp formation. It can be concluded from the above results that the CWE glasses have shown a lower exchange of ions between the glass surface and SBF in comparison to CSE glasses.

4.9.3 XRD analysis

The XRD patterns of soaked and unsoaked glasses are given in Figure 4.17 (a-c). XRD patterns of all the glasses didn't show any remarkable changes after soaking for a different time period

in SBF. These changes in comparison to virgin glass could be associated with amorphous HAp [74]. However, in the base (CSE) glass few weak diffraction peaks were observed after soaking in SBF, but in the WSA series, it has not been observed.

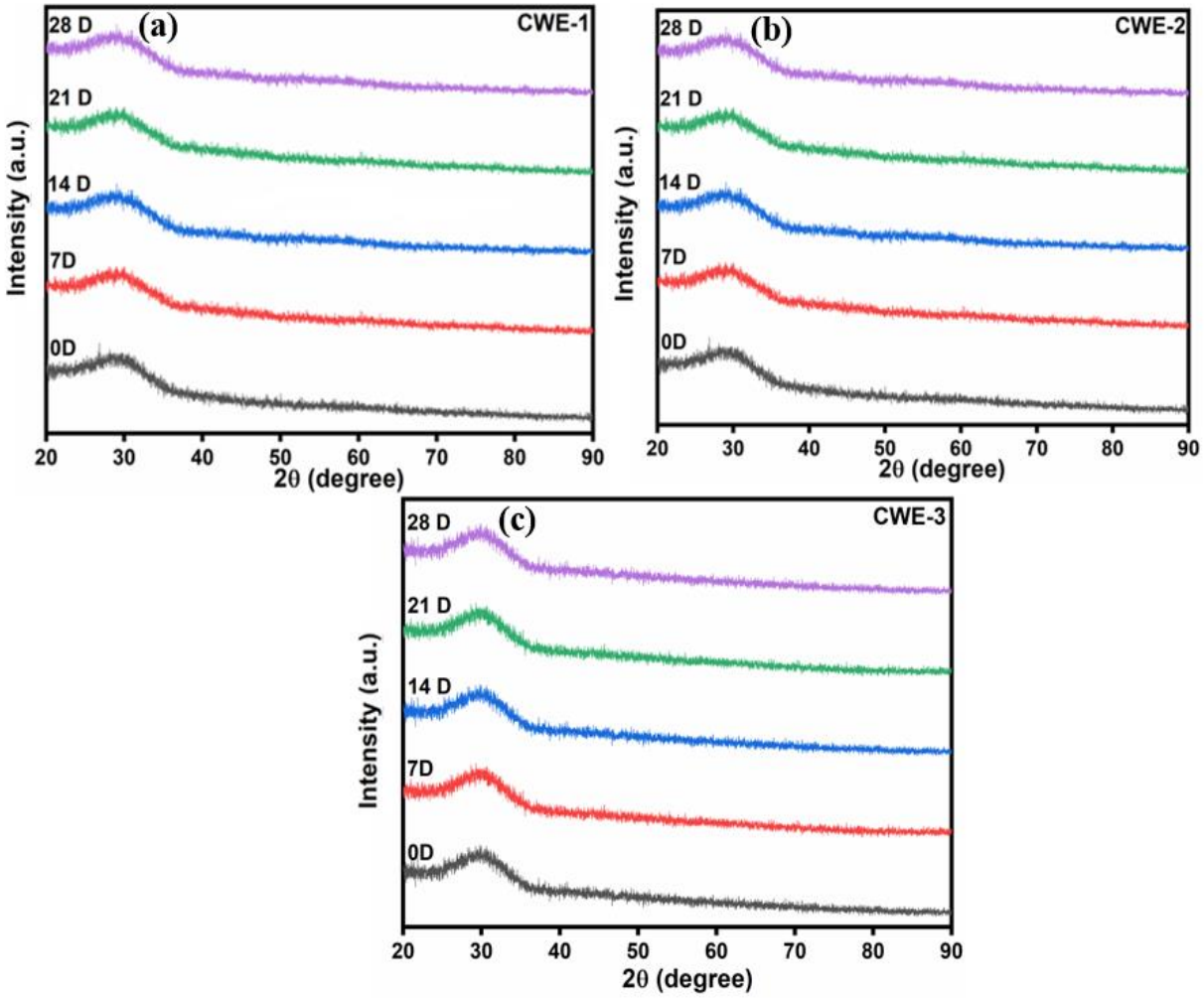

Figure 4.17 XRD patterns of unsoaked and soaked glasses (a) CWE-1, (b) CWE-2, and (c) CWE-3

4.9.4 FTIR analysis

FTIR spectra of all glasses soaked in SBF are shown in Figure 4.18 (a-f). The band is observed for glass CWE-1, and CWE-2 at 458 cm^{-1} and 462 cm^{-1}, respectively. It corresponds to bending vibrations of Si-O-Si bonds shifted towards the lower wavenumber side i.e., 456 cm^{-1} after soaking in SBF up to 28 days in comparison to CWE-3 glass.

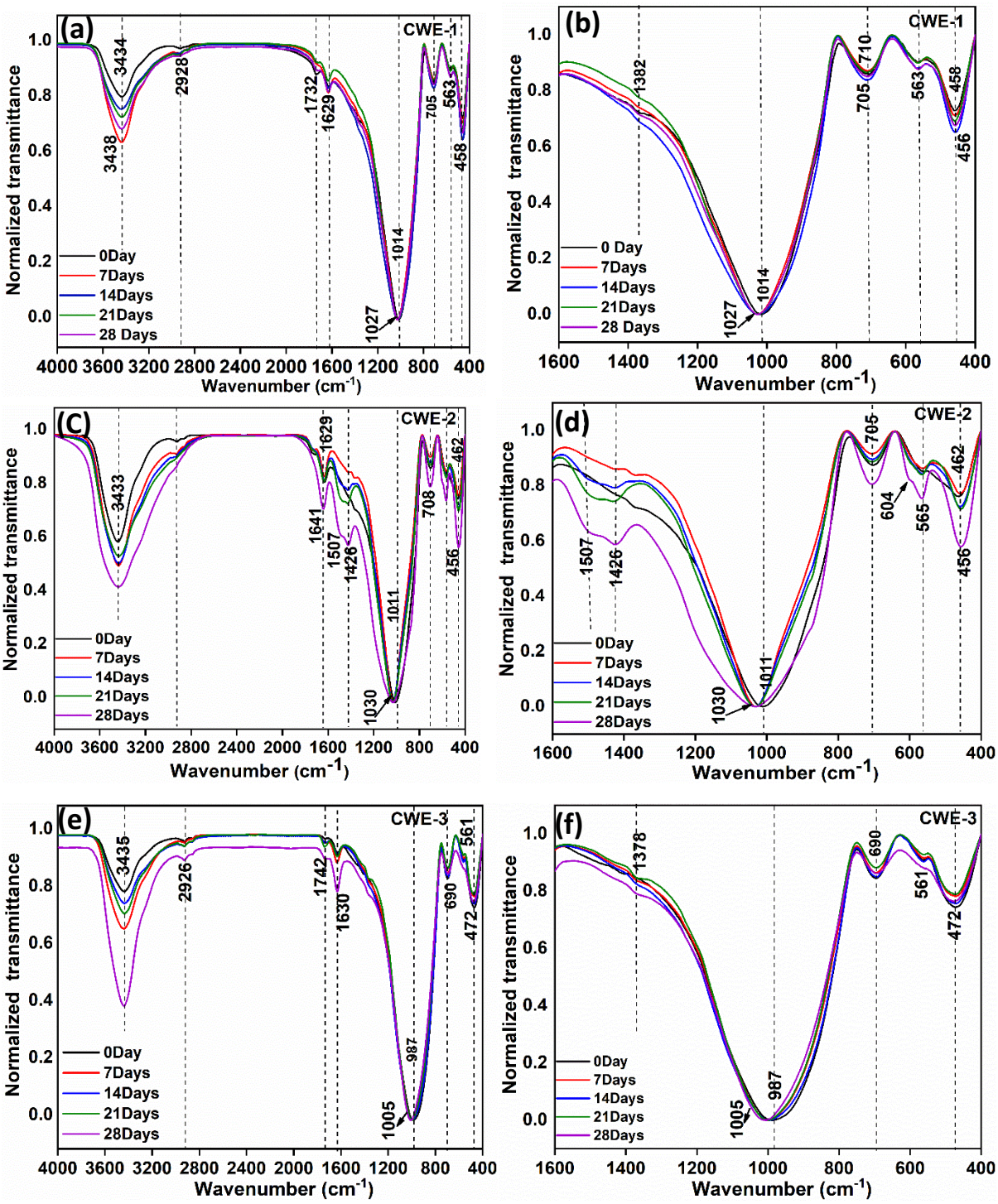

Figure 4.18 Normalized FTIR spectra of (a) CWE-1, (C) CWE-2, and (e) CWE-3 glasses before (0 day) and after soaking in SBF for 7, 14, 21, and 28 days. Figure (b), (d), and (f) are the magnified images of (a), (c), and (e) which shows the proper shifting and appearance of new bands

This showed a weakening of the glass structure due to physicochemical reactions that took place between glass and SBF. This confirmed the formation of a silica-rich layer [70]. These results also supported the MP-AES results. Furthermore, glass CWE-2 has shown new bands at 565 and 604 cm^{-1} are attributed to bending vibrations of the P-O bond after 14 to 28 days of soaking in SBF [75]. Similar bands have also been observed for glass CSE-3 and CSE-2 after 7 and 14 days of soaking in SBF, respectively. This confirmed the precipitation of the Ca-P layer on the glass surfaces. However, the band at 604 cm^{-1} is not observed in the glass CWE-1 and CWE-3 after soaking in SBF. The major and intense band 1014 cm^{-1} shifted towards the higher wavenumber i.e., 1026 cm^{-1} for glass CWE-1 and 1032 cm^{-1} for glass CWE-2 after soaking in SBF for 7 to 28 days. Similar results have also been reported for the CBGs, the P-O groups of vibrational bands also appeared near 1025-1032 cm^{-1} that confirming the formation of the Ca-P layer on the surface of CBG [24, 70]. The band at 987 cm^{-1} showed a slight shift towards higher wavenumber 1005 cm^{-1} for glass CWE-3 up to 28 days of soaking in SBF. These bands are attributed to the symmetric stretching vibrations of Si-O-Si and vibrations of silicon rings [60, 76]. The band 1629 cm^{-1} and 1732 cm^{-1} due to H_2O molecules also shifted towards the higher wavenumber side 1641 cm^{-1} and 1742 cm^{-1} for glass CWE-2 and CWE-3 in comparison to glass CWE-1. The intensity of the band 3433 cm^{-1} has also increased with the increase of soaking time in SBF after 7 days and 28 days for glass CWE-2 and CWE-3, respectively. The other bands 1426 and 1507 cm^{-1} which are attributed to stretching vibrations of the C=O group only observed for glass CWE-2 after soaking in SBF for 14 days. Similar bands have also been observed for CSE glasses after soaking in SBF for 14 days. But, these bands are more pronounced in CSE glasses in comparison to glass CWE-2. In comparison to CSE glasses, CWE-3 glass has not shown precipitations of Ca-P layer on the glass surface.

4.9.5 FESEM with EDS analysis

The FESEM micrographs of glasses CWE1 to CWE-3 before and after soaking in SBF are shown in Figures 4.19 (a) to (i). The FESEM of all glasses are distinct from each other (Figure (a)-(c)). CWE-1 and CWE-2 glasses have shown white-colored flakes like precipitates adhered on the glass surfaces after soaking in SBF for 7 days. These flakes like precipitates covered the whole surface of the glasses. As the soaking time increases for 28 days, the flakes become dense on the glass surface CWE-2 as shown in Figure 4.19 (f).

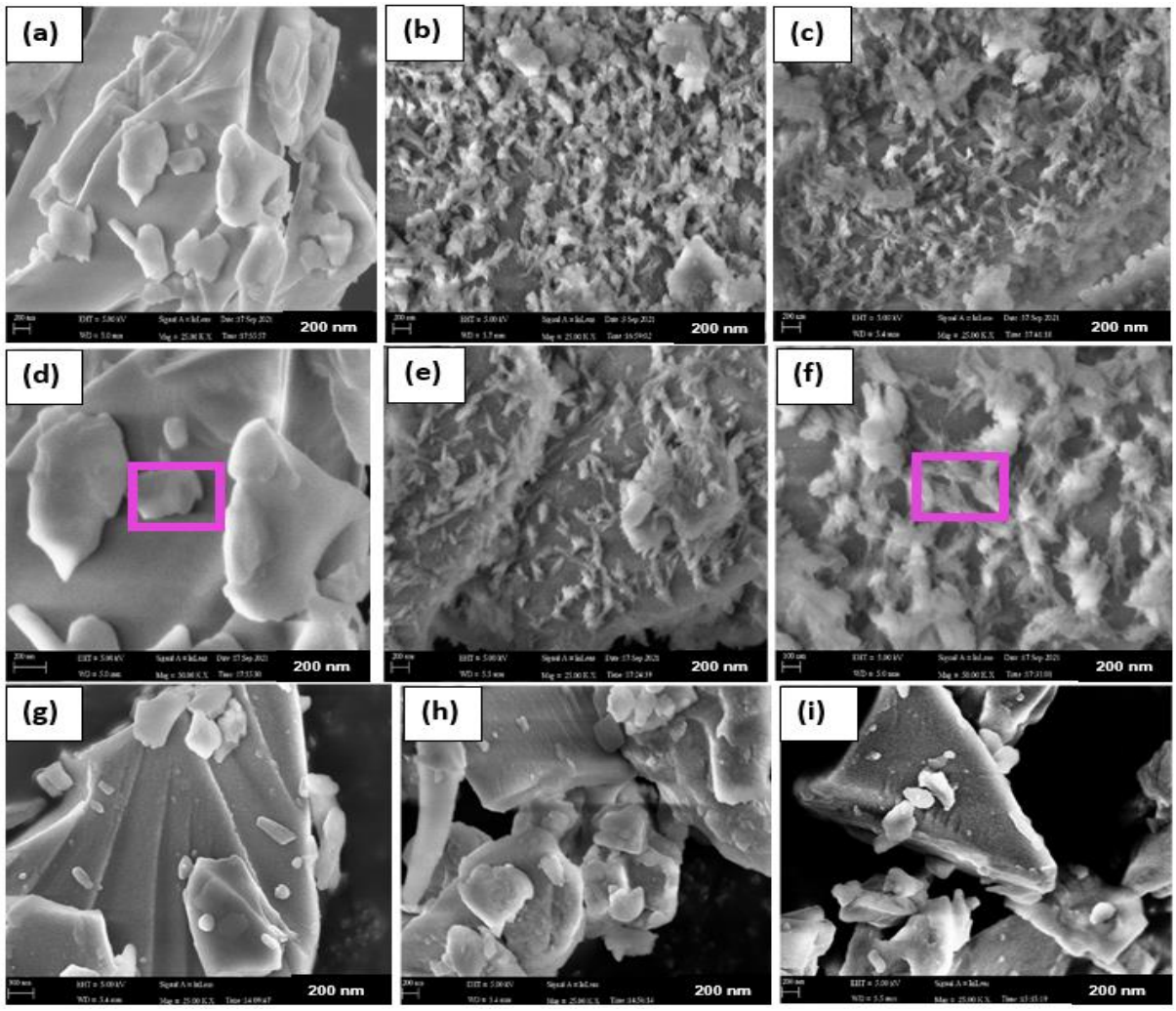

Figure 4.19 FESEM images show the development of the hydroxyapatite layer on the surface of bioactive glasses at a different soaking time in SBF. Representative FESEM images of unsoaked glasses (a) CWE-1, (d) CWE-2, (g) CWE-3 and for soaked glasses (b) 7 days of CWE-1, (c) 28 days of CWE-1, (e) 7 days of CWE-2, (f) 28 days of CWE-2, (h) 7 days of CWE-3 and (i) 28 days of CWE-3

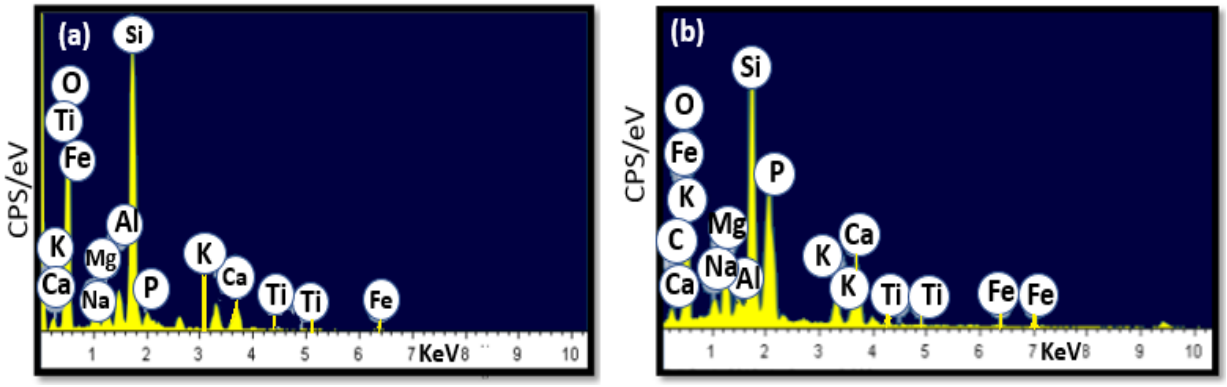

Figure 4.20 Representative EDS spectra of (a) unsoaked glass CWE-2 and (b) soaked glass CWE-2 after 28 days of soaking in SBF

Table 4.10 The glasses CWE-1, CWE-2, and CWE-3 after soaking in SBF for 7,14, 21 and 28 days show the values of Ca and P (wt %) and Ca/P (molar ratio) with an indication of mean ± standard deviation (n=3)

Days of soaking in SBF	**CWE-1**			**CWE-2**			**CWE-3**		
	Ca	**P**	**Ca/P**	**Ca**	**P**	**Ca/P**	**Ca**	**P**	**Ca/P**
7 days	13.35 ±0.35	2.32 ±0.54	4.46 ±0.14	10.97 ±0.65	2.29 ±1.13	3.85 ±0.34	12.42 ±0.04	2.05 ±0.25	4.68 ±0.42
14 days	11.66 ± 0.72	2.40 ±0.34	4.91 ±0.08	11.07 ±0.28	2.27 ±0.65	3.78 ±0.12	14.91 ±0.06	2.41 ±1.23	4.74 ±0.11
21 days	8.19 ±0.65	2.58 ±0.45	2.53 ±0.3	13.49 ±0.27	3.41 ±0.69	3.06 ±0.17	12.30 ±0.73	2.43 ±0.41	4.39 ±0.15
28 days	7.07 ±0.71	2.71 ±0.51	1.91 ±0.43	6.01 ±1.73	2.78 ± 0.11	1.69 ±0.39	11.08 ±0.51	2.02 ±0.18	4.61 ±0.64

The glasses CWE-1 and CWE-2 clearly showed some changes on the glassy surface. It could be associated with the HAp layer. Similar results were observed for conventional chemical-based derived nano HAp powder scaffolds [77]. It has also been noted that when SCLA is replaced with WSA in the base glass, the sponge-like morphology of the HAp layer changed to flakes with soaking time. On the other hand, no change has been observed for glass CWE-3 as shown in Figure 4.19 (h and i). The FESEM results have also confirmed the FTIR and MP-AES

results. The representative EDS graphs of unsoaked and soaked glass CWE-2 has given in Figure 4.20. The Ca//P molar ratio of soaked glasses CWE-1, CWE-2, and CWE-3 after 7-28 days calculated from EDS data are tabulated in Table 4.10. In order to use the glass materials as implants, the ratio of Ca/P in the HAp layer developed on its glass surface must be greater than 1(for human bone the Ca/P ratio is 1.67) [78]. However, the Ca/P ratio of as-prepared glasses is evaluated to be in the range of 1.69 to 4.91 [77, 79]. The Ca/P ratio has been found higher for CWE glasses in comparison to CSE glasses on replacing the SCLA with WSA in the base glass. The Ca/P ratio of the CWE-3 glass has not shown much variation in comparison to the other two glasses due to the lower exchange of ions. It can be concluded from the above results that the glasses CWE-1 and CWE-2 are also bioactive as CSE glasses. But glass CWE-3 has not formed HAp on the glass surfaces after soaking in SBF.

4.9.6 Biocompatibility test

The biocompatibility of glass samples is determined by varying SCLA with WSA. The MG-63 cell lines are treated with different concentrations (1 to 10 mg/ml) of glass CWE-1, CWE-2, and CWE-3 for 24 h as shown in Figure 4.21. In this case, the glasses CWE-1 and CWE-2 on human osteoblast-like cells with nearly 85 % and 76 % viability has achieved even at a higher concentration of samples, i.e., 10 mg/ml, respectively. However, the cell viability of CSE glasses is higher than that of CWE glasses. On the other hand, the glass CWE-3 has shown cell viability of 90.8 % at lower concentrations i.e., 1mg/ml. With increase of concentration the cell viability has reduced 75 %, 71 % and 66 % at concentration 2 mg/ml, 5 mg/ml and 10 mg/ml, respectively. This might be due to the presence of a higher amount of alumina in the glass CWE-3. Tripathi et al. [71] have also shown > 80 % cell viability against MG-63 cell lines by varying the Al_2O_3 (0.5 to 2.5 mol %) amount in Li_2O-CaO-Al_2O_3-P_2O_5-SiO_2 CBG composition.

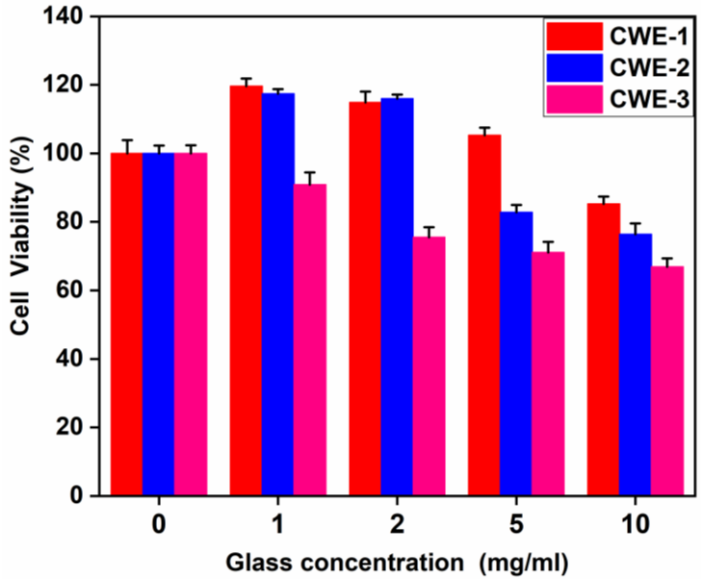

Figure 4.21 Cell growth effect of CWE-1, CWE-2, and CWE-3 glasses on human osteoblast-like (MG-63) cell lines. Cells without any treatment represent 0 mg/ml. Each experiment was performed in triplicate. The bar shows the treatments on MG-63 cells are not significantly different at $P<0.05$

The cell viability decreases with an increasing amount of Al_2O_3 beyond 1.5 mol %. Glasses CWE-1 and CWE-2 have been observed to be non-toxic with a good percentage of cell viability up to 10 mg/ml. But glass CWE-3 has become toxic at higher concentrations.

4.10 Summary

Agro-food wastes derived glasses show good bioactivity as reported for conventional chemical-derived glasses of similar glass compositions. WSA is more reactive than SCLA with recrystallized alumina crucible. The bioactivity of glasses decreases when SCLA is replaced by WSA in the glasses due to higher contents of K_2O in WSA. Phase separation and variations in characteristic temperatures of the glasses do not affect the bioactivity. SCLA glasses show sponge-like morphology of HAp which changes to flake types on varying SCLA with WSA. Initially, all glasses show Ca/P ratio is high as HAp is taken place it becomes less than ~ 2 in all the glasses. Cell viability is good in all the glasses except CWE-3 becomes toxic after a higher concentration

References

[1] G. Sharma, K. Singh, J. Mater. Cycles. Waste. Manag. 21 (2019) 801.

[2] A. Parsons, L. Burling, C. Rudd, C. Scotchford, G. Walker, J. Biomed. Mater. Res. Part B. 71 (2004) 22.

[3] D. Tulyaganov, K. Abdukayumov, O. Ruzimuradov, M. Hojamberdiev, E. Ionescu, R. Riedel, Mater. 10 (2017) 1324.

[4] B. Aktas, M. Albaskara, S. Yalcin, K. Dogru, Acta Phys. Pol. A. 132 (2017) 442.

[5] M. K. Chhina, K. Singh, Ceram. Int. 46 (2020) 9370.

[6] S. Singh, K. Singh, J. Mol. Struct. 1081 (2015) 211.

[7] P. Siriphannon, Y. Kameshima, A. Yasumori, K. Okada, S. Hayashi, J. Europ. Ceram. Soc. 22 (2002) 511.

[8] A. Balamurugan, G. Balossier, S. Kannan, J. Michel, A.H. Rebelo, J.M. Ferreira, Acta Biomater. 3 (2007) 255.

[9] A.M. Efimov, V.G. Pogareva, Chem. Geol. 229 (2006) 198.

[10] K. Singh, I. Bala, V. Kumar, Ceram. Int. 35 (2009) 3401.

[11] H.A. Mooghari, A. Nemati, B.E. Yekta, Z. Hamnabard, Ceram. Int. 38 (2012) 3281.

[12] J.E. Shelby, Introduction to Glass Science and Technology, 2nd ed.The Royal Society of Chemistry, UK 2005.

[13] G. Melinte, L. Baia, V. Simon, S. Simon, J. Mater. Sci. Mater. Electron. 46 (2011) 7393.

[14] R. Hussin, M.A. Salim, N.S. Alias, M.S. Abdullah, S. Abdullah, S.A.A. Fuzi, S. Hamdan, M.N.M. Yusuf, J. Fund. Appl. Sci. 5 (2009) 43.

[15] M. Handke, W. Mozgawa, M. Nocuń, J. Mol. Struct. 325 (1994) 129.

[16] R.M. Thomsen, J. Skibsted, Y. Yue, J. Phys.Chem. B. 122 (2018) 3184.

[17] A. Atila, S. Ouaskit, A. Hasnaoui, Ionic self-diffusion and the glass transition anomaly in aluminosilicates, Phys. Chem. Chem. Phys. 22 (2020) 17205.

[18] R. Smith, J. Phys. Chem. 60 (1956) 1293.

[19] S. Albert, K. K. Albert, H. Hollenstein, C.M. Tanner, M. Quack, J. Mass. Spectrom. 3 (2011) 117.

[20] M.M. Smedskjaer, M. Jensen, Y. Yue, J. Non-Cryst. Solids. 356 (2010) 893.

[21] B. Aktas, M. Albaskara, S. Yalcin, K. Dogru, Acta Phys. Pol. A. 13 (2017) 511.

[22] B. Aktas, M. Albaskara, K. Dogru, S. Yalcin, Acta Phys. Pol. A. 132 (2017) 436.

[23] R.B. Rao, R.A.J.M.C. Gerhardt, Physics, Mater.Chem.Phys. 112 (2008) 186.

[24] P. Jha, K. Singh, Ceram. Int. 42 (2016) 436.

[25] L.Cormier, D.R. Neuville, G. Calas, J. Am. Ceram. Soc. 88 (2005) 2292.

[26] M. Bouhadja, N. Jakse, A. Pasturel, J. Chem. Phys. 140 (2014) 234507.

[27] J. Jiusti, E.D. Zanotto, S.A. Feller, H.J. Austin, H.M. Detar, I. Bishop, D. Manzoni, Y. Nakatsuka, Y. Watanabe, H. Inoue, J. Non-Cryst. Solids. 550 (2020) 120359.

[28] R. Joshi, R.Chhibber, Ceram. Int. 44 (2018) 19084.

[29] Y. Fan, F. He, Z. Li, Z. Li, W. Zhang, J.C.S. Xie, Ceram. Sil. 65 (2021) 334.

[30] A. Cabral Jr, C. Fredericci, E. Zanotto, J. Non-Cryst. Solids. 219 (1997) 182.

[31] J. Ma, C. Chen, D. Wang, Y. Jiao, J. Shi, Colloids Surf. B. 81 (2010) 87.

[32] V. Lalzawmliana, A. Anand, V. Kumar, P. Das, K.B. Devi, J. Mukherjee, A.K. Maji, B. Kundu, M. Roy, S.K. Nandi, J. Mech. Biomed. Mater. 91 (2019) 182.

[33] R. Zia, M. Riaz, S. Maqsood, S. Anjum, Z. Kayani, T. Hussain, Ceram. Int. 41 (2015) 8964.

[34] L.L. Hench, R.J. Splinter, W. Allen, T. Greenlee, J. Biomed. Mater. Res. Part B. 5 (1971) 117.

[35] L.L. Hench, I.D. Xynos, J.M. Polak, J. Biomater. Sci. 15 (2004) 543.

[36] M. Majhi, R. Pyare, S. Singh, Int. J. Sci. Eng. Res. 2 (2011) 154.

[37] R. Bruckner, M. Tylkowski, L. Hupa, D.S. Brauer, J. Mater. Chem. B. 4 (2016) 3121.

[38] H. El Batal, E. Khalil, Y. Hamdy, Ceram. Int. 35 (2009) 1195.

[39] J. Knowles, K. Franks, I. Abrahams, Biomater. 22 (2001) 3091.

[40] K. Thind, K. Singh, G. Sharma, V. Rajendran, Phys. Status. Solidi. 206 (2009) 1447.

[41] M.M. Fereira, A.E. Clark, L.L. Hench, J. Mater. Syn. Proceed. 8 (1994) 189.

[42] J. Ma, C. Chen, D. Wang, Y. Jiao, J. Shi, J. Colloids Surf. B. 81 (2010) 87.

[43] J. Oliveira, R. Correia, M. Fernandes, Biomater. 23(2) (2002) 371-379.

[44] M.T. Souza, M. C. Crovace, C. Schroder, H. Eckert, O. Peitl, E. D. Zanotto, J. Non-Cryst. Solids. 382 (2013) 57.

[45] P. Jha, K. Singh, Ceram. Int. 42 (2016) 436.

[46] Y. Yu, Z. Bacsik, M. Eden, Mater. Chem. 11 (2018) 1690.

[47] S. Punj, K. Singh, J. Mater. Sci. Mater. Electron. 30 (2019) 3871.

[48] O.H. Andersson, K.H. Karlsson, K. Kangasniemi, J. Non-Cryst. Solids. 119 (1990) 290.

[49] A. Martinez, I. Izquierdo-Barba, M. Vallet-Regi, Chem. Mater. 12 (2000) 3080.

[50] F. Abbona, A. Baronnet, J. Cryst. Growth. 165 (1996) 98.

[51] C. Gao, S. Peng, P. Feng, C. Shuai, Bone Res. 5 (2017) 1.

[52] T. Xiu, Q. Liu, J. Wang, Chem. Lett. 36 (2007) 730.

[53] F. Naghizadeh, N. Sultana, A. Kadir, M. Rafiq, T.M. Shihabudin, T. Muzaffar, R. Hussain, T. Kamarul, J. Nanomater. 2014 (2014) 23.

[54] P. ISO, 10993–5: 2009 Biological Evaluation of Medical Devices-Part 5: Tests for In Vitro Cytotoxicity, International Organization for Standardization, Geneva (2009).

[55] A.A. Alshatwi, J. Athinarayanan, V.S. Periasamy, Mater. Sci. Eng.C. 47 (2015) 8.

[56] V. Rajendran, M. Prabhu, R. Suriyaprabha, J. Mater. Sci. Mater. Med. 50 (2015) 5145.

[57] R. Palani, J. Selvarasi, Int. J. Curr. Res. Rev. 9 (2017) 71.

[58] L. Grund Bäck, S. Ali, S. Karlsson, D. Moncke, E.I. Kamitsos, B. Jonson, Int. J. Appl. Glass Sci. 10 (2019) 349.

[59] S.Y. Venyaminov, F.G. Prendergast, Anal. Biochem. 248 (1997) 234.

[60] K.K. Dey, M. Ghosh, R. Prakash, K. Sharma, D. Singh, Appl. Phys.127 (2021) 1.

[61] H. Kamal, A. Hezma, Silicon 10 (2018) 851.

[62] G.El-Damrawi, A. Hassan, A. Shahboub, J. Mod. Phys. Appl. 5 (2018) 37.

[63] R.K. Brow, R.J. Kirkpatrick, G.L. Turner, J. Am. Ceram. Soc. 76 (1993) 919.

[64] S. Kapoor, R.E. Youngman, L. Ma, N. Lonnroth, S.J. Rzoska, M. Bockowski, L.R. Jensen, M. Bauchy, M. M. Smedskjaer, Front. Mater. 6 (2019) 63.

[65] S. Morimoto, J. Ceram. Soc. Japan. 114 (2006) 195.

[66] M. Moesgaard, D. Herfort, J. Skibsted, Y. Yue, Europ. J. Glass Sci. Technol. Part A. 51 (2010) 183.

[67] D. Carta, J.C. Knowles, M.E. Smith, R.J. Newport, J. Non-Cryst. Solids. 353 (2007) 1141.

[68] Q. Zheng, Y. Zhang, M. Montazerian, O. Gulbiten, J.C. Mauro, E.D. Zanotto, Chem. Rev. 119 (2019) 7848.

[69] I. Wacławska, M. Szumera, J. Therm. Anal. Calorim. 84 (2006) 185.

[70] S.S. Danewalia, K. Singh, Ceram. Int. 42 (2016) 11858.

[71] H. Tripathi, A.S. Kumar, S. Singh, Bull. Mater. Sci. 39 (2016) 365.

[72] M.D.O. Donnell, R.G Hill, Acta Biomater. 6 (2010) 2382.

[73] L.L. Hench, CRC Handbook of bioactive glasses and glass ceramics, CRC Press, Taylor and Francis Group, Boca Raton, (1990).

[74] R.A. Martin, H. Twyman, D. Qiu, J. C. Knowles, R.J. Newport, J. Mater. Sci. Mater. Med. 20 (2009) 883.

[75] S. Chajri, S. Bouhazma, I. Adouar, S. Herradi, M. Khaldi, B. El Bali, M. Lachkar, J. Phys. Conf. Series, IOP Publishing, (2019) 012013.

[76] J. Partyka, M. Lesniak, Spectrochim Acta A. Mol. Biomol. Spectrosc. 152 (2016) 82.

[77] P. Feng, M. Niu, C. Gao, S. Peng, C. Shuai, Sci. Rep. 4 (2014) 1.

[78] S.M. Abo-Naf, E.-S.M. Khalil, E.-S.M. El-Sayed, H.A. Zayed, R.A. Youness, Spectrochim Acta A. Mol. Biomol. Spectrosc. 144 (2015) 88.

[79] F. Naghizadeh, M.R. Kadir, A Doostmohammadi, J. Non-Cryst. Solids. 427 (2015) 54.

Chapter 5 Results and discussion-II

5. Agro-food wastes derived glasses synthesized in Pt-Rh crucible

As discussed in chapter 4, the agro-food waste/ashes derived glasses melting in an alumina crucible, showed some content of aluminum in the glasses. It is higher in the WSA-containing glasses than in SCLA glasses. It is reported that the presence of Al_2O_3 in glasses synthesized from conventional chemicals hampered bioactivity [1, 2]. Therefore, to understand the effect on bioactivity two glass compositions that had a lower and higher amount of diffused alumina (as discussed in chapter 4) were melted in Platinum-Rhodium (Pt-Rh) crucible. Thus, two samples from each series with similar compositions [60 CHA-30SCLA-10 ESP], [60 CHA-10 SCLA-30 ESP] and [60 CHA-30WSA-10 ESP], [60 CHA-10WSA-30 ESP] in wt % were selected to melt in Pt-Rh crucible. The results of these glasses are discussed in this chapter.

5.1 Chemical analysis of as-prepared samples

The as-prepared glasses were investigated by EDS to find out their compositions. A representative SEM with EDS spectra of the PCSE-1 sample is shown in Figure 5.1.

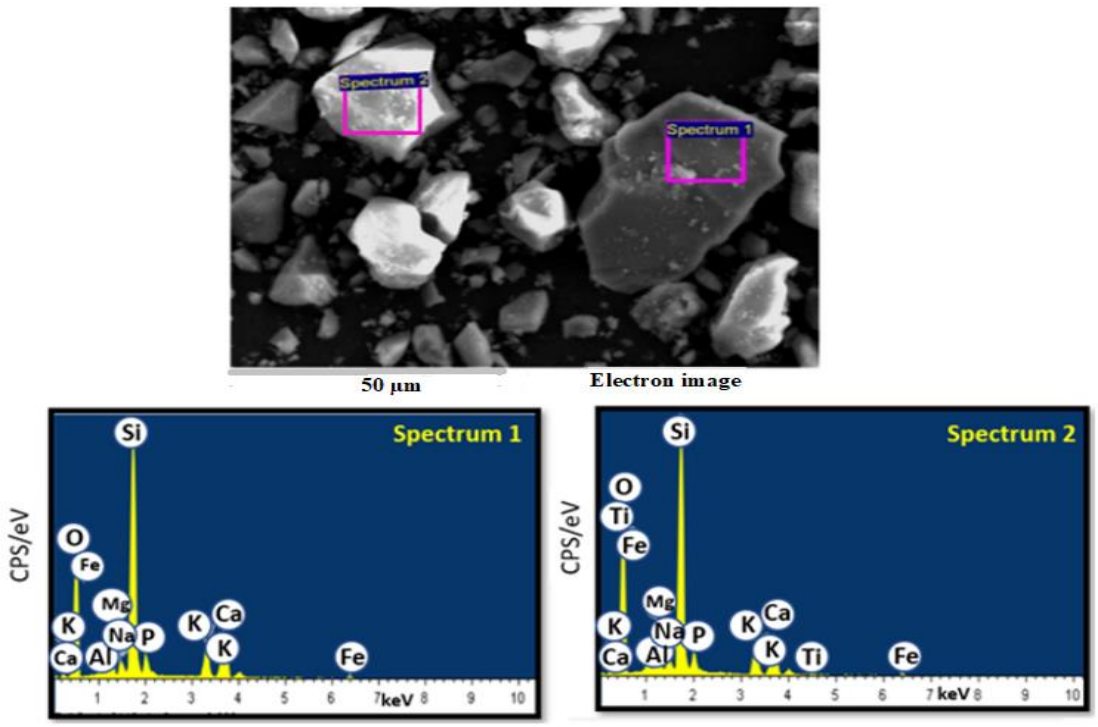

Figure 5.1 Representative SEM with EDS spectra of PCSE-1 sample

Table 5.1 The EDS analysis (wt %) of as-prepared samples synthesized in the platinum-rhodium crucible (PCSE-1, and PCSE-3) with an indication of mean ± standard deviation (n=3)

Label	Si	Ca	P	Mg	K	Na	Al	Ti	Fe	O
PCSE-1	27.09	11.07	2.86	5.25	5.95	0.75	1.20	0.10	0.72	45.10
	±0.45	±0.24	±0.49	±0.21	± 0.06	±0.25	± 0.19	±0.16	±0.31	±0.16
PCSE-3	25.46	14.43	2.14	5.15	6.15	0.97	1.02	0.21	0.66	43.77
	±0.44	±0.43	±0.43	±0.20	± 0.26	±0.06	± 0.10	±0.05	±0.14	±0.08

The SEM micrograph showed the irregular particles of the sample same as observed for CSE (synthesized in an alumina crucible) glasses. The EDS results showed almost the same trend for glass formers such as Si, P, and glass modifiers such as Ca, Mg, and K as observed for glasses synthesized in an alumina crucible. The contents of Mg, and K become higher for sample PCSE-3 in comparison to glass CSE-3. The glass modifier Na has shown an opposite trend in comparison to CSE glasses. The major difference in the composition of Pt-Rh synthesized glasses is the negligible content of Al_2O_3 in comparison to glasses synthesized in an alumina crucible (Table 5.1).

5.2 Physical properties

The apparent density is found at 2.41 and 2.67 g/cc for PCSE-1, and PCSE-3 samples, respectively. The density of the present samples is slightly lower than the density of glasses (CSE-1 and CSE-3) which were synthesized in an alumina crucible. However, the change in the densities is marginal. The change in densities is related to the change in composition. Since Al_2O_3 content is insignificant those samples were synthesized in Pt-Rh crucible. However, several other considerations such as the thermal background of the sample, field strength of the modifier, and formation of NBOs also affect the final density of the samples [3].

5.3 XRD analysis

XRD patterns of the as-prepared powder samples have shown a single broad hump, indicating that both the samples are amorphous as shown in Figure 5.2. Similar results have been obtained

for earlier (discussed in section 4.2) similar glasses (CSE-1 and CSE-3) synthesized in an alumina crucible.

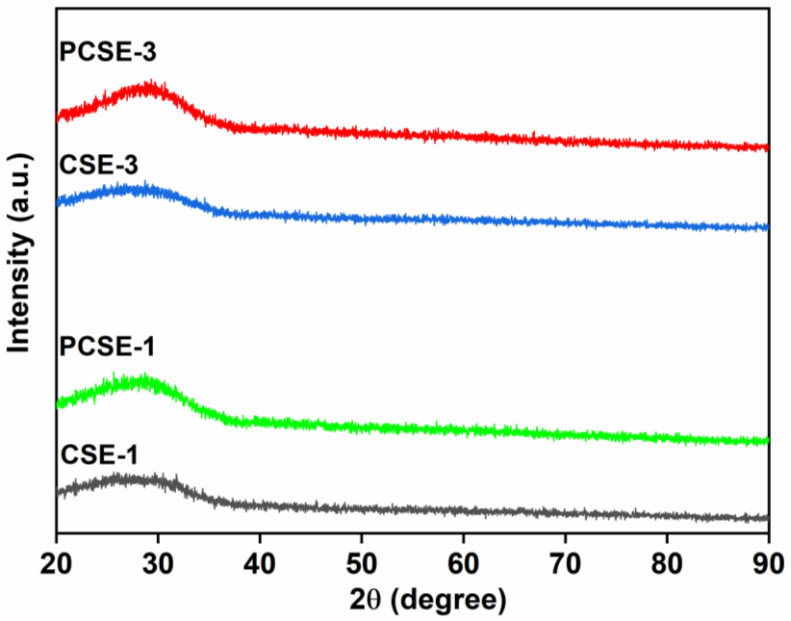

Figure 5.2 XRD patterns of as-quenched PCSE-1 and PCSE-3 samples along with glass CSE-1 and CSE-3 synthesized in alumina crucibles

5.4 FTIR analysis

The FTIR spectra of samples PCSE-1 and PCSE-3 have shown the bands at 3453, 2839-2925, 1634, 1033, 772-778, 474-468 cm^{-1} in Figure 5.3. Most of the bands lie in the same range as earlier mentioned for glasses CSE-1 and CSE-3 synthesized in an alumina crucible. The Pt-Rh synthesized samples have also shown a similar depolymerization effect of ESP (CaO) on the silica glass network [6]. However, some differences have also been observed in comparison to CSE glasses. In PCSE-1 and PCSE-3 glasses, the bands at 560 cm^{-1} (asymmetric bending vibrations of P-O bonds) and 1802 cm^{-1} (stretching mode of Si-OH group) are not present. However, new weak bands appeared at 1634 cm^{-1} and 2839-2925 cm^{-1} which can be attributed to the O-H bending vibration and stretching vibrations of the Si-OH group in different structural sites, respectively [4]. The band at 3453 cm^{-1} also shifted towards the higher wavenumber side in comparison to CSE glasses. It indicates that the adsorption capacity of

water molecules increases when samples are synthesized in a Pt-Rh crucible. In other words, the presence of Al_2O_3 has decreased the tendency of water adsorption. The band at 772 cm^{-1} is attributed to the symmetric stretching vibration of $Si\text{-}O^-$ bonds. This band slightly shifted towards the higher wavenumber side (778 cm^{-1}), which is due to the relative change in the strength of the chemical bonds by the change in glass composition [4].

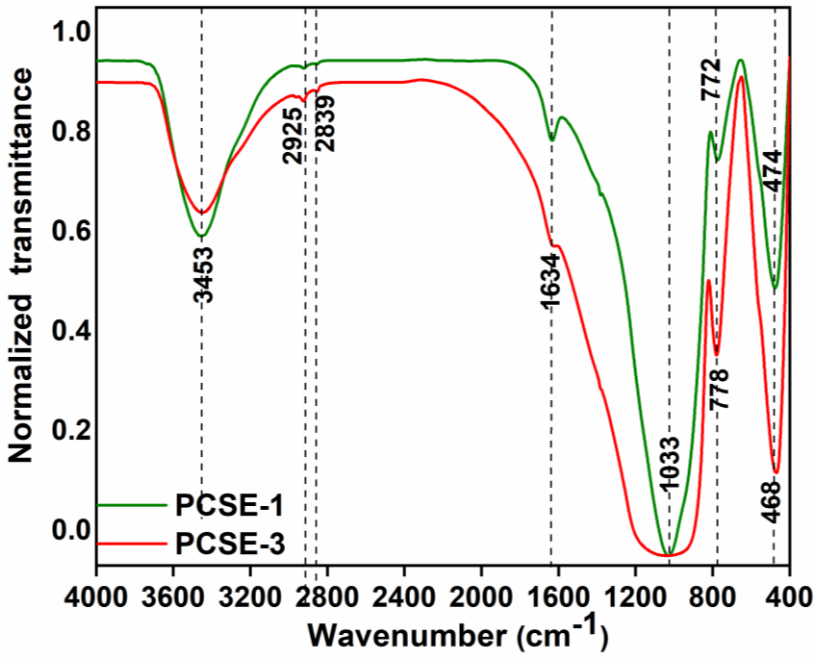

Figure 5.3 Normalized FTIR transmittance spectra of PCSE-1 and PCSE-3 samples

A similar result has also been observed for conventional chemical-derived silicate glasses, a weak band shifted 735 to 785 cm^{-1} with increasing MgO in the silicate network [4]. It can be observed that the transmission band at 1033 cm^{-1} corresponds to the vibrations of $[SiO_4]^{4-}$ and $[PO_4]^{3-}$ which is broader in glass PCSE-3 compared to glass PCSE-1 as earlier discussed in CSE glasses. It could be associated with the presence of more disorderness and defects than sample PCSE-1 [5]. It concluded from the above results, that the similar composition of glasses when synthesized in Pt-Rh crucible than alumina crucible, moreover, they have a higher tendency to adsorb water molecules from the atmosphere.

5.5 Hardness analysis

The microhardness of the samples PCSE-1 and PCSE-3 is 5.59, and 6.17 GPa, respectively. These glass samples exhibit lower microhardness than the similar composition of samples synthesized in the alumina crucibles. It corresponds to the content of Al_2O_3 in earlier samples. The intermediate oxide Al_2O_3 increases the compactness of the samples also supported by the lower density of these glasses than Al_2O_3 containing glasses. The hardness of these glasses is within the reported range of silicate glasses i.e., 4-10 GPa [3, 6].

5.6 DSC analysis

Figure 5.4 depicts the DSC curves of the glasses PCSE-1 and PCSE-3 synthesized in the Pt-Rh crucible. It is noted that the value of T_g decreases with an increase of ESP contents on replacing SCLA as given in Table 5.2. A similar trend was observed for alumina synthesized glasses CSE-1 and CSE-3. This result also agreed with the FTIR results. Here, glass PCSE-1 and PCSE-3 have shown a slight decrease in T_g values corresponding to the silicate phase (majority phase due to its concentration) occurring between (710 ^oC - 690 ^oC). It is almost in the same range as observed for glass CSE-1 and CSE-3. In contrast, a significant displacement of the crystallization peak has been observed in Pt-Rh synthesized glasses occurring at T_c (1010 ^oC-997 ^oC). Both the glasses exhibited higher T_c in comparison to glasses (CSE-1 and CSE-3) synthesized in an alumina crucible. It might be due to glasses having multicomponent compositions that have higher combinational entropy which plays an important role to enhance the glass-forming ability [7]. It can also be clearly seen in Table 5.2. Further, the melting temperature (T_m) of these glasses has decreased (1156 ^oC-1154 ^oC) in comparison to glasses synthesized in an alumina crucible. It could be possible that CSE-1 and CSE-3 glasses are inhomogeneous and phase-separated as observed in section 4.6. Similar results have been observed by Watts et al. [8] for conventional chemical-derived glasses ($49SiO_2$-$1.1P_2O_5$-23(1-x) CaO-xMgO-$26.4Na_2O$ mol %, where x=0,7, 9) on replacing CaO with partial MgO contents.

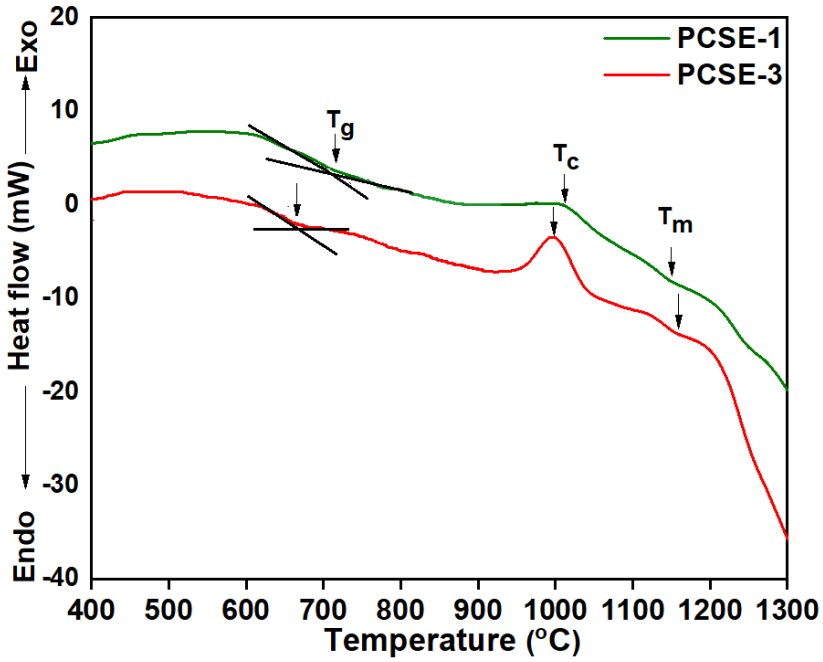

Figure 5.4 DSC curves for glasses PCSE-1, and PCSE-3, thermal signals showing the glass transition (T_g), crystallization temperature (T_c) and melting temperature (T_m)

Table 5.2 T_g , $T_{c,}$ and T_m for the PCSE-1, and PCSE-3 glasses

Sample	T_g (°C)	T_c (°C)	T_m (°C)	K_H Parameter
PCSE-1	710	1010	1154	2.14
PCSE-3	690	997	1156	1.92

This might be due to the effect of MgO_4 tetrahedra which causes the distribution of the local symmetry of the silicate network, results in a decrease in $T_{g,}$ and inhibit the crystallization that enhances the sintering window required for coating procedures for dental applications [9]. So, similar results can be associated with the Pt -Rh synthesized glasses. The above results indicated that the SCLA-based glasses synthesized in Pt-Rh crucible have to increase the sintering window that enhances the glass-forming ability in comparison to glasses (CSE-1 and CSE-3) synthesized in an alumina crucible.

5.7 Assessment of bioactivity (*in-vitro*)

5.7.1 Weight change and pH variation of glasses soaking in SBF

The weight change of the glass PCSE-1 and PCSE-3 has been observed after soaking in SBF as shown in Figure 5.5 (a).

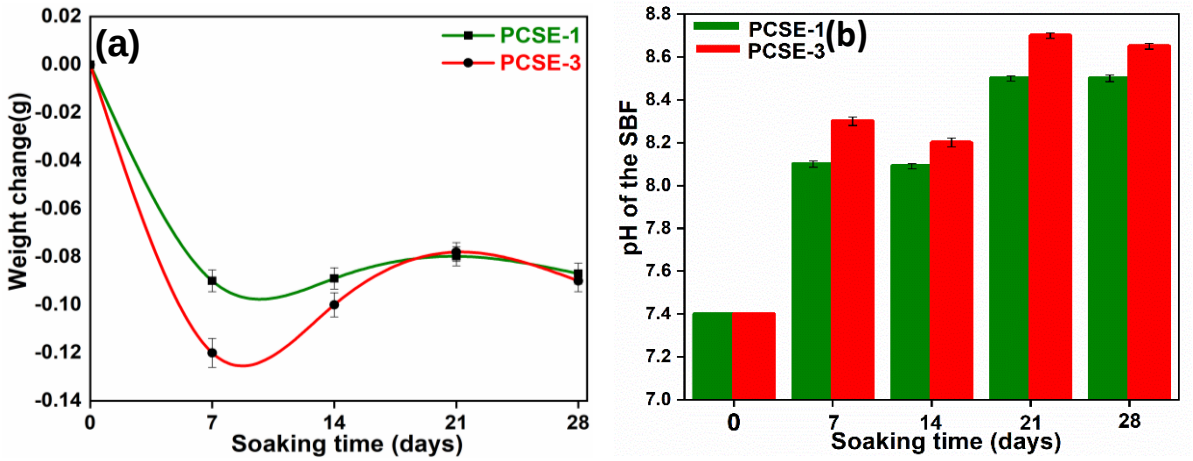

Figure 5.5 (a) Weight change of PCSE-1 and PCSE-3 glasses (b) Variation in pH of the SBF before (0 day) and after 7, 14, 21, and 28 days, error bars indicate the standard deviation

Glass PCSE-1 and PCSE-3 have shown higher weight loss than CSE-1 and CSE-3 glasses. The weight loss in PCSE-1 and PCSE-3 is 9 % and 12 %, respectively, which is higher than the samples synthesized in an alumina crucible of similar agro-food waste ashes. It indicated that the decrease of alumina contents in the Pt-Rh synthesized glasses increases the degradability of the glasses [6]. Further, the glass PCSE-1 and PCSE-3 have shown slightly lower weight gain after 14 days of soaking in SBF, in comparison to glasses synthesized in an alumina crucible. This might be due to less heavy ions moving from SBF to the glass surfaces as observed for conventional chemical-derived glasses after soaking in SBF [9]. Further, soaked glasses up to 28 days in SBF exhibit weight loss, which is in accordance with the pH changes (Figure 5.5 (b)). The changes in pH of the SBF solution after soaking the glasses (PCSE-1 and PCSE-3) for 7, 14, 21, and 28 days are shown in Figure 5.5(b). It has been observed that the overall pH of the SBF solution increases from 7.4 to 8.5 and 8.7 for glass PCSE-1 and PCSE-

3, respectively. The glass PCSE-1 and PCSE-3 have shown a 0.1-0.2 rise in pH values which are slightly higher than the similar composition of glasses synthesized in an alumina crucible. But, the pH values of agro-food wastes derived glasses have lower than the conventional chemical-derived glasses as earlier discussed for glasses synthesized in an alumina crucible [10].

5.7.2 MP-AES analysis

Table 5.3 shows the release of ions in the SBF solution after soaking the glass powder for 28 days with respect to the original SBF. In the present glasses, the release of a higher amount of Na^{2+}, K^{+}, and Mg^{2+} ions in comparison to glasses synthesized in an alumina crucible. But, the amounts of Mg^{2+} ions are lower than the CSE-1 glass. However, the release of trace elements is also too less than in CSE-1 and CSE-3 glasses. The concentration of silica ions has also higher for glass PCSE-1and PCSE-3 than the earlier mentioned glass CSE-1 and CSE-3 i.e., 43.6 mg/l and 63.2 mg/l after 28 days of soaking in SBF, respectively. This indicated that the concentration of Si^{4+} ions also increased with the increase of Mg^{2+} and K^{+} ions in SBF.

Table 5.3 Si, Ca, Mg, K, Na, Ti, and Fe ions concentration in SBF after 28 days of soaking. The results are taken by mean ± standard deviation (mg/l, n=3)

Label	Si	Ca	Mg	K	Na	Ti	Fe	Al
Pure SBF	0	113.5 ±1.5	62.5 ±3.5	351 ±2	2980 ±10	0	0	0
PCSE-1 (28 days)	82.1 ±1.1	197 ±1	267 ±2	489 ±2	4840 ±12	0.65 ±0.03	0.10 ±0.01	<0.01 ±0.00
PCSE-3 (28 days)	83.2 ±1.2	218 ±3	176 ±4	512 ±1	4735 ±13	0.62 ±0.05	0.10 ±0.01	<0.01 ±0.00

Similar results were also reported for conventional chemical used glasses [9, 11]. However, the value of Ca^{2+} ions has not decreased as compared to pure SBF after 28 days of soaked glasses in SBF as observed for alumina synthesized glass CSE-3. It might be due to the release of more Mg^{2+} ions that retards the apatite forming process as observed for conventional chemical-

derived bioglasses [9]. It is also reported that reduces the incorporation of P^{5+} ions on the Ca-P rich layer with an increase of Mg^{2+} ions in SBF (as discussed in the 5.7.3 section) [6]. It can be concluded from the above results, that in Pt-Rh synthesized glasses release more alkali and alkaline earth metal ions in comparison to CSE-1 and CSE-3 glasses. The release of more Mg^{2+} ions retard the apatite forming ability in comparison to alumina synthesized glasses in the present glasses.

5.7.3 XRD analysis

The XRD patterns of PCSE-1 and PCSE-3 before and after 7, 14, 21, and 28 days of soaking in SBF are represented in Figure 5.6 (a-b). There were no diffraction peaks observed after soakings of these glasses in SBF up to 28 days. However, very few weak diffraction peaks of HAp have been observed for CSE glasses. This showed that the soaked glasses might be formed amorphous HAp on the surface of these glasses.

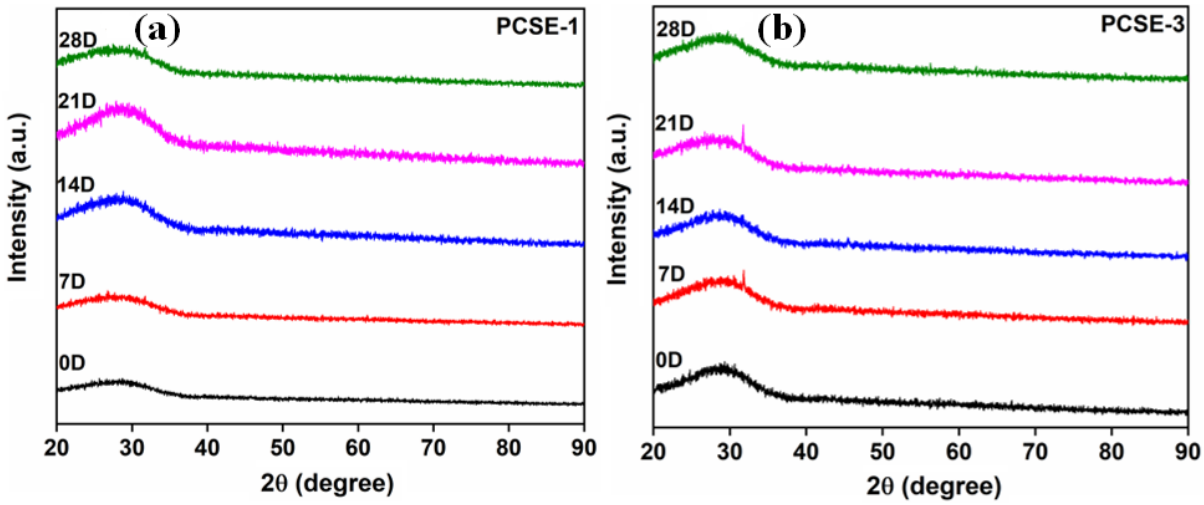

Figure 5.6 XRD patterns before (0 day) and after soaked in SBF solution (a) PCSE-1 and (b) PCSE-3 samples for 7, 14, 21 and 28 days

5.7.4 FTIR analysis

The FTIR spectra of glasses PCSE-1 and PCSE-3 before and after soaking for 7, 14, 21, and 28 days in SBF are shown in Figure 5.7. After soaking both glasses in SBF solution for 7 to 28

days, the bands 474 cm^{-1} and 468 cm^{-1} are attributed to vibration of the Si-O-Si bond, shifted to the lower wavenumber.

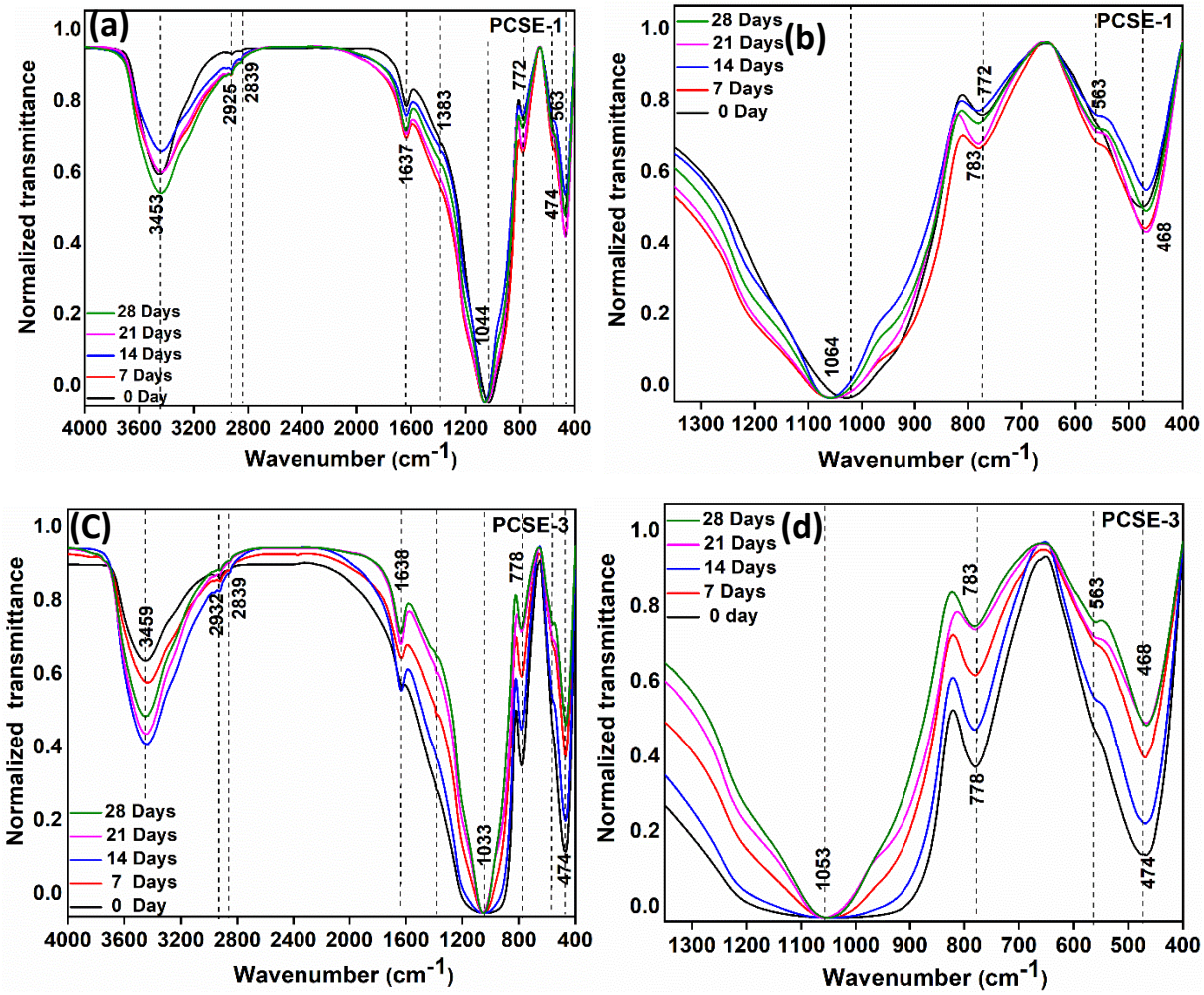

Figure 5.7 Normalized FTIR spectra before (0 day) and after soaked in SBF solution PCSE-1 and PCSE-3 glasses for 7, 14, 21, and 28 days. The figures (b) and (d) are the extended images of (a) and (c) which show the proper shifting and appearance of new bands

This contributes to the formation of silica gel on the surface of glasses. These results also supported the MP-AES results conducted on these glasses. The band at 772-778 cm^{-1} shifted towards a higher wavenumber 783 cm^{-1} for both glasses after soaking in SBF. This might be due to the leaching of alkali and alkaline earth metal ions that make the surface free of NBOs [5]. In fact, the frequency of transmittance of the Si-O bond increases with the decrease of NBOs. Both soaked glasses (PCSE-1 and PCSE-3) show the new weak band at 563 cm^{-1}, which corresponds to the P-O bonding (amorphous) indicated by the formation of the amorphous Ca-

P layer [12]. In comparison to glass CSE-1 and CSE-3, band 602 cm^{-1} corresponds to the P-O bonding that has not been observed for PCSE-1 and PCSE-3 glasses [13]. These results also agreed with the XRD results. The highest intensity of the major band ~1033 cm^{-1} shifted to the higher wavenumber ~1064 cm^{-1} after soaking in SBF from 7 to 28 days for both glasses as observed for (CSE) glasses synthesized in an alumina crucible. The glass PCSE-3 has also been shown to reduce the broadness of the major band. The same band 1060 cm^{-1} which is corresponding to the P-O vibration modes of regular phosphate tetrahedral (PO_4^{3-}) group observed for conventional chemical-derived bioglasses [14, 15]. In both glasses, it is found blue-shift of the most intense band at ~1033 cm^{-1} to 1064 cm^{-1} after soaking in SBF solution for up to 28 days confirming the precipitation of Ca-P species onto the glass surfaces [16]. The bands 1638, 2839, 2925, and 3453-3459 cm^{-1} correspond to the O-H group observed for glass PCSE-1 and PCSE-3 that are in accordance with CSE bioglasses. However, in comparison to CSE-1 and CSE-3 glasses, the carbonate bands at 1423 and 1465 cm^{-1} have not been observed in PCSE-1and PCSE-3 glasses after soaking in SBF. It can be concluded from the above results that the Pt-Rh synthesized glasses could form only an amorphous HAp layer on the glasses instead of the c-HAp layer as formed on glasses synthesized in an alumina crucible.

5.7.5 SEM with EDS analysis

SEM images for PCSE-1 and PCSE-3 glasses after soaking in SBF are given in Figure 5.8. After 7 days of soaking, the glass PCSE-1 has shown the formation of HAp as compared to the glass CSE-1 synthesized in an alumina crucible. This might be due to the release of lower Mg^{2+} ions in comparison to glass CSE-1 [17]. Glass PCSE-1 has shown cauliflower-like agglomerated morphology after 28 days of soaking in SBF [18]. On the other hand, glass PCSE-3 shows flakes or needle-like morphology. With the increase in soaking time (28 days), precipitates of the apatite phase become dense for both the glasses as shown in Figure 5.8.

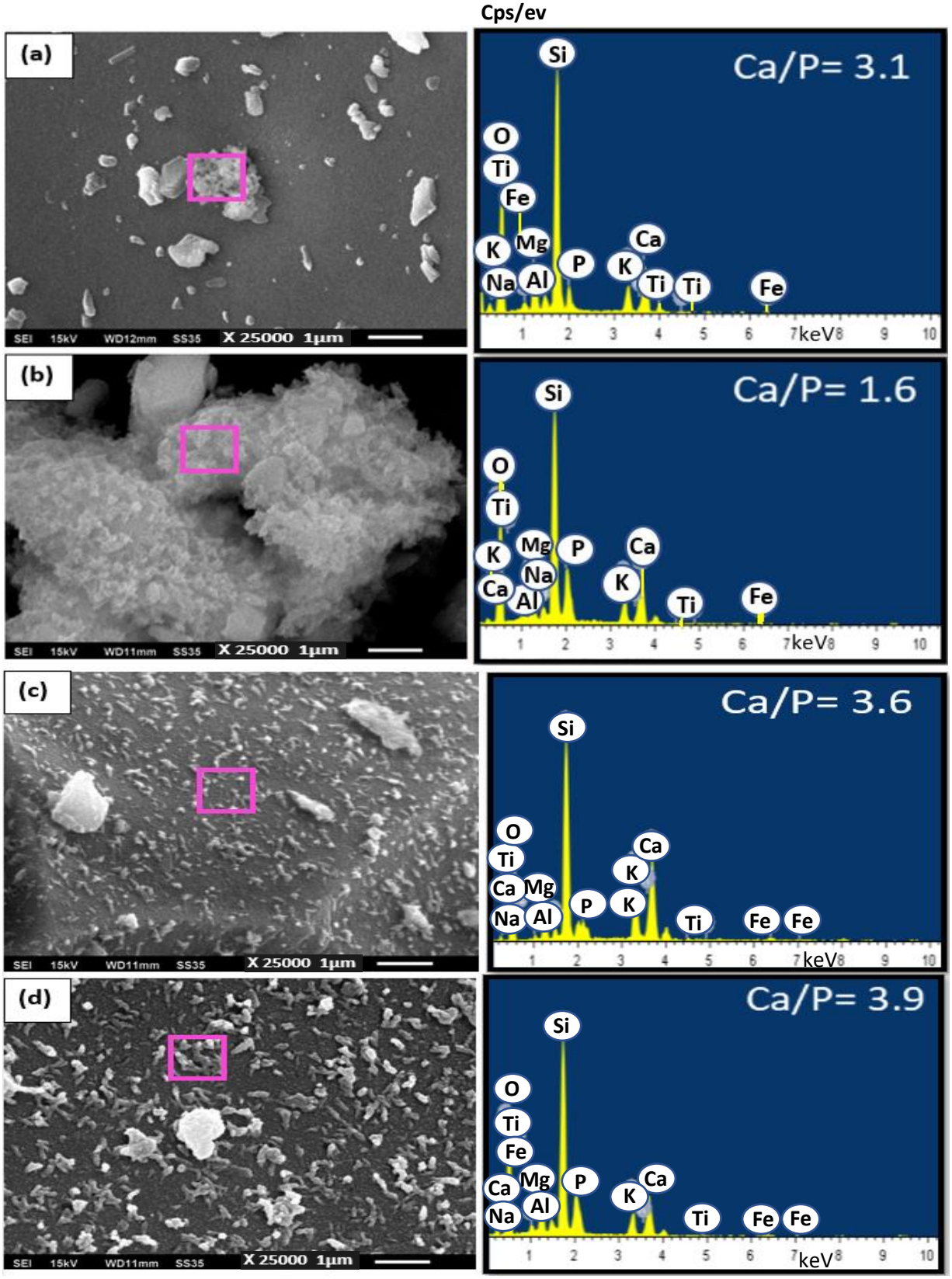

Figure 5.8 Representative SEM with EDS images for glasses after soaking in SBF (a) 7 days of PCSE-1, (b) 28 days of PCSE-1, (c) 7 days of PCSE-3, (d) 28 days of PCSE-3 glass

The surface of both the glasses exhibits different morphology of HAp in comparison to glasses synthesized in an alumina crucible. The results obtained from SEM are also confirmed by EDS analysis on soaked glasses. After soaking both glasses in SBF for 7 to 28 days, the Ca/P ratio lies in the range of 1.6 to 3.9 obtained from EDS spectra. The value of the Ca/P ratio is also lower than the glasses synthesized in an alumina crucible. This might be due to the absence of the carbonate (C) element as confirmed in the EDS spectra as shown in Figure 5.8.

5.7.6 Biocompatibility test

The MG-63 cell lines are exposed to various concentrations of 1, 2, 5, and 10 mg/ml following 24 h incubation as shown in Figure 5.9.

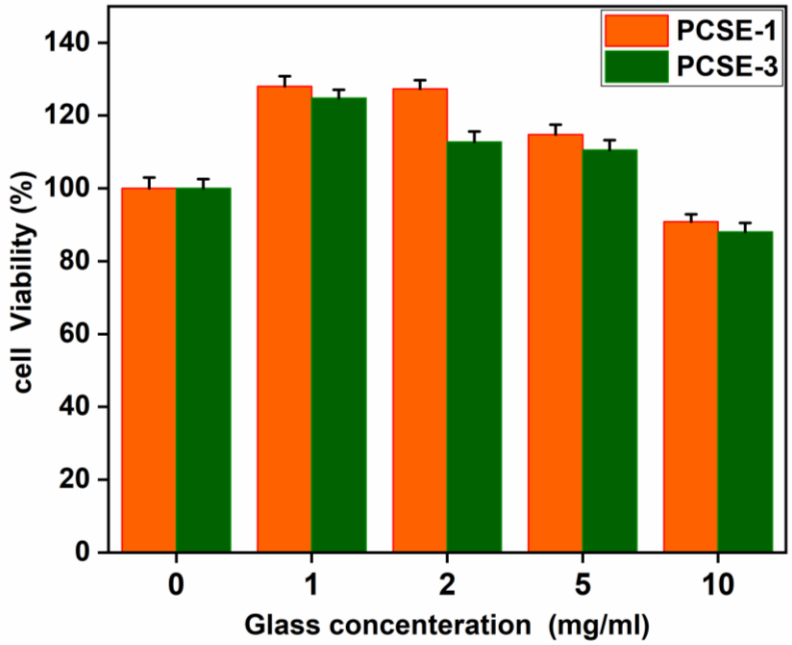

Figure 5.9 Cell growth effect of PCSE-1, and PCSE-3 glasses on human osteoblast-like (MG-63) cell lines. Cells without any treatment represent 0 mg/ml. Each experiment was performed in triplicate. The bar shows the treatments on MG-63 cells are not significantly different at $P<0.05$

In comparison to alumina synthesized glasses, these glasses have also shown almost similar behavior. At a lower concentration of glasses i.e. 1mg/ml, the maximum cell viability is 124.56 %. On the other hand, at a higher concentration of 10 mg/ml, the cell viability has reduced to 88 %. However, it is slightly lower than the CSE glasses. This can be concluded that the glasses

synthesized in the Pt-Rh crucible are also non-toxic as observed for glasses synthesized in an alumina crucible.

5.8 Effect of the platinum crucible on WSA-based glasses

5.8.1 Chemical analysis of as-prepared samples

The FESEM and EDS spectra of the PCWE-1 sample are shown in Figure 5.10. The glass formers Si, P, and glass modifiers Ca, Mg, K, and Na shows a similar trend as observed for alumina synthesized glasses on replacing WSA with ESP. The EDS results exhibit that the samples synthesized in the Pt-Rh crucible have a very lower amount of alumina in comparison to glasses synthesized in an alumina crucible as composition shown in Table 5.4. However, in comparison to CSE and PCSE glasses, the amount of alumina is lower for sample PCWE-3. Another difference in the composition of the present samples, the trace element titania (Ti) has not been observed in these glasses.

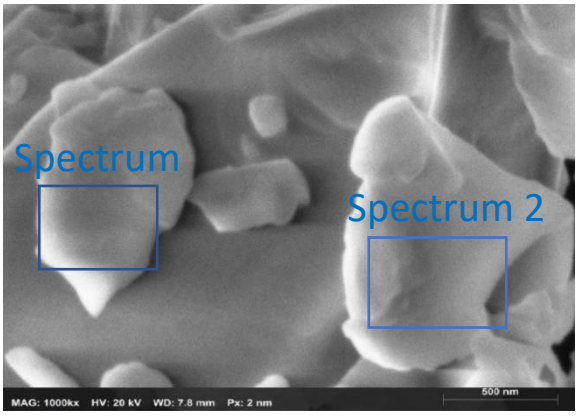

Figure 5.10 Representative FESEM with EDS spectra of PCWE-1 sample

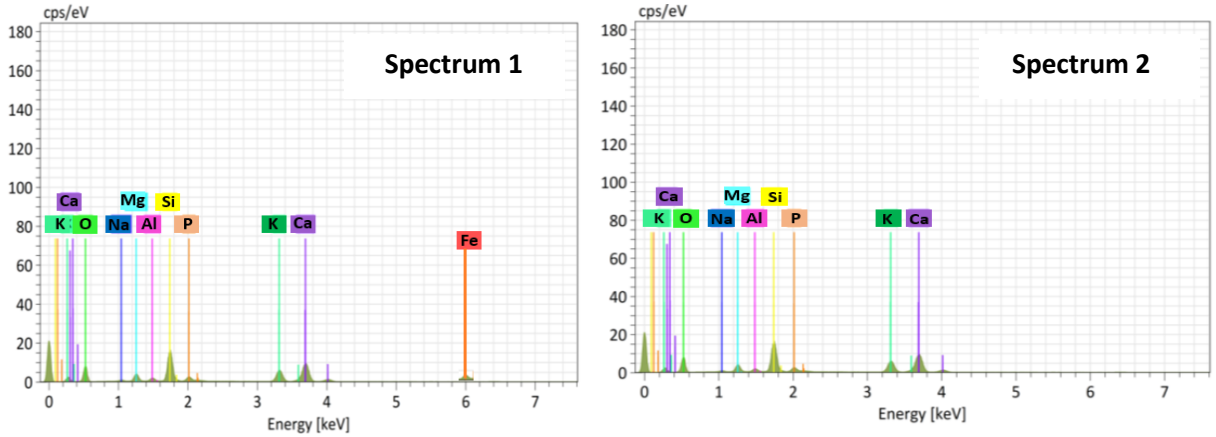

Table 5.4 The EDS analysis (wt %) of PCWE-1, and PCWE-3 samples before soaking in SBF solution with an indication of mean ± standard deviation (n=3)

Sample label (wt %)	Si	Ca	P	Mg	K	Na	Al	Fe	O
PCWE-1	20.08 ±0.45	7.89 ±0.24	2.08 ±0.49	3.42 ±0.21	14.57 ±0.06	0.91 ±0.25	1.06 ±0.19	0.11 ±0.31	49.88 ±0.16
PCWE-3	18.92 ±0.44	10.45 ±0.43	2.19 ±0.43	4.61 ±0.20	11.10 ±0.26	0.71 ±0.06	0.78 ±0.10	1.20 ±0.14	50.04 ±0.08

5.8.2 Physical properties

The apparent density is observed at 2.40 and 2.84 g/cc for PCWE-1 and PCWE-3 glasses prepared in a Pt-Rh crucible. The density of glass PCWE-1 and PCWE-3 is slightly higher than the density of CWE glasses synthesized in an alumina crucible. However, the change in the values of density is only 0.02 to 0.03 %, which is insignificant and within the measurement error range.

5.8.3 XRD analysis

XRD patterns of as-prepared powder samples do not show any peaks, indicating that both the samples are amorphous in nature. The XRD pattern of both glasses is shown in Figure 5.11.

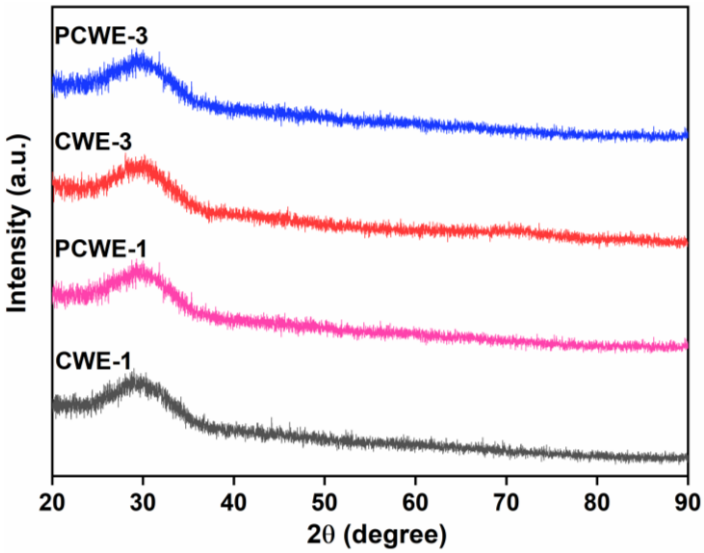

Figure 5.11 XRD patterns of as quenched PCWE-1 and PCWE-3 samples along with glass CWE-1 and CWE-3 synthesized using alumina crucibles

Similar results have been obtained for earlier reported similar CWE-1 and CWE-3 glasses synthesized in an alumina crucible.

5.8.4 FTIR analysis

FTIR spectra of the samples PCWE-1 and PCWE-3 are shown in Figure 5.12. A few new bands are observed in these glasses, in comparison to the similar glasses (CWE-1 and CWE-3) synthesized in an alumina crucible. The different bands appeared at 482, 619, 761, 1044, 1384, 1615, and 2073-3943 cm^{-1}. The more intense and broader bands appeared in the region 1615-3934 cm^{-1} in comparison to glasses synthesized in an alumina crucible. This indicated that the samples synthesized in the Pt-Rh crucible, are more hydrophilic in comparison to alumina synthesized glasses (CWE), CSE, and PCSE glasses as earlier discussed in section 5.4. This might be due to a decrease of intermediate oxide, Al_2O_3 [19, 20]. The new very weak vibration band 1384 cm^{-1} ascribed to stretching of the carbonate group (C-O) found in both glasses. The band at 482 cm^{-1} corresponds to the O-Si-O bending mode that shifted towards the higher wavenumber side (487 cm^{-1}) on replacing WSA at the cost of ESP. It might be due to the presence of different alkali and alkaline earth metal ions in the WSA instead of ESP may be responsible to shift these bands to the higher wavenumber side. Similar behavior has been observed for conventional chemical-derived orthosilicate glasses that attributed to the increasing strength of cation-oxygen bonds with an increase of MgO contents on replacing CaO contents [21]. The new band at 619 cm^{-1} is assigned P-O vibration modes of regular phosphate tetrahedral (PO_4^{3-}) group that only observed for PCWE glasses [22]. A weak band at 761 cm^{-1} is attributed to bending vibrations of the Si-O-Si bond observed for glass PCWE-1. However, the intensity of this band is very low in comparison to glass CWE-1 and the band disappeared in glass PCWE-3. The band at 1044 cm^{-1} is ascribed to stretching vibrations of both Si-O-Si and P-O bonds, shifted towards the higher wavenumber side (1068 cm^{-1} assigned to Q^3, BO = 3) for glass PCWE-3.

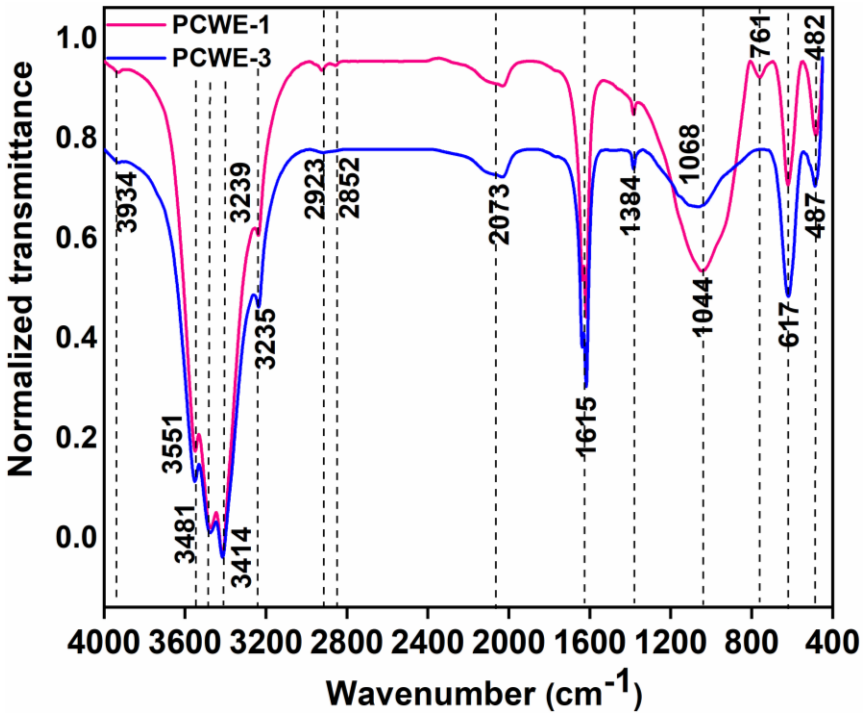

Figure 5.12 Normalized FTIR transmittance spectra of PCWE-1 and PCWE-3 samples

The intensity of the major band has also decreased after replacing WSA with ESP content. This glass has shown the opposite trend in comparison to glasses (CWE) synthesized in an alumina crucible. This indicated that the Pt-Rh synthesized (PCWE) glasses have shown more adsorption of water molecules and also increase the polymerization in the silica-phosphate glass network in comparison to glasses (CWE) synthesized in an alumina crucible. The water adsorption in these glasses is higher than in the CSE-1, CSE-3, PCSE-1, and PCSE-3 glasses.

5.8.5 Hardness analysis

The microhardness of the sample PCWE-1 and PCWE-3 is 5.67, and 6.57 GPa, respectively. These samples have also shown an increasing trend similar to the glasses synthesized in an alumina crucible. The value of hardness of these glasses is higher than CSE-1, CSE-3, PCSE-1, and PCSE-3 glasses. Moreover, the hardness of these samples is comparable to the glasses synthesized using conventional chemicals [23].

5.8.6 DSC analysis

In the present glasses, T_g increases (PCWE-3 > PCWE-1) with a decrease of silica contents on replacing WSA at the cost of ESP as shown in Figure 5.13. It has shown a similar trend as observed for previously discussed alumina synthesized glass CWE-3 > CWE-1. However, in such glasses, the concentration of alumina is lower than the glasses synthesized in an alumina crucible. It might be due to the presence of different concentrations of alkali and alkaline earth metal ions in agro-food wastes also play a significant role in the glass networks. These results are also in a similar line as observed in FTIR and hardness. The major difference observed for PCWE glasses is that they have shown single T_g , T_c , and T_m. Further, the glass PCWE-1 has shown broad and non-distinctive T_c in comparison to glass PCWE-3 and CWE-1. In the case of glass PCWE-1, the content of Al is 1.06 wt % and K is 14 wt % has shown broad and non-distinctive T_c . However, in glass CWE-1 the content of Al is 5.29 wt % and K is 12.5 wt % has shown sharp and distinctive T_c . It means that decreasing alumina contents suppress clear T_c, even though the presence of higher K contents.

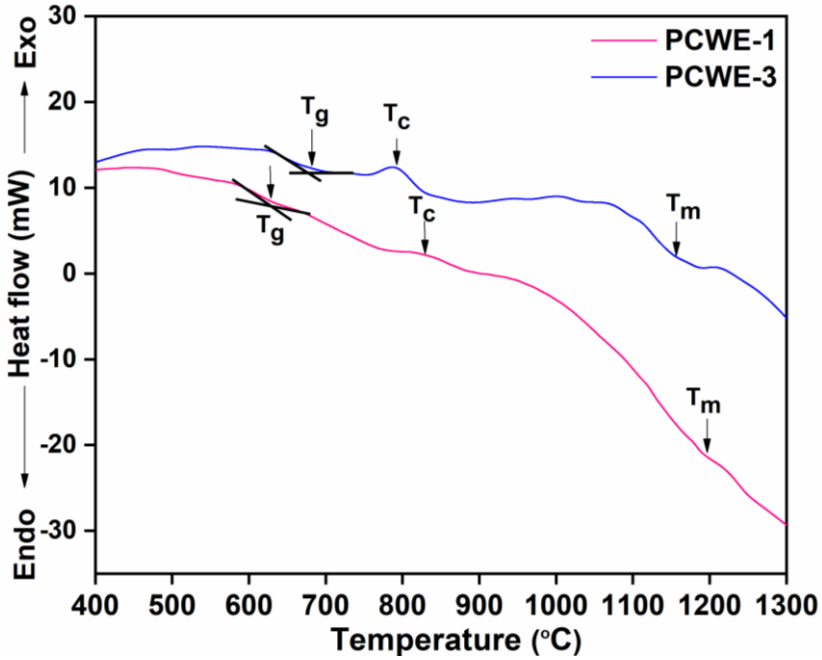

Figure 5.13 DSC curves for glasses PCWE-1, and PCWE-3, thermal signals showing the glass transition (T_g), crystallization temperature (T_c), and melting temperature (T_m)

According to earlier studies, also reported that silica-phosphate glasses that contain a higher amount of K have diminished the crystallization [24]. In fact, ionic radii of K^+ ions are larger than that of Ca^{2+} ions and therefore NBOs are less attracted [25, 26]. It could also be associated with the presence of some minor crystalline or nano crystalline phases [27]. Further, in glass PCWE-3, Ca contents increase and K contents decrease in the glass structure show ability to crystallize even in during quenching. The ability of glasses to crystallize also depends upon the mutual proportion between the components that form the glass network [28]. The T_c and T_m also depend upon the cross-link density, composition, etc [20].

Table 5.5 T_g , T_c, and T_m for the PCWE-1, and PCWE-3 glasses

Sample	**T_g (°C)**	**T_c (°C)**	**T_m (°C)**	**K_H Parameter**
PCWE-1	631	823	~1191	0.52
PCWE-3	671	786	~1151	0.32

From Table 5.5, K_H parameter indicated that the glass-forming ability has reduced with reducing of alumina contents in WSA glasses when synthesized in Pt-Rh crucible. The above results can be concluded that the Pt-Rh synthesized glasses also form homogenous glasses in comparison to glasses synthesized in an alumina crucible. The glass-forming ability decreases of Pt-Rh synthesized glasses in comparison to glasses synthesized in an alumina crucible. In other words, the presence of Al_2O_3 enhances the glass formation in agro-food wastes derived from present glasses.

5.9 Assessment of bioactivity (*in-vitro*)

5.9.1 Weight change and pH variation of glasses soaking in SBF

The weight change of the glass PCWE-1 and PCWE-3 after soaking in SBF is given in Figure 5.14 (a). After 7 days of soaking in SBF solution, glass PCWE-1 and PCWE-3 have shown slightly higher weight loss (8 %) in comparison to glasses synthesized in an alumina crucible.

Further, these glass PCWE-3 show weight gain after 14 to 28 days of soaking which is higher than PCWE-1 and alumina synthesized glasses CWE-1 and CWE-3. This might be due to heavier ions moving from SBF to the glass surfaces [29]. On the other hand, changes in pH of the SBF solution after soaking the glasses PCWE-1 and PCWE-3 for 7, 14, 21, and 28 days are shown in Figure 5.14 (b).

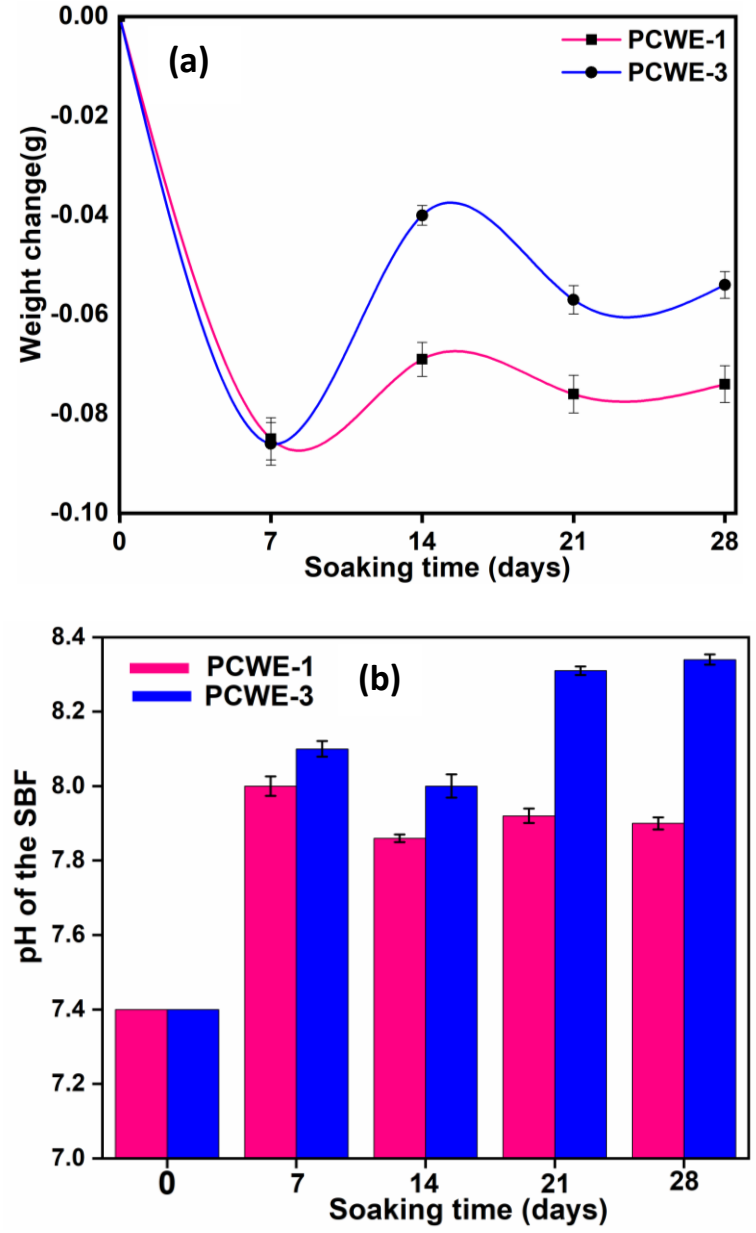

Figure 5.14 (a) Weight loss of PCWE-1 and PCWE-3 glasses (b) Variation in pH of the SBF before (0 day) and after 7, 14, 21, and 28 days of soaking in SBF, error bars indicate the standard deviation

The glass PCWE-1 has shown almost similar behavior as earlier mentioned for the similar composition of the glass (CWE-1) synthesized in an alumina crucible. However, at the initial stage (7 days), the value of pH slightly increases by 0.2 to the glass CWE-1. On the other hand, PCWE-3 glass has shown more variations in pH in comparison to similar compositions of glass (CWE-3). In glass PCWE-3, a fast release of alkali and alkali metal ions to the SBF solution increases the pH (8.1) up to 7 days of soaking. Later on, as soaking days increase, the pH decrease, and drop-down up to 8.0 (14 days). These results are consistent with the weight change results also. The gradual pH rises again observed after 21 days of soaking. Small changes in these pH values are also observed for the next 28 days of soaking. It has been observed that the overall pH of the SBF solution increased from 7.4 to 8 and 8.3 for glass PCWE-1 and PCWE-3, respectively, which is higher than the similar composition of glasses synthesized in an alumina crucible. It indicated that the WSA glasses synthesized in the Pt-Rh crucible have shown more weight change and pH change in comparison to the glasses synthesized in an alumina crucible. However, this weight change and pH change are lower than the CSE glasses in which SCLA is used as resource materials.

5.9.2 MP-AES analysis

PCWE-1 and PCWE-3 glasses released a higher amount of K^+, Na^{2+}, and Mg^{2+} ions in comparison to glasses (CWE-1 and CWE-3) synthesized in an alumina crucible. These results are shown in Table 5.6. The release of Si^{4+} ions has also increased after 28 days of soaking of glass PCWE-1 and PCWE-3. Similar behavior is also observed for PCSE glasses as discussed in section 5.7.2. However, in comparison to CWE, CSE, and PCSE-based glasses, PCWE glasses have shown a higher release of K^+ ions. Obviously, the K_2O contents in these glasses are higher than in other glasses (Table 5.6). On the other hand, the trace elements such as Fe, and Al is present in a very lower amount in comparison to CWE-3 glass. Ti ions have also not been observed in the MP-AES results of these glasses.

Table 5.6 Si, Ca, Mg, K, Na, Al, and Fe ions concentration in SBF after 28 days of soaking. The results are taken by mean ± standard deviation (mg/l, n=3)

Label	Si	Ca	Mg	K	Na	Fe	Al
Pure SBF	0	117 ±1.5	61.8 ±2.2	207 ±2	2890 ±5	0	0
PCWE-1 (28 days)	56.4 ±1.6	98 ±1	88.7 ±1.2	567 ±1	3543 ±5	<0.01 ±0.03	<0.01 ±0.00
PCWE-3 (28 days)	58.3 ±0.4	129 ±2	148 ±2	560 ±1	3323 ±6	<0.01 ±0.04	<0.01 ±0.00

Further, after 28 days of soaking, the concentration of Ca^{2+} ions in the SBF solution decreased for glass PCWE-1 as observed for glass CWE-1. But, glass PCWE-3 has released more Ca^{2+} ions in comparison to glass CWE-3. The results indicated that the WSA-based glasses synthesized in the Pt-Rh crucible have released more alkali and alkaline earth metal ions in comparison to CWE-based glasses synthesized in an alumina crucible.

5.9.3 XRD analysis

The XRD patterns of PCWE-1 and PCWE-3 before and after 7, 14, 21, and 28 days of soaking in SBF represented are given in Figure 5.15 (a-b). There no diffraction peaks are observed after soakings of these glasses in SBF even up to 28 days. This showed similar results as observed for (CWE) glasses synthesized in an alumina crucible.

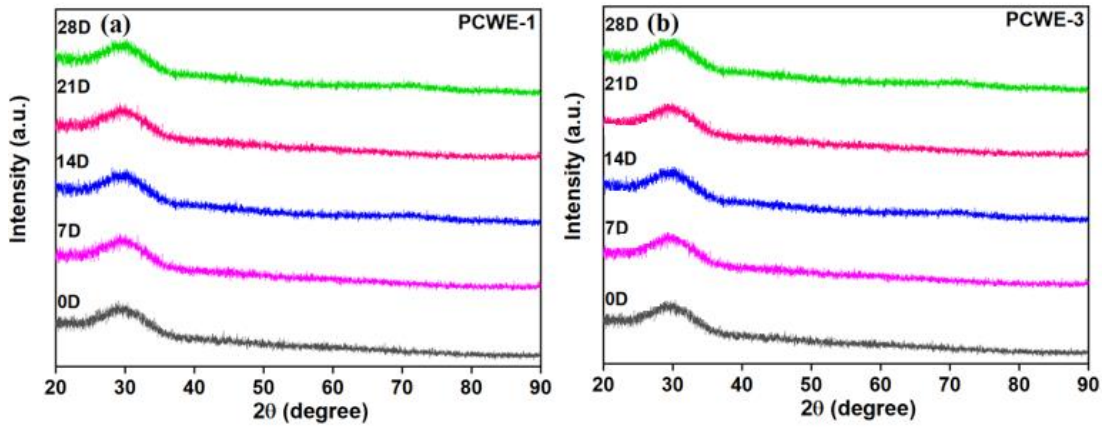

Figure 5.15 XRD patterns before (0 day) and after soaked in SBF solution (a) PCWE-1 and (b) PCWE-3 samples for 7, 14, 21, and 28 days

5.9.4 FTIR analysis

The FTIR spectra of soaked glasses PCWE-1 and PCWE-3 revealed some differences observed in comparison to unsoaked glasses. These differences can be seen in the region between 484-487,761, 1044-1068 cm^{-1}, and 1384-1470 cm^{-1} in Figure 5.16. After soaking the glasses in SBF solution, the bands 484 and 487 cm^{-1} are attributed to vibration of the Si-O-Si band, shifted to the lower wavenumber side as observed for soaked glass CWE-1 and CWE-3. Furthermore, as the soaking time increased to 21 and 28 days, the bands at 484 cm^{-1} and 761 cm^{-1} disappeared in PCWE-1 glass. However, this behavior has not been observed in CWE glasses. This contributes to the formation of complete silica gel on the glass surface [30].

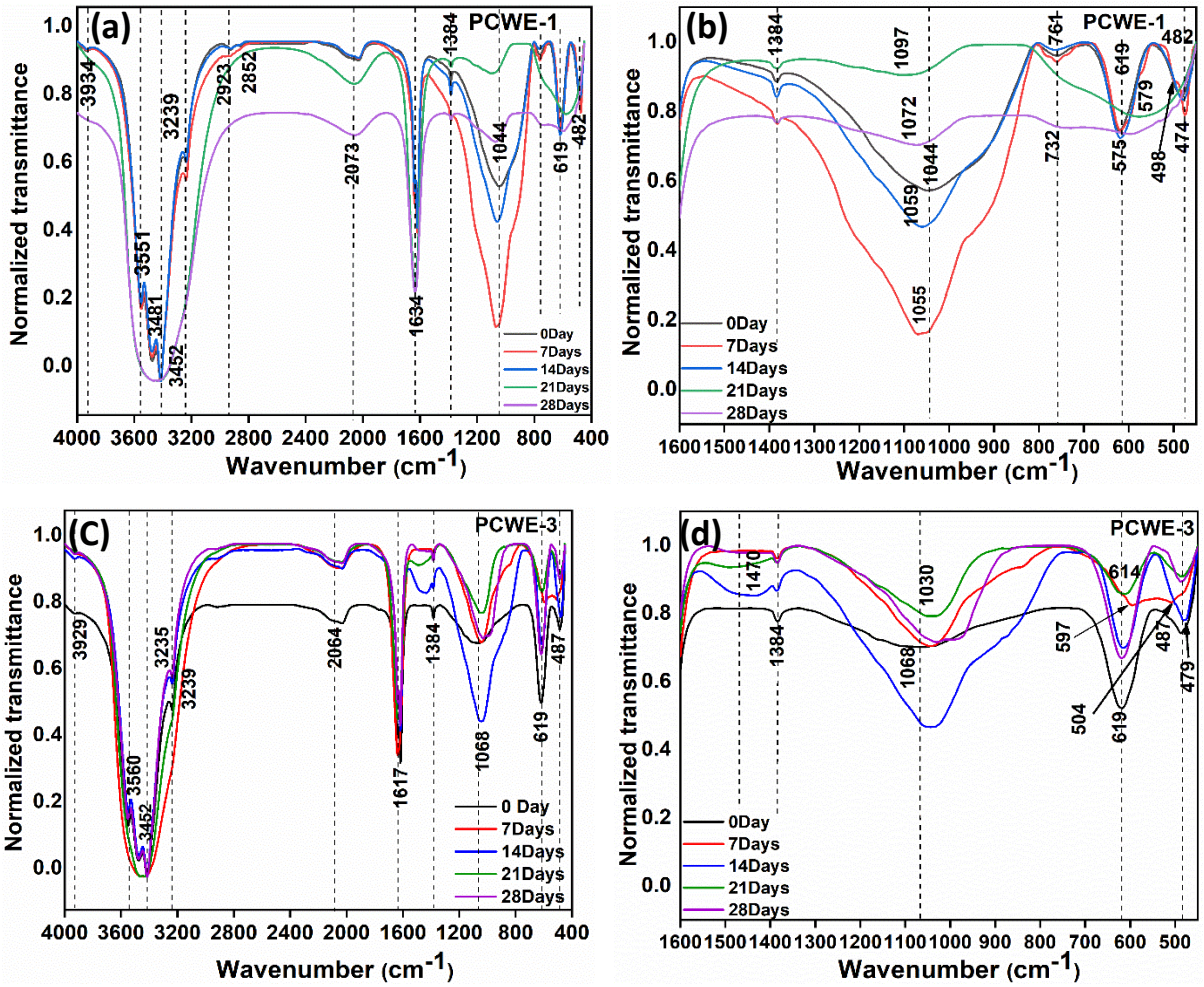

Figure 5.16 Normalized FTIR spectra before (0 day) and after soaked in SBF solution PCWE-1 and PCWE-3 glasses for 7, 14, 21, and 28 days. The figures (b) and (d) are the magnified images of (a) and (c) which show the proper shifting and appearance of new bands

After 7 days of soaking, PCWE-1 and PCWE-3 glasses have shown new bands in the region at 504-597 cm^{-1}. This corresponds to the P-O bonding (amorphous) bands that indicate the formation of the Ca-P layer [12]. The band appeared at 619 cm^{-1} and slightly shifts towards the lower wavenumber side for glass PCWE-3. On the other hand, with an increase of soaking up to 28 days, the water bands at 1617-3934 cm^{-1} become broader. It indicated that more silanol group (OH) groups might be formed on PCWE glasses in comparison to CWE glasses. Another (C-O) band at 1470 cm^{-1} has only been observed for glass PCWE-3 after 14, 21, and 28 days of soaking in SBF. These results are consistent with the results of weight change and pH change of these glasses during soaking in SBF. The highest intensity of the major band ~1044 cm^{-1} was attributed to Si-O-Si stretching, as well as P-O stretching mode [13]. After soaking in SBF, this band shifted to the higher wavenumber side ~1097 cm^{-1}. The blue shift of the most intense peak at ~1044 cm^{-1} to 1097 cm^{-1} after soaking in SBF solution for up to 28 days confirms the precipitation of Ca-P species onto the glass surface [16]. On the other hand, glass PCWE-3 has shown the opposite behavior with respect to glass CWE-3. The major band shifted towards the lower wavenumber side i.e.,1068 cm^{-1} to 1030 cm^{-1} up to 28 days. The transmittance peaks located at 1097 cm^{-1} and 1030 cm^{-1} for glass PCWE-1 and PCWE-3 originated from asymmetric stretching (V_3) of PO_4^{3-} group [31]. The shifting of bands to lower wavenumber or higher wavenumber after soaking in SBF indicates that there is an exchange of alkali and alkaline earth metal ions between glass and SBF that plays an important role in bioactivity [32]. However, this change has not been observed for similar glass (CWE-3) when synthesized in an alumina crucible. The results indicated that Pt-Rh synthesized glasses are more bioactive in comparison to alumina synthesized glasses.

5.9.5 FESEM with EDS analysis

FESEM images for PCWE-1 and PCWE-3 glasses after soaking in SBF are given in Figure 5.17.

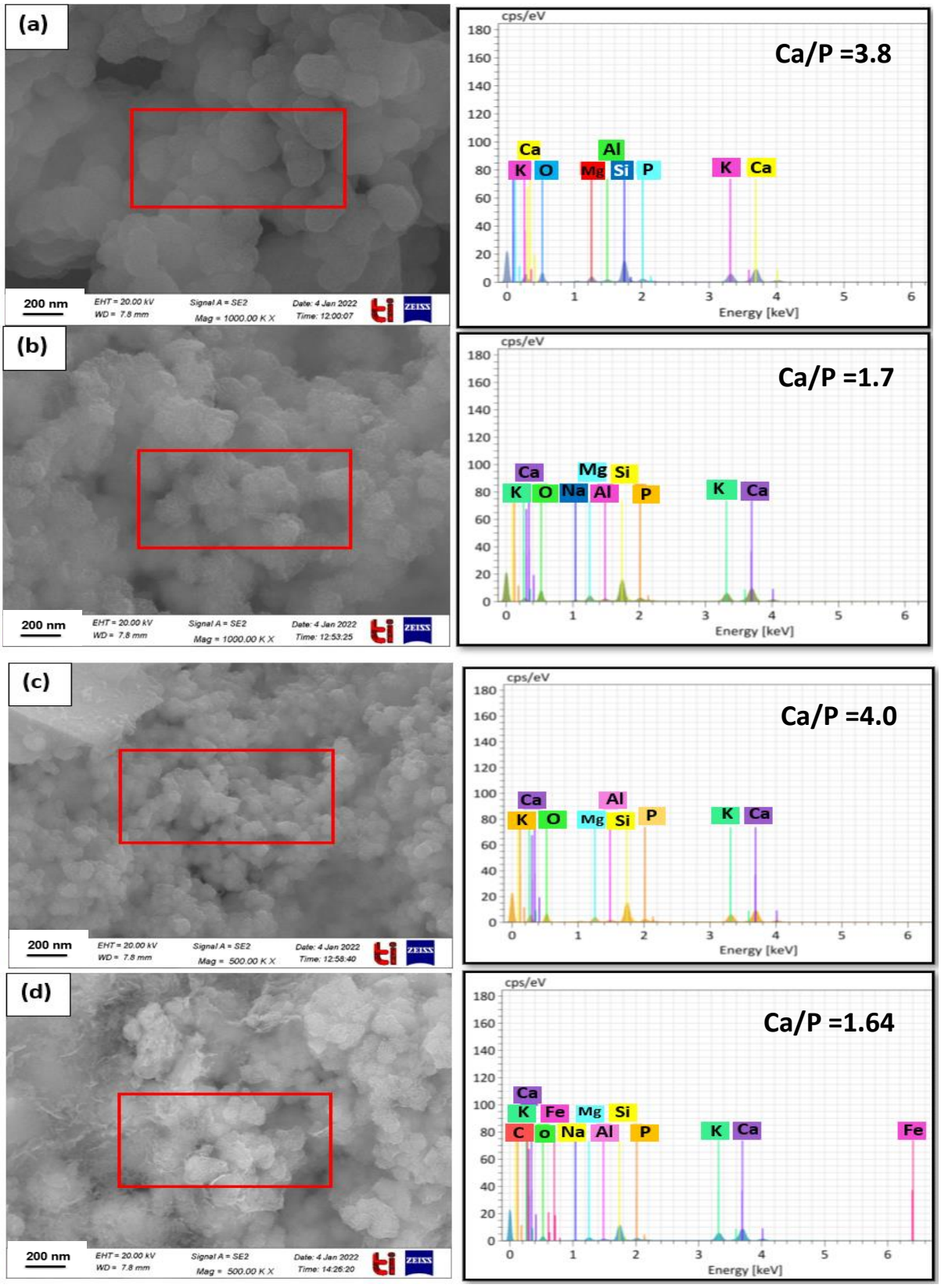

Figure 5.17 Representative FESEM with EDS images for glasses after soaking in SBF (a) 7 days of PCWE-1, (b) 28 days of PCWE-1, (c) 7 days of PCWE-3, (d) 28 days of PCWE-3

It also gives direct evidence of the surface modifications that occurred on the sample surface after soaking in SBF. After 7 days of soaking, PCWE-1 and PCWE-3 glasses showed a globular shape of HAp that covered the entire surface of both the glasses as shown in Figures 5.17 (a) and (c). With an increase in soaking time for the next 28 days, thicker and homogenous HAp formed on both the glass surfaces as shown in Figures 5.17 (b) and (d). It indicated that a lower amount of alumina in the present glasses has also changed the morphology of HAp. The formation of HAp is further confirmed by the EDS results, that the calcium phosphorous (Ca/P) ratio is determined based on the peak intensity of the EDS spectra. The calculated values of the Ca/P ratio of the apatite layer from the EDS microanalysis are 1.7 to 3.8 for PCWE-1 and 1.64 to 4.0 for PCWE-3 corresponding to 7, 14, 21, and 28 days of soaking. However, these values are lower than the glasses synthesized in an alumina crucible.

5.9.6 Biocompatibility test

In comparison to glasses that are synthesized in the Al_2O_3 crucible, the glass PCWE-1 has shown similar behavior.

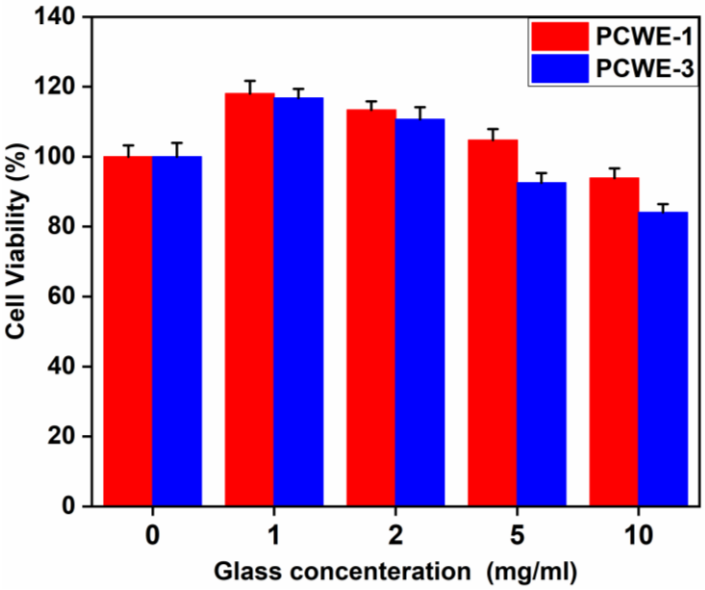

Figure 5.18 Cell growth effect of PCWE-1, and PCWE-3 glasses on human osteoblast-like (MG-63) cell lines. Cells without any treatment represent 0 mg/ml. Each experiment was performed in triplicate. The bar shows the treatments on MG-63 cells are not significantly different at $P<0.05$

The PCWE-3 glass exhibits cell viability ~ 118 % at a lower concentration of i.e., 1mg/ml, which is higher than the glass CWE-3 (90.8 %) as shown in Figure 5.18. It indicates that a decrease of alumina contents from 10.76 wt % to 0.78 wt % in glass PCWE-3, also increases the cell viability [10]. Glass PCWE-3 has also shown a similar trend as observed for glass PCWE-1. The cell viability of glass PCWE-3 is not less than 80 % even at a higher concentration of 10 mg/ml, which is higher than the glasses synthesized in an alumina crucible. Thus, it can be concluded that both glasses synthesized in a Pt-Rh crucible are also non-toxic and could be used for further applications.

5.10 Summary

Pt-Rh synthesized SCLA-derived glasses show the density and hardness lie in the same range as observed for glasses synthesized in an alumina crucible. However, density and hardness increase on replacing SCLA with WSA. The glass-forming ability decreases when SCLA is replaced with WSA. The water adsorption tendency increases when agro-food wastes derived glasses synthesized in Pt-Rh crucible. It increases the bioactivity of WSA glasses instead of SCLA glasses, due to the release of more Mg^{2+} ions from soaked SCLA glass in the SBF. All Pt-Rh synthesized glasses show a change in morphology of HAp from spherical and flakes to globular type due to a decrease in alumina contents. The Ca/P ratio lies in the range of 1.6 to 4.0, which is slightly lower than similar glasses synthesized in an alumina crucible. All Pt-Rh synthesized glasses also show good cell viability even at a higher concentration of 10 mg/ml in comparison to glasses synthesized in the Al_2O_3 crucible.

References

[1] A. El-Kheshen, F. Khalifa, E. Saad, R. Elwan, Ceram. Int. 34 (2008) 1667.

[2] S. Melchers, T. Uesbeck, O. Winter, H. Eckert, D. Chem. Mater. 28 (2016) 3254.

[3] J. Shelby, Introduction to Glass Science and Technology, 2nd ed. The Royal Society of Chemistry, UK (2005).

[4] A. Silva, C. Queiroz, S. Agathopoulos, R. Correia, M. Fernandes, J. Oliveira, J. Mol. Struct. 986 (2011) 16.

[5] P. Jha, K. Singh, Ceram. Int. 42 (2016) 436.

[6] A.K. Varshneya, T.P . Seward, in Handbook of ceramics, glasses and diamonds, C. A. Harper (ed.) Mc Graw Hill, USA (2001).

[7] M. Brink, J. Biomed. Mater. Res. 36 (1997) 109.

[8] S. Watts, R. Hill, M. O'Donnell, R. Law, J. Non-Cryst. Solids. 356 (2010) 517.

[9] A. Al-Noaman, S.C. Rawlinson, R.G. Hill, J. Non-Cryst. Solids. 358 (2012) 3019.

[10] H. Tripathi, A.S. Kumar, S. Singh, Bull. Mater. Sci. 39 (2016) 365.

[11] M. Majhi, R. Pyare, S. Singh, Int. J. Sci.Eng. Res. 2 (2011) 154.

[12]M. Priya, K.S. Thind, K. Singh, V. Kumar, D.P. Singh, J. Phys. Chem. Solids. 8 (2009) 1137.

[13] T. Himanshu, S. Singh, K. Sampath, M. Prerna, J.J. Ashish, Bioceram. Dev. Appl 6 (2016) 1.

[14] T. Charoensuk, C. Sirisathitkul, U. Boonyang, I.J. Macha, J. Santos, D. Grossin, J. Non-Cryst. Solids. 452 (2016) 62.

[15] F. Hmood, O. Goerke, F. Schmidt, Biomed. Glas. 4 (2016) 82.

[16] S. Agathopoulos, D. Tulyaganov, J. Ventura, S. Kannan, M. Karakassides, J. Ferreira, Biomater. 27 (2006) 1832.

[17] B. Abd Aladel, I.K. Sabree, S. Edrees, Int. J. Mech. Eng. Technol.10 (2019) 97.

[18] S. Son, D.-H. Kim, K.-H. Yoo, S.-Y. Yoon, Y.-I. Kim, Nanomater. 10 (2020) 621.

[19] K.K. Dey, M. Ghosh, R. Prakash, K. Sharma, D. Singh, Appl.Phys.127 (2021)1.

[20] R. Balzer, H. Behrens, T. Waurischk, S. Reinsch, R. Muller, P. Kiefer, J. Deubener, M. Front. Mater.7 (2020) 85.

[21] V. Farmer, Orthosilicates, Pyrosilicates, and other finite-chain silicates, Chapter 13 (1974).

[22] C. Rey, C. Combes, C. Drouet, D. Grossin, G. Bertrand, J. Soulie, Phys. Chem. Comp. Biomater. 2 (2017) 244.

[23] M.M. Smedskjaer, M. Jensen, Y. Yue, J. Non-Cryst. Solids. 356 (2010) 893.

[24] I. Wacławska, M. Szumera, J. Therm. Anal. Calorim. 84 (2006) 185.

[25] D. Bellucci, A. Sola, R. Salvatori, A. Anesi, L. Chiarini, V. Cannillo, Mater. Sci . Eng. C. 72 (2017) 566.

[26] N. Lotfibakhshaiesh, D.S. Brauer, R.G. Hill, J. Non-Cryst. Solids. 356 (2010) 2583.

[27] P. Pernice, A. Aronne, V. Sigaev, M. Kupriyanova, J. Non-Cryst. Solids. 275 (2000) 216.

[28] F. Branda, A. Costantini, G. Luciani, G. Laudisio, J. Therm. Anal. Calorim. 64 (2001) 1017.

[29] M. Araujo, M. Miola, G. Baldi, J. Perez, E.J.M. Verne, Mater. 9 (2016) 226.

[30] C. Ohtsuki, T. Kokubo, T. Yamamuro, J. Non-Cryst. Solids. 143 (1992) 84.

[31] L. Radev, V. Hristov, I. Michailova, B. Samuneva, Europ. J. Chem. 7 (2009) 322.

[32] R.A. Martin, H. Twyman, D. Qiu, J.C. Knowles, R.J. Newport, J. Mater. Sci. Mater. Med. 20 (2009) 883.

Chapter 6 Results and discussion-III

6. Glasses synthesized using conventional chemicals

Based on bioactivity, biocompatibility, and other properties of glasses, two of the best compositions are also synthesized using conventional chemicals. These glasses are synthesized by the melt-quench technique for comparison and study the effect of conventional and agro-food wastes derived glasses. Glasses with composition $47.9SiO_2$-$23.7CaO$-$4.6P_2O_5$-$6.4MgO$-$7K_2O$-$8Al_2O_3$-$0.8Na_2O$-$0.2TiO_2$-$1.4Fe_2O$ and $43.6SiO_2$-$21CaO$-$1.5P_2O_5$-$5.5MgO$-$15K_2O$-$12Al_2O_3$-$0.7Na_2O$-$0.3TiO_2$-$0.4Fe_2O_3$ in wt %, are designated as MCSE-3 and MCWE-2, respectively. The results of these two glasses are discussed in this chapter.

6.1 Physical properties

The apparent density is found at 2.80 and 2.84 g/cc for MCSE-3 and MCWE-2, respectively. The density of the present glasses is higher than the density of the glasses derived from agro-food wastes i.e., CSE-3 (2.67 g/cc) and CWE-2 (2.73 g/cc). This might be due to agro-food waste materials having inherent porosity that increase the volume of the materials and decrease the density [1]. The density of MCSE3 and MCWE-2 samples is within the reported range of calcium silicate conventional chemical-based glasses (CBG) i.e., 2.75 to 3.02 g/cc [2].

6.2 XRD analysis

Figure 6.1 (a) and (b) depict the XRD patterns of the conventional chemical-derived samples MCSE-3 and MCWE-2, respectively. For comparison, the XRD patterns of glass CSE-3 and CWE-2 are also shown along with MCSE-3 and MCWE-2 in Figures 6.1 (a) and (b), respectively. These samples show similar amorphous nature as found for the similar composition of glasses (CSE-3 and CSE-2) synthesized using agro-food waste materials. Based on the broadness of the hump, it could be concluded that the CSE-3 glass is more amorphous than other glasses reported in this thesis. However, these observations can be correlated with other results as discussed in the following sections.

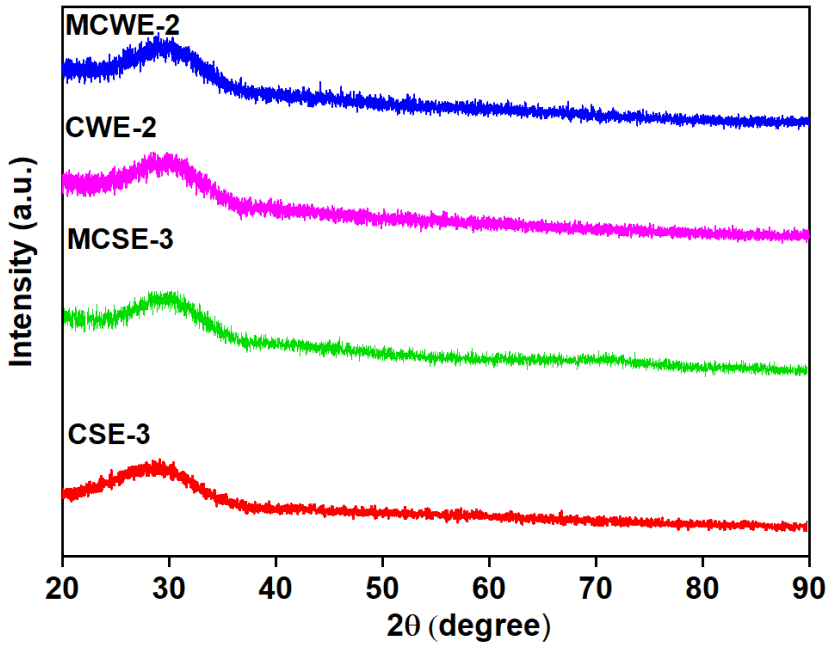

Figure 6.1 (a) XRD patterns of as-quenched CSE-3, MCSE-3, CWE-2 and MCWE-2 samples

6.3 FTIR analysis

The FTIR spectra of the samples MCSE-3 and MCWE- 2 are shown in Figures 6.2 (a-b) and (c), respectively. The sample MCSE-3 show bands at 3453, 1631, 1465, 1006, 766, 507-560, 494 cm^{-1} and sample MCWE-2 having bands 3443, 2030,1634, 1413,1056, 543 cm^{-1}. Most of the bands are in the same range as observed (discussed in sections 4.4 and 4.8.4) for glasses CSE-3 and CWE-2 synthesized using agro-food wastes. However, some distinctions can be observed in the FTIR of these glasses. For comparison, the band positions of all glass samples and their assigned chemical bonds are given in Table 6.1. In sample MCSE-3, the band at 494 cm^{-1} corresponds to bending vibrations of Si-O-Si shifted towards the higher wavenumber side in comparison to glass CSE-3. A similar band at 494 cm^{-1} is also found for MgO containing $4.9Na_2O$-$7.8MgO$-$2.9CaO$-$55.8P_2O_5$-$2.5Al_2O_3$ conventional chemical-derived glasses [3]. The new three bands appeared at 507, 540, and 560 cm^{-1} corresponding to a phosphate group. However, these phosphate bands were not observed in agro-food wastes derived glass such as CSE-3. A very weak band at 766 cm^{-1} slightly shifted towards the higher wavenumber side and its intensity decreased in comparison to glass CSE-3.

Table 6.1 FTIR bands positions of samples CSE-3, MCSE3, CWE-2, and MCWE-2, and their assigned chemical bonds. Where, v, v_s, and δ, mean vibrations, symmetric stretching vibrations, and bending vibrations, respectively

Assigned chemical bonds (references)	**Band positions (cm^{-1})**			
	CSE-3	**MCSE-3**	**CWE-2**	**MCWE-2**
δ Si-O-Si [3, 4]	470	494	462	-
PO_4^{3-}, Si-O-Al/ δ Si-O-Mg [5]	-	507,540, 560	567	543
Si-O-Si/Si-O-Al/ P-O-Al [6]	764	766	708	-
Si-O-Si P-O-P, v_s (PO_4) [7]	1035	1006	1011	1056
v_s C-O [8]	-	1465		1413
$v H_2O$ [5]	-	1631	1624	1634
v_s Si-OH [5, 8, 9]	1802	-	1732	-
$v H_2O$ [10]	3624	3424	3434	2030,3443

This might be due to the formation of P-O-Al bonds [6]. A similar band at 770 cm^{-1} was reported for Al_2O_3 doped calcium phosphate glasses, in which the intensity of this band decreases by forming a P-O-Al bond and strengthening the glass network [11]. The lower wavenumber region (400-766 cm^{-1}) indicated that the silica-phosphate network is more polymerized in the sample MCSE-3 in comparison to CSE-3. On the other hand, the major band at 1006 cm^{-1} corresponds to SiO_4 chains of Q^2 units when NBOs are bonded to alkali metal ions [12]. This band shifted towards a lower wavenumber in comparison to glass CSE-3 due to the weakening of the network. A similar band at 1006 cm^{-1} was observed by Mocioiu et al. [13] for conventional chemical-derived SiO_2-Na_2O-PbO glass. The bands 1802 cm^{-1} (stretching mode of Si-OH group) are not present in glass MCSE-3. However, a very weak new OH band and C-O band appeared at 1631 cm^{-1} and 1465 cm^{-1}, respectively.

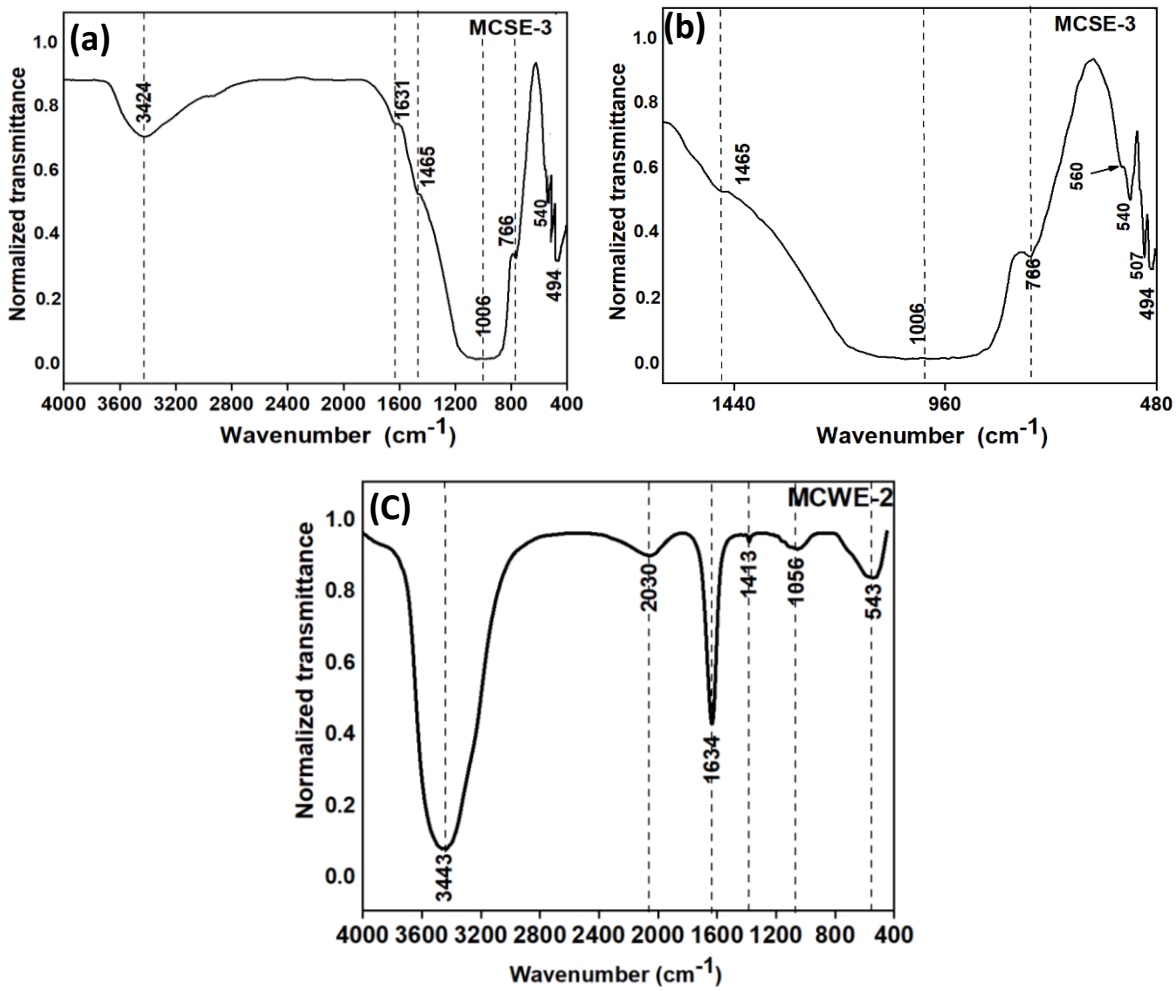

Figure 6.2 Normalized FTIR transmittance spectra of samples (a) MCSE-3, (b) the extended image of (a) which show the proper shifting and appearance of new bands, and (c) sample MCWE-2

The H_2O band at 3424 cm^{-1} in the MCSE-3 sample shifted towards the lower wavenumber side in comparison to agro-food wastes derived glass CSE-3. It indicated that this band might be formed by hydrogen bonding with the non-bridging oxygen [14]. However, the water adsorption tendency of glass MCSE-3 has reduced in comparison to agro-food wastes derived glass CSE-3. On the other hand, bands at 458 cm^{-1}, and 708 cm^{-1} correspond to bending vibrations of Si-O-Si, and Si-O-Al are disappeared in MCWE-2 glass, respectively. The band at 543 cm^{-1} is assigned to bending vibrations of Si-O-Mg, Si-O-Al, or P-O-P for glass MCWE-2. A similar band at 550 cm^{-1} was observed for phosphate-silicate glasses. It was combined with Moroccan red clay in which P_2O_5-SiO_2-CaO-Al_2O_3-K_2O-MgO-Fe_2O_3-Na_2O-TiO_2 were

present [5]. The intensity of the major band at 1056 cm^{-1} corresponds to the PO_4 group, has reduced and this band shifted towards a higher wavenumber in comparison to the glass CWE-2 as given in Table 6.1. The wavenumber shifted towards the higher wavenumber side indicated the increasing number of Q^n units (BOs) and containing lesser NBOs in the glass [15]. A similar result has also been observed for glass MCSE-3, which form P-O-Al bonds. On the other hand, the intensity of water bands at 1643 to 3443 cm^{-1} has the same as observed for glass CWE-2. It can be concluded from the above finding that the silica phosphate networks are less depolymerized in the glass and lower water adsorption ability from the atmosphere of the sample MCSE-3 in comparison to glass CSE-3. On the other hand, sample MCWE-2 shows more polymerization than glass CWE-2. However, the WSA-based sample MCWE-2 has shown almost similar water adsorption ability as glass CWE-2. Basically, the presence of hydroxyl and water in a glass might increase the surface activity of the glasses. It could increase the bioactivity of the glasses.

6.4 Hardness analysis

The microhardness of the samples MCSE-3, and MCWE-2 is 6.47 and 6.83 GPa, respectively. Sample MCSE-3 and MCWE-2 have shown a higher value of hardness in comparison to the glass CSE-3 (6.26 GPa) and CWE-2 (6.39 GPa). These changes might be due to the formation of more covalent Si-O-M or P-O-M (M=Al or Mg) bonds, which increase the rigidity and compactness of the structure [5, 16]. These results are also consistent with the density and FTIR results of conventional chemical-derived glasses [16]. This concludes that the similar composition of agro-food wastes based on conventional chemical-derived samples has more rigidity in comparison to agro-food wastes derived glasses CSE-3 and CWE-2. However, the hardness of these glasses is also within the range as earlier reported for CBG and higher than the agro-food wastes derived glasses [17].

6.5 DSC analysis

The characteristic glass transition temperatures of the glasses MCSE-3 and MCWE-2 are determined by DSC as shown in Figure 6.3.

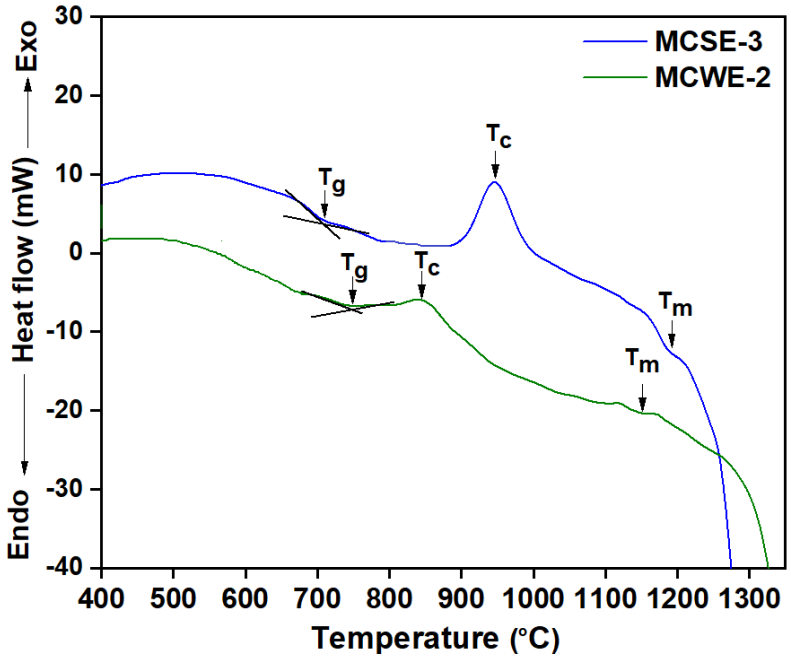

Figure 6.3 DSC curves of glasses (a) MCSE-3 and (b) MCWE-2

Table 6.2 T_g , T_c, and T_m for the glasses CSE-3, MCSE-3, CWE-2, and MCWE-2

Sample	T_g (°C)	T_{C1} (°C)	T_{C2} (°C)	T_{m1} (°C)	T_{m2} (°C)	K_H Parameter
CSE-3	698	967	-	1245	-	0.96
MCSE-3	708	948	-	1198	-	0.93
CWE-2	726	903	1014	1075	1140	1.09
MCWE-2	730	840	-	1145	-	0.35

The values of T_g, T_c, and T_m of glass CSE-3, CWE-2, MCSE-3, and MCWE-2 are given in Table 6.2 for comparison. According to the DSC curve, in the glass MCSE-3, and MCWE-2 single endothermic peak (T_g) is observed at 708 °C and 730 °C which is higher than the agro-food wastes derived glass CSE-3 and CWE-2, respectively. This indicated that the glass network is more rigid than agro-food wastes derived glasses. The hardness and FTIR results

also supported these results. Further, the glass MCSE-3 and MCWE-2 show a single exothermic peak (T_c) at 945 ^oC and 840 ^oC which is lower than the agro-food wastes derived glass CSE-3 and CWE-2, respectively. Similar, results have been observed for alumina calcium phosphate in conventional chemical-based glasses, the value of T_g increases and value of T_c decreases, as the Al_2O_3 breaks the P-O bonds and forms P-O-Al bonds in the glass [11]. The endothermic point (T_m) effect after the crystallization points is observed at 1188 ^oC and 1145 ^oC for glass MCSE-3 and MCWE-2, respectively. However, the melting point of these glasses is not very clear in DSC curves. It could be associated with the different structural units with different bond strengths present in these glasses. It can be seen that the crystallization temperature decreased for glass MCSE-3 in comparison to glass CSE-3. But, for glass MCWE-2 slightly increased the value of T_C in comparison to glass CWE-2. Similarly, the value of the K_H parameter has also lower for glass MCSE-3 and MCWE-2 than the glass CSE-3 and CWE-2 as given in Table 6.2. It can be concluded that the conventional glasses synthesized from conventional chemicals than agro-food wastes derived glasses of similar compositions have less tendency to form glass.

6.6 Assessment of bioactivity (*in-vitro*)

6.6.1 Weight change and pH variation of glasses soaking in SBF

The weight and pH change of glass MCSE-3 and MCWE-2 after soaking in SBF as shown in Figures 6.4 (a) and 6.4 (b), respectively. After 7 days of soaking in SBF, the weight loss in glass MCSE-3 and MCWE-2 is 10.3 % and 7.9 %, respectively. The weight losses of the present glasses are higher than the glass CSE-3 (9 %) and CWE-2 (7 %) derived from agro-food wastes. This influence that conventional chemical glasses are more reactive and leached out more ions in the initial stage in comparison to agro-food wastes derived glasses. However, these glasses show lesser changes after 14, and 21 days of soaking in SBF, in comparison to glass CSE-3. Further, after 28 days of soaking, MCSE-3 shows weight gain in comparison to

glass CSE-3. On the other hand, glass MCWE-2 shows a similar trend as glass CWE-2 up to 28 days of soaking in SBF. The variations in pH of the SBF solution after soaking the glass MCSE-3 and MCWE-2 for 7 to 28 days are shown in Figure 6.4 (b). The change in pH results also agreed with weight change results.

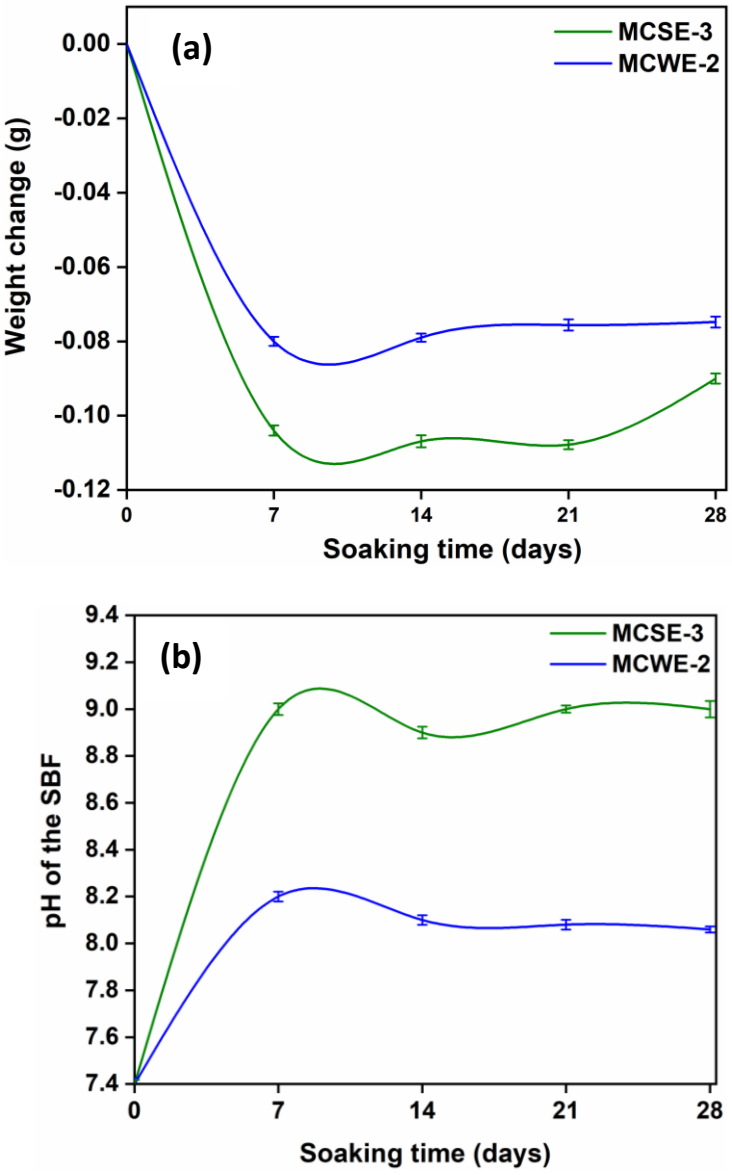

Figure 6.4 (a) Weight change of MCSE-3 and MCWE-2 glasses (b) Variation in pH of the SBF before (0 day) and after 7, 14, 21 and 28 days, error bars indicate the standard deviation

The glass MCSE-3 and MCWE-2 have achieved maximum pH values of 9.0 and 8.2 which is higher than the glass CSE-3 (8.6) and CWE-2 (8.1). Further, up to 28 days of soaking in SBF,

the glass MCSE-3 shows a lower change in pH value in comparison to glass CSE-3. On the other hand, the glass MCWE-2 has shown a slight decrease in pH value after 7 days of soaking in SBF and then saturated as observed for glass CWE-2. The results can be concluded that the glass MCSE-3 and MCWE-2 show maximum release of ions only in the initial stage of soaking (after 7 days) in both glasses. After that, up to 28 days these conventional chemical-based glasses MCSE-3 and MCWE-2 have shown lesser changes in pH value in comparison to the glasses CSE-3 and CWE-2.

6.6.2 MP-AES analysis

Table 6.3 shows that the glass MCSE-3, releases a higher amount of Ca^{2+}, Na^{+}, Mg^{2+}, and K^{+} ions than the glass CSE-3. On the other hand, glass MCWE-2 releases more amount of Na^{+} and K^{+} ions than glass CWE-2. The concentration of silica ions is also higher than the glass CSE-3 and CWE-2 due to the release of more alkali earth metal ions [18]. The leaching of other ions such as Ti^{4+}, $Fe^{3+/2+}$, and Al^{3+} from the glasses MCSE-3 and MCWE-2 into the SBF solution is almost in the same range as observed for glass CSE-3 and CWE-2.

Table 6.3 Si, Ca, Mg, K, Na, Al, Ti, and Fe ions concentration in SBF after 28 days of soaking. The results are taken by mean ± standard deviation (mg/ml, n=3)

Label	**Si**	**Ca**	**Mg**	**K**	**Na**	**Ti**	**Fe**	**Al**
Pure SBF	0	117 ±1	61.8 ±1.8	207 ± 2	2890 ± 6	-	-	-
CSE-3 (28 days)	63.2 ±1.1	110 ±1	136 ±3	504 ±3	3947 ±13	0.68 ±0.02	0.19 ±0.02	<0.01 ±0.00
MCSE-3 (28 days)	66.1 ±0.5	280 ±3	168 ±1	510 ±4	4654 ±8	0.65 ±0.03	0.10 ±0.01	<0.01 ±0.00
CWE-2 (28 days)	38.8 ±1.1	245 ±1	148 ±3	488 ±3	3256 ±8	0.65 ±0.02	<0.01 ±0.00	<0.01 ±0.00
MCWE-2(28 days)	41.1 ±1.3	240 ±2	146 ±2	519 ±2	3743 ±10	0.68 ±0.02	<0.01 ±0.00	<0.01 ±0.00

But, the concentrations of Ca^{2+} ions are not lower than the pure SBF in comparison to glass CSE-3. This might be due to the release of higher Mg^{2+} ions from glass MCSE-3 [18]. Forming a HAp layer on the glasses is taken place due to the leaching of ions from glasses and SBF solution. This physicochemical phenomenon changes the concentrations of SBF solution. To confirm this, the MP-AES was done of SBF after soaking the glasses for 28 days. On the other hand, no difference has been observed for Ca^{2+} ions in glass MCWE-2, it exhibits the same behavior as glass CWE-2. These results agreed with the weight change and pH changes during the *in-vitro* testing of these glasses. It can conclude from the above results that the conventional chemical-based glass MCSE-3 released more ions than agro-food waste derived glass CSE-3. But, due to the release of more Mg^{2+} ions in glass MCSE-3 retard the apatite formation on the surface of these glasses [18]. On the other hand, the glass MCWE-2 has shown almost similar behavior as observed for agro-food wastes derived CWE-2 glass.

6.6.3 XRD analysis

The XRD patterns of glasses MCSE-3 and MCWE-2 before and after 7, 14, 21, and 28 days of soaking in SBF are represented in Figures 6.5 (a) and (b), respectively.

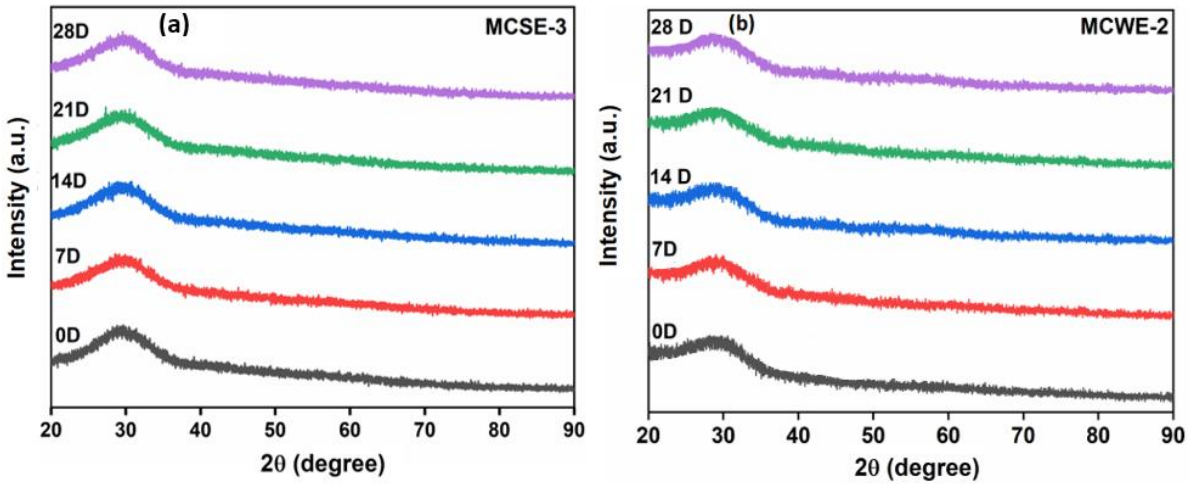

Figure 6.5 XRD patterns before (0 day) and after soaked in SBF solution (a) MCSE-3 and (b) MCWE-2 samples for 7, 14, 21 and 28 days

Glass MCSE-3 has shown no diffraction peaks related to HAp in comparison to glass CSE-3 derived from agro-food wastes. This might be due to the release of more Mg^{2+} ions than the glass CSE-3 which leads to inhibiting the crystallinity of HAp [19]. However, glass MCWE-2 has shown similar amorphous HAp as observed for agro-food wastes derived glass CWE-2. However, the change in XRD patterns of soaked glasses and unsoaked glasses is not showing any remarkable change as shown in Figures 6.5 (a) and (b), respectively.

6.6.4 FTIR analysis

The FTIR spectra of glasses MCSE-3 and MCWE-2 before and after soaking 7, 14, 21, and 28 days in SBF are shown in Figures 6.6 (a-b) and 6.6 (c-d), respectively. Glass MCSE-3, after 7 days of soaking in SBF solution, the band 494 cm^{-1} attributed to vibration of the Si-O-Si bond, shifted to the lower wavenumber 462 cm^{-1} and becomes broad in comparison to unsoaked glasses. This could be related to the formation of silica gel on the surface of the glass. On the other hand, the bands 507-560 cm^{-1} disappeared after soaking in SBF. It indicates the release of P^{5+} ions after soaking of glass in SBF. However, the glass CSE-3 has shown two bands at 562 and 602 cm^{-1} corresponding to (PO_4^{3-}) phosphate group, after 14 days of soaking in SBF. But, such PO_4^{3-} bands are not observed in glass MCWE-3 up to 28 days of soaking in SBF. It indicated that reduces the incorporation of phosphate ions on the Ca-P layer due to the release of more Mg^{2+} ions in SBF [18]. These results supported the MP-AES results also. The band at 766 cm^{-1} shifted towards a higher wavenumber (780-790 cm^{-1}) due to the release of ions in SBF and a physicochemical reaction occurred between glass and SBF [19]. The highest intensity of the major band ~1006 cm^{-1} shifted to the higher wavenumber ~1068 cm^{-1} and broadness reduced for 14 and 21 days of soaking in SBF. Further, after 28 days of soaking, the band again becomes broad. The same band 1060 cm^{-1} which corresponds to the P-O vibration modes of regular phosphate tetrahedral (PO_4^{3-}) group also observed for glass CSE-3 [20, 21]. The new weak vibration band at 1425 cm^{-1} and 1494 cm^{-1} ascribed to stretching of the carbonate

group (C-O) observed in glass MCSE-3 after 28 days of soaking in SBF. However, in glass CSE-3, C-O bands were observed after 14 days of soaking in SBF. It indicated that the glass MCSE-3 has formed amorphous HAp and is slow to form c-HAp in comparison to glass CSE-3. The other glass MCWE-2 has shown similar behavior as observed for glass CWE-2 during soaking in SBF solution for 28 days.

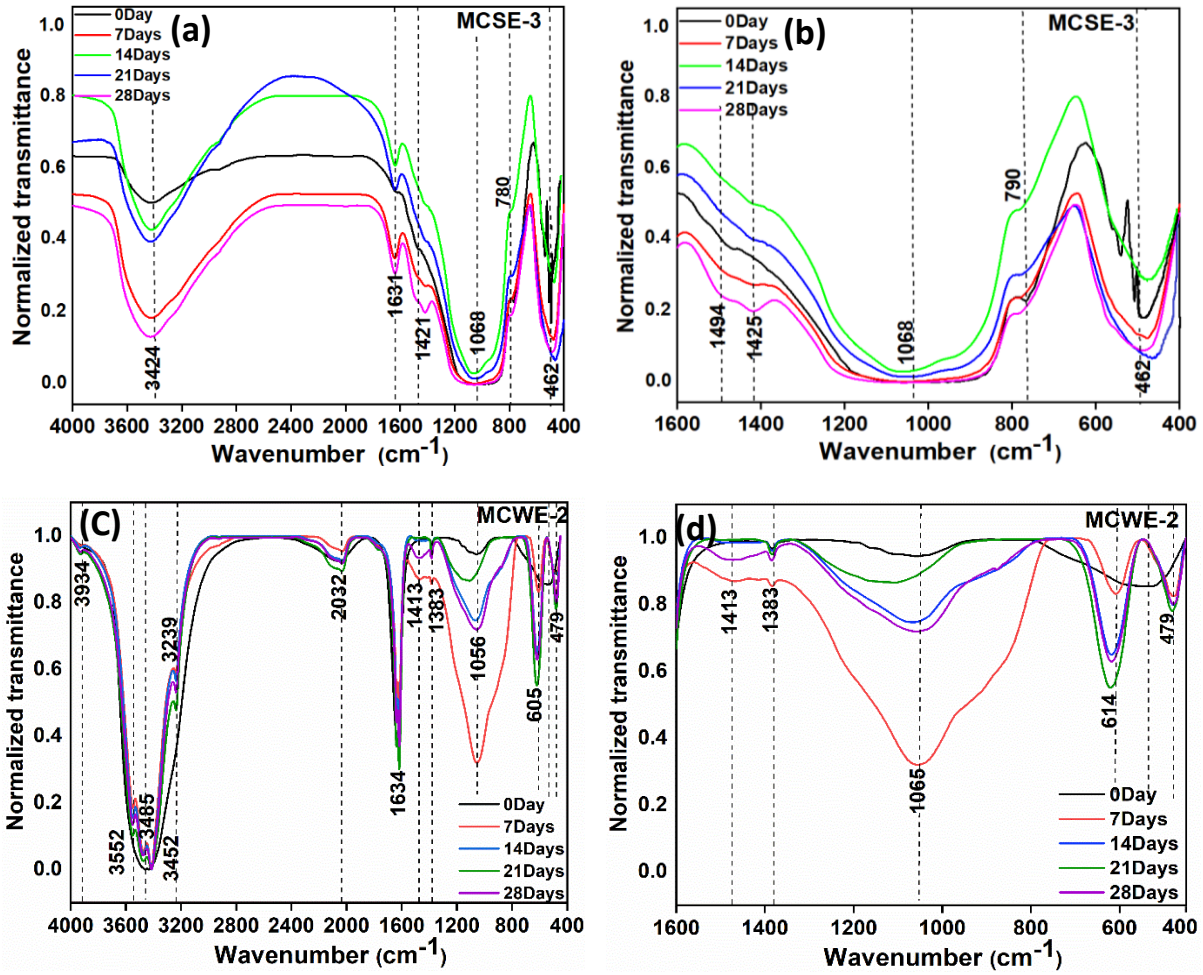

Figure 6.6 Normalized FTIR spectra of (a) MCSE-3, (c) MCWE-2, before (0 day) and after soaking in SBF for 7, 14, 21 and 28 days. The figures (b) and (d) are the magnified images of (a) and (c), respectively, which show the proper shifting and appearance of new bands

The major difference is that band at 605-614 cm^{-1} ascribed to bending vibrations of the P-O bond becomes more intense with an increase of soaking time up to 28 days. The most intense peak also shifted towards a higher wavenumber at 1065 cm^{-1} after soaking in SBF solution for

up to 28 days confirming the precipitation of Ca-P onto the glass surface [15]. The C=O band at 1413 cm^{-1} has also been observed for glass MCWE-2 after 7 and 28 days of soaking as observed for glass CWE-2. The water bands 2032-3443 cm^{-1} also shifted towards higher wavenumber 2035-3934 cm^{-1} after soaking in SBF. The results indicated that the glass MCWE-2 has formed a similar c-HAp as observed for glass CWE-2. The glass MCSE-3 has formed HAp but delay to form amorphous c-HAp than glass CSE-3.

6.6.5 SEM with EDS analysis

SEM images for MCSE-3 and MCWE-2 glasses after soaking in SBF are given in Figure 6.7 (a-d).

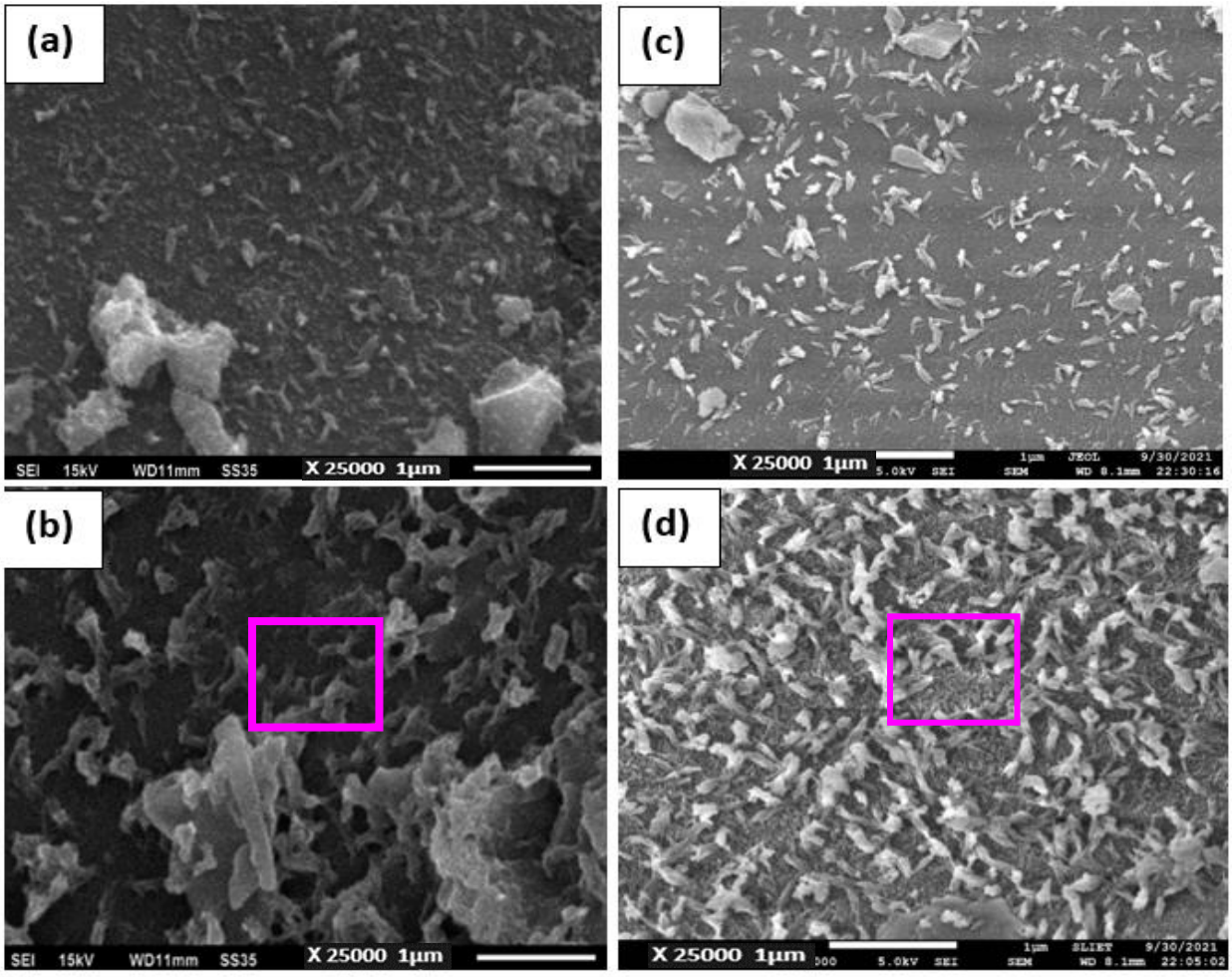

Figure 6.7 Representative SEM images for glasses after soaking in SBF (a) 7 days of MCSE-3 (b) 28 days of MCSE-3 (c) 7 days of MCWE-2 (d) 28 days of MCWE-2

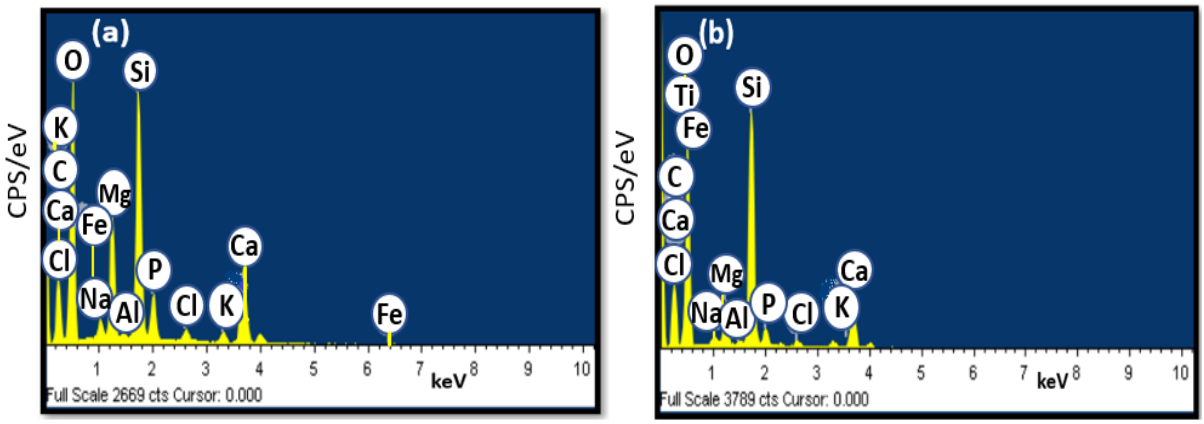

Figure 6.8 Representative EDS spectra of (a) soaked glass MCSE-3 and (b) soaked glass MCWE-2 after 28 days of soaking in SBF

Table 6.4 The glasses MCSE-3, and MCWE-2 after soaking in SBF for 7, 14, 21, and 28 days show the values of Ca and P (wt %) and Ca/P (molar ratio) with an indication of mean ± standard deviation (n=3)

Days of soaking in SBF	**MCSE-3**			**MCWE-2**		
	Ca	**P**	**Ca/P**	**Ca**	**P**	**Ca/P**
7 days	14.16 ± 0.15	3.21 ± 0.22	3.98 ±0.12	11.32 ± 0.09	2.21 ±0.03	3.76 ±0.38
14 days	11.03 ± 0.32	2.22 ± 0.07	3.80 ±0.10	10.10 ± 0.54	3.23 ±0.19	2.53 ±0.44
21 days	8.06 ±0.15	2.52 ± 0.42	2.40 ± 0.33	9.40 ±0.21	2.72 ±0.38	2.56 ±0.58
28 days	8.20 ±0.16	2.44 ± 0.37	2.18 ± 0.21	9.30 ±1.26	3.89 ±1.72	1.72 ±0.52

After 7 days of soaking, glass MCSE-3 and MCWE-2 show flakes like precipitates adhered on the surface of the glasses. However, the glass CSE-3 formed a spherical shape of precipitates on its surface after 7 days of soaking in SBF (discussed in section 4.7.6). The change in morphology might be due to the release of more Mg^{2+} ions in MCSE-3. It has been reported

that the release of more Mg^{2+} ions in SBF, reduced the size of HAp and inhibits the formation of crystalline HAp [22, 23].

On the other hand, glass CWE-2 shows similar morphology after 7 days of soaking in SBF. With an increase in soaking time for the next 28 days, precipitates of apatite phase become dense on the glass MCSE-3 and MCWE-2. Glass MCWE-2 has shown (Figure 6.7 (d)) similar flakes-like morphology as found for glass CWE-2. However, glass MCSE-3 has formed a less spongy c-HAp layer in comparison to agro-food wastes derived glass CSE-3. The representative EDS graphs also show the occurrence of Ca, P, C, Cl, O, and other elements as observed for glass CSE-3 and CWE-2 after soaking in SBF in Figure 6.8. The comparison of the Ca/P molar ratio for glass MCSE-3 is (2.18 -3.98) and for MCWE-2 is (1.72-3.76) after 7-28 days of soaking in SBF is shown in Table 6.4. The glass MCSE-3 has shown a slightly lower Ca/P ratio in comparison to CSE-3 glass. On the other hand, the glass MCWE-2 has an almost similar range of Ca/P ratio.

6.6.6 Biocompatibility test

Figure 6.9 depicts the biocompatibility test of the conventional chemical-derived bioglasses i.e., MCSE-3, and MCWE-2. It is performed on MG-63 cell lines using MTT assay using the same concentrations (1, 2, 5, and 10 mg/ml) as used for the agro-food waste derived glasses CSE-3 and CWE-2. In comparison to agro-food waste derived glasses, these glasses MCWE-3 show cell viability up to 5 mg/ml. With an increase of concentration up to 10 mg/ml, the cell viability has reduced (70 %) in comparison to glass CSE-3 (98 %). It might be due to the release of more Ca^{2+} ions in comparison to CSE-3 glass (discussed in section 6.6.2) [24]. Similar results have been reported for osteoblastic-like human cell lines MG-63 used to study the cell viability of hydroxyapatite nanoparticles with concentrations 100 to 500 ug/ml via MTT and fluorescent staining assay [25].

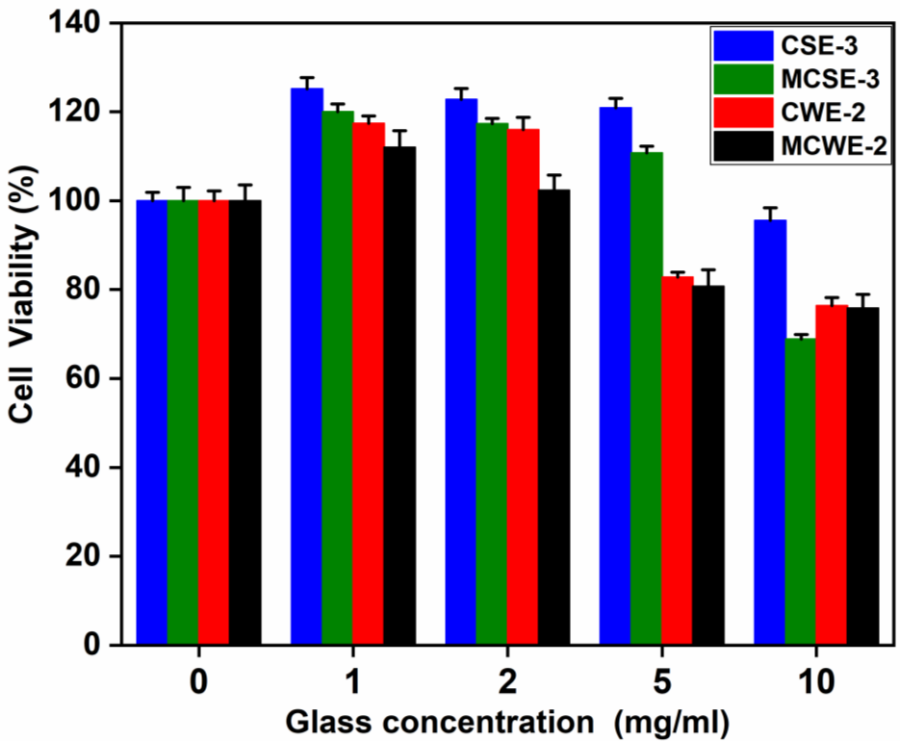

Figure 6.9 Cell growth effect of MCWE-3, and MCWE-2 glasses on human osteoblast-like (MG-63) cell lines. Cells without any treatment represent 0 mg/ml. Each experiment was performed in triplicate. The bar shows the treatments on MG-63 cells are not significantly different at $P<0.05$

The results exhibited that the viability of the cells is reduced and showed cytotoxicity at a greater concentration of 250 µg/ml, due to the release of more Ca^{2+} ions assessed in dissolution tests [25]. On the other hand, glass MCWE-2 has shown ~ 75 % cell viability at a higher concentration of 10 mg/ml, which is the same as glass CWE-2 [26]. Thus, it can be concluded that the glass MCSE-3 is non-toxic up to a concentration of 5 mg/ml, but at a higher concentration of 10 mg/ml, this glass becomes toxic. Glass MCWE-2 is also non-toxic as glass CWE-2.

6.7 Summary

All conventional chemical-derived glasses show more compactness and rigidity in the glass structure than agro-food wastes derived glasses. Higher T_g is not affecting the bioactivity of the glasses. All conventional chemical-derived glasses show bioactivity. But, slow formation of amorphous c-HAp in comparison to agro-food wastes derived glass due to the release of

more Mg^{2+} ions in the SBF. Conventional chemical-derived glasses show a change in morphology of HAp from spherical to flakes types, due to the release of more Mg^{2+} ions confirmed by EDS analysis. These glasses also show initially high Ca/P ratio of ~ 3.9 as HAp is taken place then it becomes less than ~ 2 same as observed for agro-food wastes derived glasses. Conventional chemical-derived based glasses show good cell viability up to the concentration of 5 mg/ml and become toxic at a higher concentration of 10 mg/ml. On the other hand, agro-food wastes derived glasses exhibit higher cell viability than these glasses. Further, the cost analysis of conventional chemicals and agro-food waste ashes derived glasses and glass-ceramics has done. The agro-food wastes derived glasses and glass-ceramics are more cost effctive than conventional chemical derived glasses and glass-ceramics.

Chemical derived glasses	**Agro-food waste derived glasses**
Cost of energy consumption =23.73 USD	Cost of energy consumption = 24.80 USD
Cost of chemicals = 2.3 USD	Cost of chemicals = 0 USD
Total = 26.03 USD	**Total = 24.80 USD**

References

[1] G. Sharma, K. Singh, J. Mater. Cycles Waste Manag. 21 (2019) 801.

[2] H. Jabraoui, M. Malki, A. Hasnaoui, M. Badawi, S. Ouaskit, S. Lebegue, Y. Vaills, Phys. Chem. Chem. Phys. 19 (2017) 19083.

[3] N.A. Wojcik, S. Ali, J.L. Karczewski, B. Jonson, M. Bartmanski, R.J. Barczynski, Mater. 14 (2021) 2626.

[4] L. Grund Back, S. Ali, S. Karlsson, D. Möncke, E.I. Kamitsos, B. Jonson, Int. J. Appl. Glass Sci. 10 (2019) 349.

[5] O.J. Eddine, M. El Bouchti, O. Cherkaoui, H. Hannache, S. Gmouh, J. Chem. 9 (2019) 222.

[6] E. Metwalli, R.K. Brow, J. Non-Cryst. Solids. 289 (2001) 113.

[7] A. Silva, C. Queiroz, S. Agathopoulos, R. Correia, M. Fernandes, J. Oliveira, J. Mol. Struct. 986 (2011) 16.

[8] J. Huang, S. Best, R. Brooks, N. Rushton, W. Bonfield, J. Biomed. Mater. Res. Part A. 87 (2008) 598.

[9] A.M. Efimov, V.G. Pogareva, Chem. Geol. 229 (2006) 198.

[10] S.Y. Venyaminov, F.G. Prendergast, Anal. Biochem. 248(1997) 234.

[11] H. Liu, Y. Lu, Y. Qu, H. Lu, Y. Yue, J. Non-Cryst. Solids. 450 (2016) 95.

[12] I.F. Kadikova, E.A. Morozova, T.V. Yuryeva, I.A. Grigorieva, Mater. Res. 24 (2020) 025203.

[13] O.C. Mocioiu, M. Popa, E.I. Neacsu, M. Zaharescu, J. Non-Cryst. Solids 361 (2013) 130.

[14] Y. Sun, Z. Zhang, L. Liu, X. Wang, J. Non-Cryst. Solids. 420 (2015) 26.

[15] S. Agathopoulos, D. Tulyaganov, J. Ventura, S. Kannan, M. Karakassides, J. Ferreira, Biomater. 27 (2006) 1832.

[16] A. Tilocca, A.N. Cormack, The J. Phys. Chem. B 111 (2007) 14256.

[17] G. Sani, R. Limbach, J. Dellith, I. Sokmen, L. Wondraczek, J. Am. Ceram. Soc. 104 (2021) 3167.

[18] J. Ma, C. Chen, D. Wang, Y. Jiao, J. Shi, Colloids Surf B. 81 (2010) 87.

[19] P. Jha, K. Singh, Ceram. Int. 42 (2016) 436.

[20] T. Charoensuk, C. Sirisathitkul, U. Boonyang, I.J. Macha, J. Santos, D. Grossin, J. Non-Cryst. Solids. 452 (2016) 62.

[21] F. Hmood, O. Goerke, F. Schmidt, Biomed. Glas. 4 (2016) 82.

[22] Z. Geng, Z. Cui, Z. Li, S. Zhu, Y. Liang, W.W. Lu, X. Yang, J. Mater. Chem. B. 3 (2015) 3738.

[23] B. Gayathri, N. Muthukumarasamy, D. Velauthapillai, Santhosh, Arabian J. Chem. 11 (2018) 645.

[24] E. Filova, T. Suchy, Z. Sucharda, M. Supova, M. Zaloudkova, K. Balik, V. Lisa, M. Slouf, Int. J.Nanomed. 9 (2014) 3687.

[25] F. Qing, Z. Wang, Y. Hong, M. Liu, B. Guo, H. Luo, X. Zhang, J. Mater. Sci. Mater. Med. 23 (2012) 2245.

[26] P. ISO, 10993–5: 2009 Biological Evaluation of Medical Devices-Part 5: Tests for In Vitro Cytotoxicity, International Organization for Standardization, Geneva (2009).

Chapter 7 Conclusion and future scope

7.1 Conclusion

In the present work, appropriate agro-food wastes ashes/powder such as corn husk, sugarcane leaves, wheat straw, and eggshell powders were used as resource materials to synthesize glass/glass-ceramics in two different crucibles i.e., Al_2O_3 and Pt-Rh by melt quench technique. For comparison, two glasses were also synthesized using conventional chemicals. These as-prepared glasses/glass-ceramics are characterized and tested by various experimental techniques to check bioactivity and biocompatibility as biomaterials. The following conclusions have been drawn.

All selected glass compositions have formed the glasses irrespective of the crucibles, in which these glasses are melted. Some of the glasses are phase-separated since exhibited two T_c in DSC measurement. The hardness of the present glasses (synthesized from agro-food wastes) is comparable to the conventional chemical used glasses. Even better than conventional chemical glasses i.e., 5.64-6.57 GPa. The agro-food derived glasses form the amorphous c-HAp in 14 days of soaking in SBF solution. The leaching of Mg^{2+} ions from the glass might be the absence of crystalline HAp formation on these glasses. The eggshell powder (CaO) replacement in place of SCLA increases the bioactivity of the glasses. The present glasses have also shown a controlled dissolution rate due to the presence of different alkali and alkaline earth metal ions in comparison to conventional glasses. The Ca/P molar ratio lies between 1.78 to 4.1, which is greater than standard HAp (1.67). These glasses showed cell viability > 90 % on MG-63 osteoblast-like human cell lines even at a higher concentration (10 mg/ml), which could be used for bone regenerative applications. The replacement of SCLA by WSA in glass composition reduces the bioactivity of the glasses. It might be related to the increase of K and alumina in WSA than SCLA. WSA is more reactive than SCLA with the alumina crucible. The higher content of Al_2O_3 increases the hardness, and density of the glasses but decreases the

bioactivity. However, increase the glass formation tendency. The WSA glasses (up to 20 wt % ESP) formed flakes type amorphous c-HAp after 14 days of soaking in SBF. When alumina contents become ~ 11 wt %, inhibits the bioactivity as well as showed toxicity on MG-63 osteoblastic-like human cell lines at a higher concentration (10 mg/ml). WSA glasses (at 30 % ESP) could be useful only when synthesized in a platinum-rhodium crucible since no diffusion of alumina from the alumina crucible. The absence of alumina also increases the tendency of homogeneous glasses. It showed a dense globular shape of amorphous c-HAp after 28 days of soaking in SBF with a Ca/P molar ratio of 1.64 to 4.0, and become non-toxic even at a higher concentration of glass (10 mg/ml).

The dissolution of all conventional chemical-derived glasses is more in SBF and leach out more ions in the SBF than agro-food wastes derived glasses. However, they alter the HAp on the surface of these glasses due to the higher release of Mg^{2+} ions in SBF as compared to agro-food wastes derived glasses. It also released more Ca^{2+} ions in SBF than agro-food wastes derived SCLA glass, which makes the glass toxic at a higher concentration (10 mg/ml). Agro-food wastes derived glass composition [(60 CHA-10SCLA-30 ESP] is most bioactive and biocompatible on human osteoblastic-like cell lines (MG-63) than conventional chemical-derived glasses. This glass is cost-effective and expected to be useful for bone bonding applications.

7.2 Future Scope of the work

The fracture toughness of these glasses can be studied after applying different loads. Young's modulus of these glass/glass-ceramics can also be tested to be used as biomaterials. The bioactivity of the present glasses can also be tested *in in-vitro* using different media such as saline water, tris buffer solution, phosphate alkaline buffer solution, deionized water, etc. to confirm their versatile nature. The *in-vivo* studies could be conducted on the glass CSE-3 to check their performance in the physicochemical environment. As it has been suggested that the formation of an amorphous c-HAp layer *in-vitro* is indicative of the material's bioactive potential *in-vivo*. The antimicrobial tests on these glasses/glass-ceramics may also be performed. These agro-food wastes ashes derived glasses/glass-ceramics may be further explored to form scaffolds used for bone tissue engineering due to their inherent porosity and good bioactivity and biocompatibility. The adhesion, wear and corrosion studies of developed hydroxyapatite surfaces can also be explored.